1-1-1980

Component magnetization of the iron formation and deposits at the Moose Mountain Mine, Capreol, Ontario.

David Stephen Walley
University of Windsor

COMPONENT MAGNETIZATION OF THE IRON FORMATION AND DEPOSITS AT THE MOOSE MOUNTAIN MINE, CAPREOL, ONTARIO.

by

David Stephen Walley

A Thesis
submitted to the Faculty of Graduate Studies
through the Department of
Geology in Partial Fulfillment
of the requirements for the Degree
of Master of Science at
The University of Windsor

Windsor, Ontario, Canada.

1980

ACA 24

740103

TABLE OF CONTENTS

TABLE OF CONTENTS - cont'd.

CHAPTER

ABSTRACT

The object of this project is to study the magnetic characteristics and the ore genesis of the Algoma-type iron formation (IF) near Capreol, including both the Moose Mountain iron deposit and the other host rock (HR) units. A total of 115 IF blocks (4 to 5 specimens each) and 37 HR sites (5 cores or 10 specimens each) were oriented in situ, cored, and sliced into specimens. The specific gravity (S.G.) of the IF specimens give a normal distribution with a mean of 3.56: i.e. mixed ore and lean IF. The low field susceptibility perpendicular to bedding (k_1) for HR and IF is lognormally distributed with a lognormal mean ratio: k_{IF}/k_{HR} of $\sim$1200, so that HR values can be neglected in the magnetic anomaly computation (k_{IF} = 6210 x 10^{-5} cgscm^{-3}). The relationship k_1 = 0.0912S.G. - 0.249 gives an excellent correlation coefficient of 0.84; thus k_1 for economic iron ore at Moose Mountain is 0.11 cgscm^{-3}. The IF shows strong anisotropy of susceptibility with $k_{min} = k_1$ and $k_{11} = 1.75k_1$. Both the HR and IF natural remanent magnetization (NRM) intensities are lognormally distributed with means of 2.00 x 10^{-6} and 11,000 x 10^{-6} emucm^{-3} respectively giving Koenigsberger ratios (Q) of 0.063 and 0.63 respectively. HR NRM can be neglected for anomaly calculation. However, the IF NRM augments the induced component (J_i) by an effective 24%.

After AF cleaning, thermal cleaning and chemical cleaning

70% of the IF samples survive screening tests. After combining normal and reversed components, a stable prefolding A component is isolated at (354^{o},3^{o}), that is thought to represent a metamorphic event associated with emplacement of the Algoman granite and giving an apparent age of 2.5Ga. A second stable, prefolding B component is isolated in all cases at (79^{o},1^{o}), giving an age of 2.7Ga and which is thought to represent the primary remanence of the IF acquired during deposition. Least squares analysis isolates a 'soft', third prefolding remanence component at (278^{o},78^{o}); the significance of it is not as yet understood. A total of $\sim$40% HR sites survive screening tests after AF and thermal cleaning and give poorly defined components in similar directions to the A and B components which are not significantly different to the initial HR NRM site mean directions when grouped in populations.

Using our computer model to incorporate the induced component, the NRM component, the anisotropy of susceptibility, and the demagnetizing factor of 2π, our computed peak value for the Pit 11 aeromagnetic anomaly at the Moose Mountain mine is in excellent agreement with the observed anomaly if a depth extent of 150m is assumed for the IF. Other pits give similar results, inferring a definite depth extent for the IF. Also, if the deposits were flat-lying, the anomalies would be reduced to $\sim$22% of their present value.

ACKNOWLEDGEMENTS

I am most grateful to Dr. D.T.A. Symons for suggesting this project, for his supervision of this work and of course for his tireless reading of this dissertation in manuscript.

I am also in debt to Dr. M. Stupavsky for the numerous suggestions, explanations and critical assistance I received from him.

Thanks are also extended to the Personnel at the Moose Mountain mine for their co-operation during the sampling stage of this study, to Joe Huschilt and Dennis Dunsmore for their enthusiastic assistance both in the field and in the laboratory, and to Gayna Sinclair for her drafting services.

Furthermore, I am most grateful to the Ontario Geological Survey for their financial support.

Finally, I would like to thank Mr. and Mrs. S.D. Walley, Anne and Catherine Walley and complete family tree, not for having anything to do with the compilation of this thesis, but for helping to further my career either deliberately or by accident.

LIST OF FIGURES

LIST OF FIGURES - cont'd.

Figure

LIST OF TABLES

Table

LIST OF APPENDICES

CHAPTER I

INTRODUCTION

1.1 THE PROBLEM AND PROPOSAL

Three years ago, there were eight major iron ore producing mines in Ontario (Fig. 1). In one years' time there will probably be only four because of dwindling reserves and unsuccessful exploitation and exploration of major prospects (C.M.Y. 1976).

The exploration for iron ore deposits in Ontario has been done primarily by airborne and ground magnetic surveys measuring the vertical magnetic component. Only the most intense magnetizations are targets for examination. The vertical magnetization in Ontario iron formations and deposits varies significantly with: 1) the nature and abundance of the magnetic minerals, 2) the anisotropy of magnetic susceptibility 3) the attitude of the bedding, and 4) the direction and intensity of the remanence.

In this study it is proposed to:

a) define the magnetic properties of the iron formation at the Moose Mountain mine and to establish the relationships between bedding attitude, magnetic susceptibility, magnetic anisotropy, magnetic mineralogy and natural remanence with the aim of constructing a magnetic model to aid interpretation of aero-

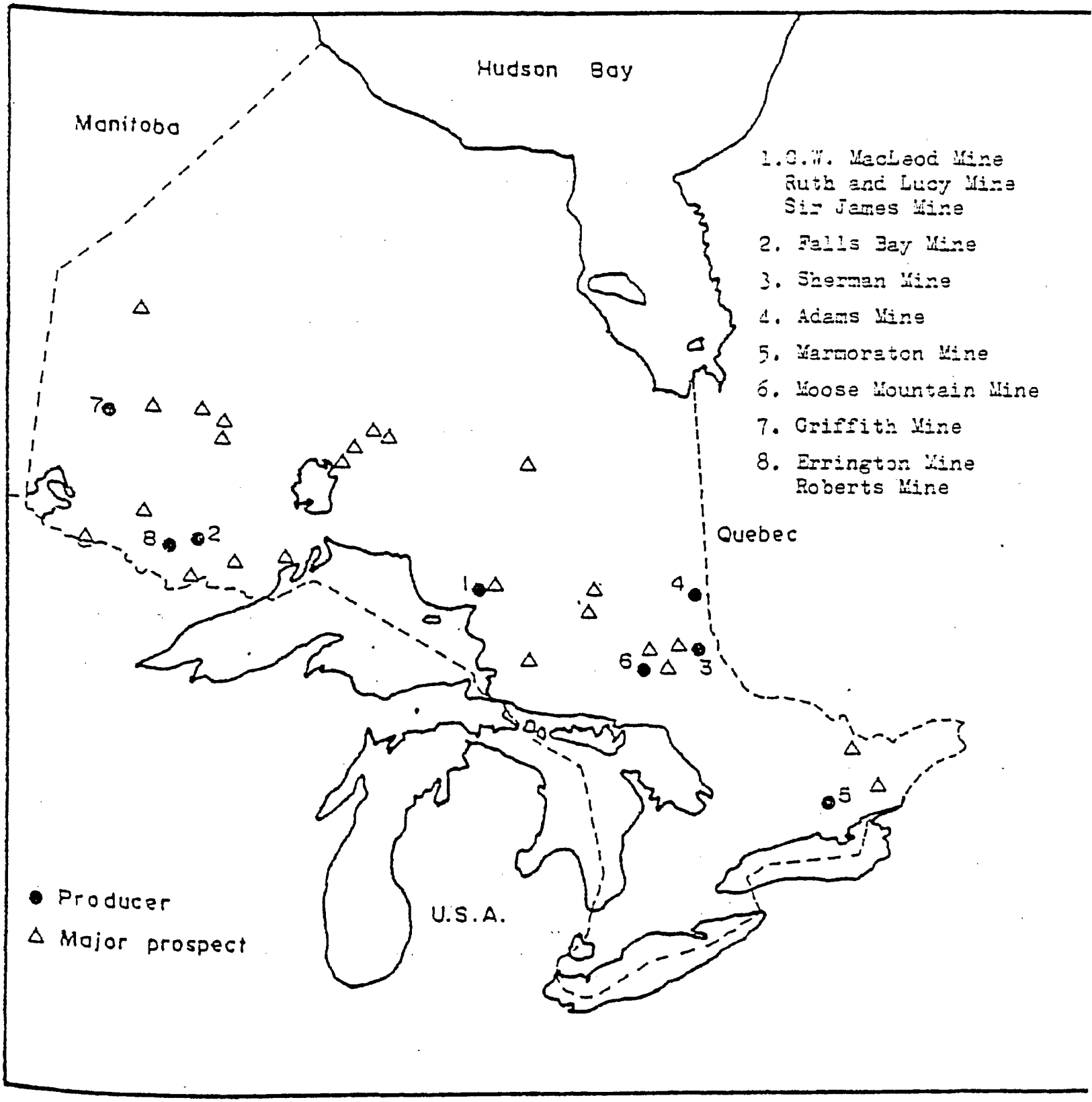

FIG. 1. Map of iron ore producing mines and major prospects in Ontario (modified after Shklanka, 1968).

magnetic maps and ground magnetometer surveys, and b) to look at the paleomagnetic characteristics of the iron formation and the associated host rock in order to provide genetic information on the age and mode of ore formation.

This information will assist in the exploration of new iron ore deposits by more closely defining their magnetic geophysical parameters and their genetic geological control.

1.2 PREVIOUS SIMILAR WORK AND LOCATION OF THE AREA

The suitability of Precambrian iron formations for paleomagnetic studies has been discussed at length by Seguin (1976). Several successful studies in the Precambrian of Canada have been made (Symons 1966,1967; Seguin 1972,1975; Symons and Stupavsky 1979). The latter paper looks at the iron formation and associated host rocks of the Sherman mine, Temagami and is a similar study to the one proposed here. Stable remanences are isolated and the indications are that the iron formation is ideal for paleomagnetic studies. Wherever possible and relevant, comparison will be made to the results of this previous study.

This study examines the Moose Mountain deposit near Capreol. The mine is situated in Hutton Township, Northern Ontario about 32km north of Sudbury (Fig. 2). The geographic co-ordinates of the mine are Long.: 81.00^{o}W, Lat.: 46.80^{o}N.

1.3 HISTORY OF THE MINE

The Moose Mountain deposits have been known since the

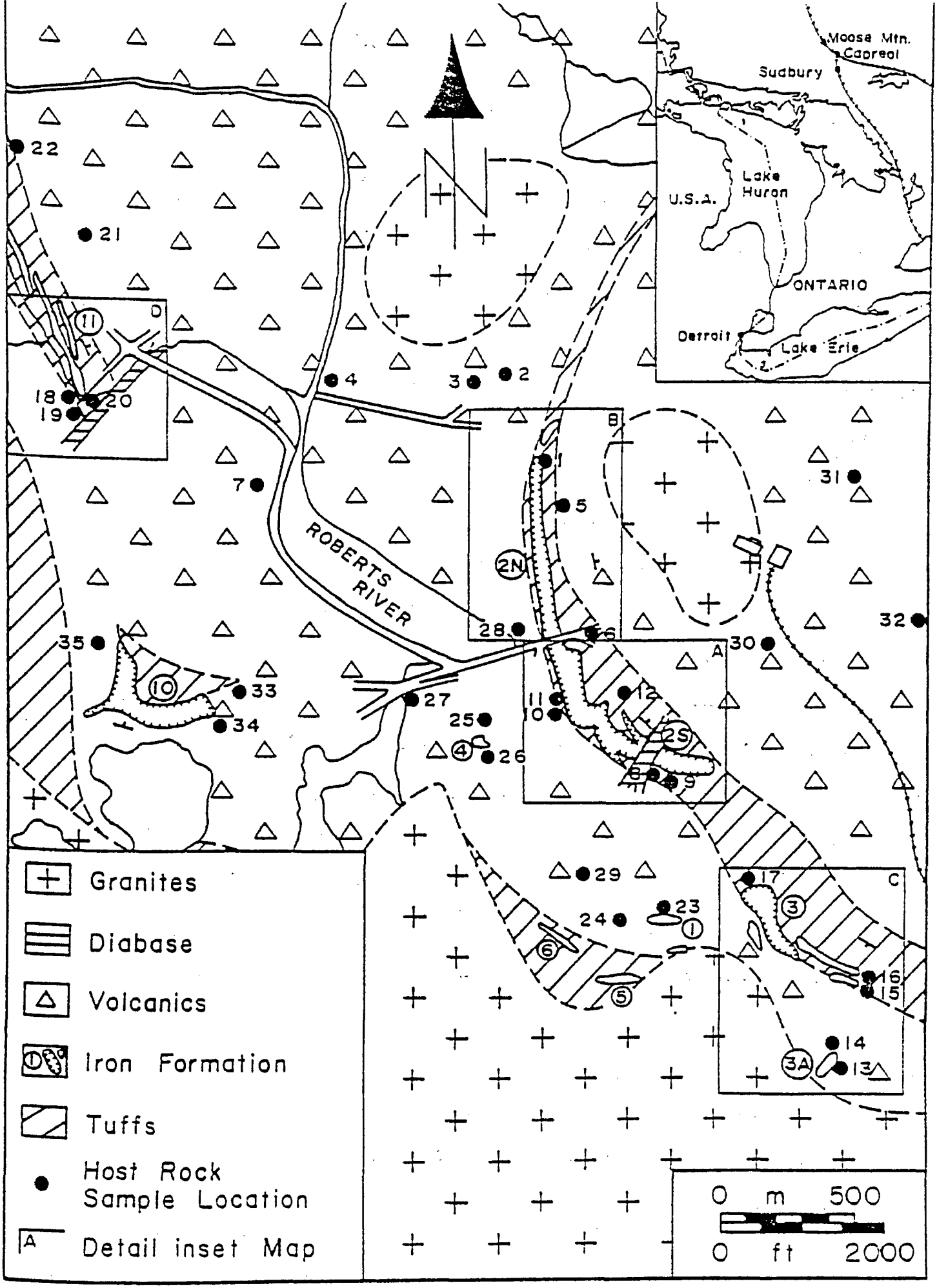

FIG. 2. Regional geology and location of the Moose Mountain mine. (modified after Markland, 1966).

1890's. A financially unsuccessful attempt was made to mine the ores from 1901-1920 (O.D.M. 1967). The early production came from an open pit excavated on the No. 1 body (Fig. 2). The ore consisted of relatively massive, coarse grained magnetite intergrown with recrystallized mafic volcanics, and yielded a product containing about 55% iron and less than 14% silica. However, the treatment produced a high percentage of fines and operations were subsequently shifted to the No. 2 body. It consists of typical Algoma-type oxide facies iron formation composed of an intimate mixture of fine-grained magnetite and quartz yielding a concentrate averaging 69% iron and less than 6% silica.

In 1937, the M.A.Hanna Co. became interested in the property and after studies and further exploration brought the property into production in 1959. The benefication plant turned out 625,000 tons of concentrate per year. A pellet plant was opened in 1963 and produced 600,000 tons of pellets per year. Reserves in 1966 were quoted as 14 million tons, of which 80% assay approximately 33% Fe or 28% magnetic Fe and yield a concentrate of 68% Fe with 40% weight recovery. The other 20% of reserves assay approximately 28% Fe or 21% magnetic Fe and yield a concentrate of 66% Fe with 31% weight recovery.

The National Steel Corporation of Canada Limited continued production and in 1969 produced 669,900 tons of iron ore pellets (O.D.M. 1969). During 1975, extraction of

ore from the No. 3 pit was terminated and temporarily suspended from the No. 10 pit. Development work was carried out on the No. 11 pit (O.D.M. 1975).

Originally scheduled to cease operations in 1980, the plant closure was accelerated by severe spring flooding and closed in early 1979.

CHAPTER II

GEOLOGY

The geology in the vicinity of the mine is shown in Figure 2. It has been described by Markland (1966) from which most of this discussion is taken.

2.1 REGIONAL GEOLOGY

The mine area lies approximately 16km north of the Sudbury Irruptive where Huronian sediments lie unconformably over older Archean rocks of the Superior Geologic Province. The Archean Keewatin volcanic strata lie in steeply dipping isolated segments surrounded by subsequently emplaced Algoman granite. The known iron formation occurrences of the district lie within these volcanic remnants.

The Moose Mountain ore bodies occur within a large belt of Keewatin rocks comprising mafic metavolcanics, felsic metavolcanics, sedimentary schists, tuffs and iron formation. A group of mafic dikes, probably Matachewan in age, intrude both this greenstone belt and the Algoman granite. Still later dikes and sills of Keweenawan olivine and quartz diabase, striking in a north-westerly direction, intrude all of the other rocks. Table 1 shows the lithologic units present along with the available radiometric age data.

TABLE 1. Table of lithologic units (after Kindle, 1932 and Meyn, 1970)

		Approx. Radiometric Age (Ma)
CENOZOIC		
Recent:	Fluvial clays and silts, and swamp deposits	
Pleistocene:	Clay, sand, gravel and till	0.1 to 1[5]
	Unconformity	
PRECAMBRIAN		
PROTEROZOIC		
Keweenawan:	Olivine diabase dikes Quartz diabase dikes and sills	1250[1]
	Intrusive contact	
Nickel Irruptive:	Quartz diorite breccia	1840[5]
	Intrusive contact	
Nipissing:	Quartz diabase and diorite	2150[5]
	Intrusive contact	
Huronian:		
Cobalt Group;	Lorrain Fm. -Quartzite Gowganda Fm. -Argillite, quartzite & conglomerate	2200[2]
	Unconformity	
Bruce Group;	Serpent Fm. -Quartzite & conglomerate Espanola Fm. -Limestone & greywacke Bruce Fm. -Conglomerate & quartzite	
	Unconformity & Faulting	
ARCHEAN		
Matachewan:	Diabase dikes	2485[3], 2690[4]
	Intrusive contact	
Algoman:	Massive pink granite, granite gneiss and pegmatite dikes	2500[5]
	Intrusive contact	
Keewatin:	Basaltic lava, mafic to intermediate flows and iron formation	

NOTES: 1. van Schmus (1965); 2. Fairbairn et al (1969); 3. Wanless et al (1965); 4. Gates and Hurley (1973); 5. Card (1978).

2.2 MINE GEOLOGY

2.2a General

The Archean iron formation in the mine occurs as eleven discontinuous lenses aligned in a general north-westerly direction over a strike length of 8km. It is interbedded with flows and tuffs of basaltic to rhyolitic composition. The lenses range in length from 90 to 1200m and have an average width of 50m (Shklanka 1968).

The metavolcanics and metasediments have been intruded by dikes and sills of granite, pegmatite and diabase. The mafic volcanics are now largely recrystallized hornblende schists (Markland 1966, p51).

2.2b Local Members

Figure 2 shows the distribution and numbering of the deposits and their relation to the regional geology.

The prevalent host rocks to the iron formation are mafic volcanic flows and tuffs of generally basaltic composition. The mafic tuff near the deposits commonly grades to an intermediate dacitic composition by the addition of lenticular felsic inclusions.

The felsic volcanics are hard grey rhyolitic rocks found flanking some deposits and as minor lenses within mafic tuff.

Chert, in addition to forming the major gangue constituent of the iron formation, occurs as fine interbeds with

tuff and as laminated units with amphibole, graphitic material or fine granular pyrite. The chert, now recrystallized to a very fine textured quartz, is always in close association with the iron formation.

The Matachewan mafic intrusives include massive diabase and a biotite-rich dense basalt. They intersect all of the formations as small dikes and sills. The Algoman felsic intrusives include granite and pegmatite dikes and sills. They increase in abundance close to the main granite contacts (Markland 1966, p54).

2.2c Alteration

The Archean volcanic complex has been subject to shearing and metamorphism ranging from the greenschist to the epidote-amphibolite facies.

In the iron formation, original mafic tuffaceous material is believed to be now represented by amphibole, chlorite and biotite. The magnetite and chert have been recrystallized, but to a degree where only the coarsest grains are macroscopically visible. The alteration is attributed to the intrusion of the Algoman granite. In some instances the magnetite is locally remobilized, while in other places this alteration has caused considerable martitization and the production of localized hematite-rich zones (Markland 1966, p54)

2.2d Stratigraphy

The general depositional sequence across the lenses of

iron formation from the footwall on the southwest to the hanging wall on the northeast is:

1) massive volcanics containing pockets and small erratic concentrations of tuff or low-grade iron formation;
2) cherty tuff, occasionally with appreciable pyrite and graphite;
3) cherty gruneritic iron formation;
4) banded iron formation with included interbeds of tuff or sheared volcanic rocks;
5) cherty tuff which is garnetiferous in part;
6) banded mafic to intermediate tuff; and,
7) pillow lava.

The sequence listed above is seldom complete in any one deposit. Due to widespread shearing and alteration, no definite top determinations have yet been made. The sequence assumes that volcanic stratigraphy is generally from mafic to felsic volcanic rocks, and that such a stratigraphic sequence may be repeated a number of times in a volcanic pile. On this basis it is assumed that the sequence tops are to the northeast (Fig. 3; Meyn 1970).

2.2e Structure

In addition to the regional tilting of the Keewatin belt, there is evidence of cross-folding in a NNE direction with steep northerly plunges.

Two main patterns of faulting are recognized. Longitudinal faults, believed to be related to the general shearing, closely follow the bedding but curve and bifurcate

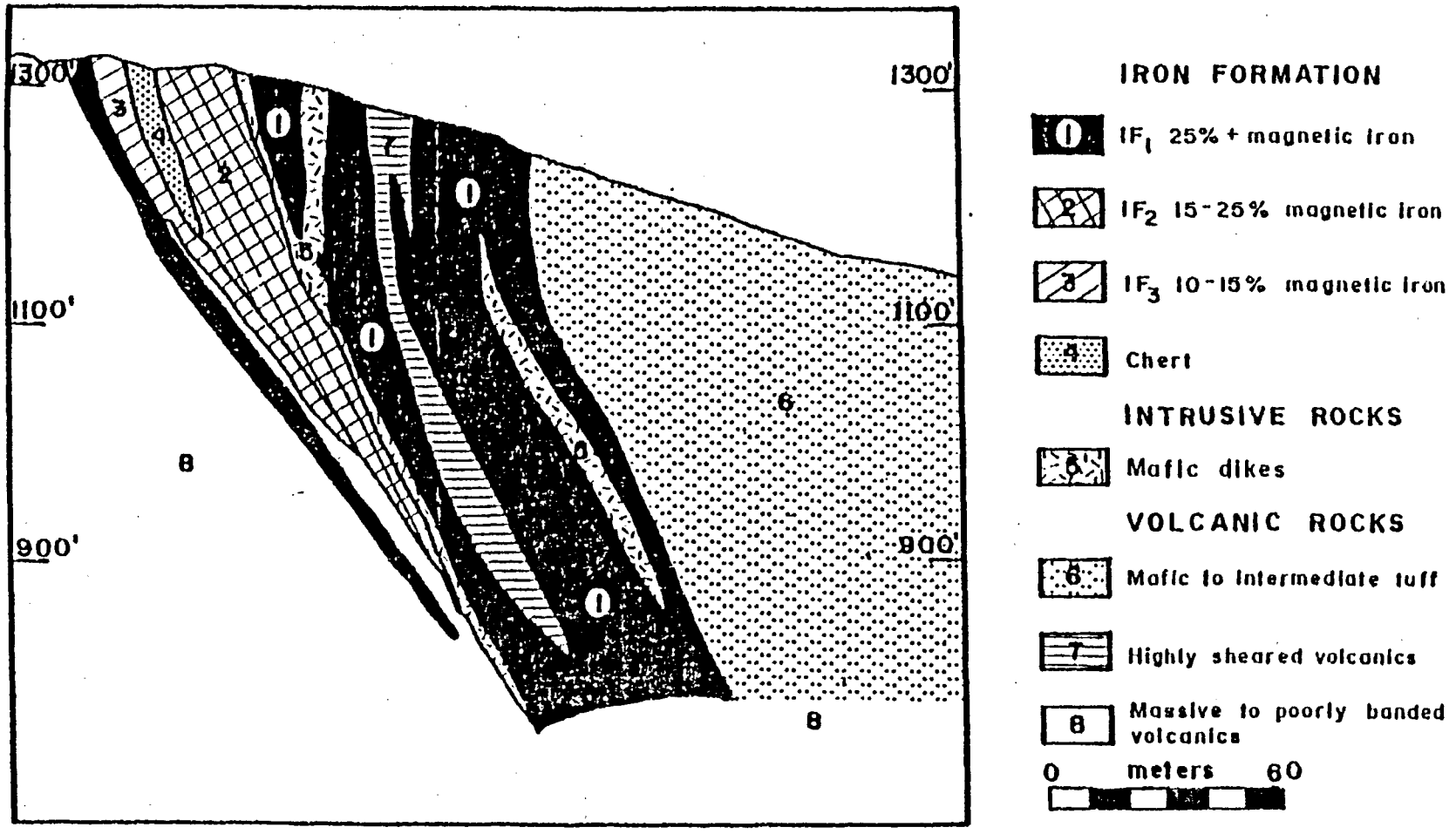

FIG. 3. Cross-section of Pit 2S, Moose Mountain mine; modified after Meyn, 1970, Fig. 7 p.48.

across the strata in strike and dip. Faults of this system appear to be related to the cross-folding and to have caused most of the deformation of the ore bodies. A younger steeply dipping set of north-easterly striking faults provide openings for diabase dikes. Horizontal offsets are small but the vertical component of movement may be large.

2.3 IRON FORMATION

The Moose Mountain iron formation is of the Algoman type. It is composed of magnetite and chert with varying admixtures of tuffaceous material, now chiefly in the form of amphibole.

2.3a Classification

The iron formation can be divided into three general types: siliceous, amphibolitic, and gruneritic depending upon the chief gangue constituent. Each type may be further classified and described on the basis of certain structural relations which have a practical significance when applied to ore.

The ore is divided into classes 1,2,3 and 4 based on the magnetic iron content being greater than 25,15,10 and 5% respectively.

The iron formation may be fine or coarsely banded. Fine banded ore is most prominent. It normally shows alternating 3mm thick magnetite-rich and magnetite-poor bands. Occasionally, ore of the amphibole type will be coarsely banded to

massive with no fine banding or foliation in evidence.

Magnetite occurs as grains and aggregates which are intercrystallized with gangue minerals in all proportions. The grains and aggregates vary from 0.3mm in diameter in iron-rich bands down to 0.04mm grains disseminated throughout the iron-poor bands, and to 0.01mm and smaller inclusions in the gangue minerals. Size is fairly uniform in any one band.

Hematite occurs in three types of association in the ore. It forms alteration rims around the very fine magnetite grains in some of the iron-poor bands. It also occurs in local zones where it is closely associated with epidote and granite dikes as a martitization product of magnetite. The most prominent occurrence, however, is again in localized zones where specular hematite forms iron-rich bands in the same manner as magnetite. The average hematite content of the ore is approximately 4 percent (Meyn 1970).

Amphibole is present as the major gangue material in about 20% of the ore and as a minor constituent approaching 20% in the remainder. The iron content of the amphibole is indeterminate because of the variable composition and the enclosed, ultra-fine magnetite. It should not be more than 10 percent (Meyn 1970).

Pyrite occurs in the ore as scattered grains along dike borders and in some volcanic interbeds (Markland 1966,p55-56).

2.3b Siliceous Iron Formation

Siliceous iron formation comprises 80% of the ore. It

is composed of magnetite and chert with minor amphibole. Recrystallized grains of quartz and amphibole, 0.02mm to 0.3mm in size, form crude layers with magnetite distributed throughout as very fine inclusions, fine scattered grains, and coarse aggregates in ragged bands (Markland 1966, p56).

2.3c Amphibolitic Iron Formation

This type of iron formation comprises about 20% of the ore. It is composed of magnetite and amphibole with minor chert. The distribution of magnetite is most commonly in the form of coarse irregular aggregates which are arranged in rough, narrow, but closely spaced bands with the fibrous amphibole. Coarser and more sparsely distributed grains are disseminated with the gangue minerals (Meyn 1970).

2.3d Gruneritic Iron Formation

A third type of iron formation is found along the low grade borders of several deposits. In it, the amphibole mineral grunerite forms the dominant gangue mineral, and is interbedded with chert and magnetite. The grunerite forms dominant bands, but occasionally appears as irregular cross-cutting masses and veinlets. The magnetite occurs as very fine (0.05mm) grains and thin beds. The gruneritic iron formation appears to represent a transition stage between the deposition of pure chert and the normal siliceous banded ore (Markland 1966, p58).

2.3e Genesis

The lenticular nature of the ore, its distribution and the volcanic environment suggest that the iron formation was deposited in local basins, possibly as a colloidal gel during a period of active volcanism. Fluctuating conditions of concentration and Eh-pH due to weathering and volcanic activity, may have caused the alternate layers of iron-rich and iron-poor silica to be deposited together with varying quantities of ash. The conditions of deposition with subsequent diagenetic and metamorphic effects have produced magnetite in a wide range of associations (Markland 1966, p58).

CHAPTER III

EXPERIMENTAL METHODS

3.1 SAMPLING

Immediately after the closure of the Moose Mountain mine, 115 iron formation (IF) oriented hand samples and 37 field drilled host rock (HR) sites were collected in a period of 10 days. The sites were distributed both within the several pits and the surrounding HR so as to adequately represent each pit (Figs. 2,2a-d).

At each HR site a mimimum of five cores were drilled several metres apart and oriented in situ using a solar compass with Brunton compass and topographic sitings to an accuracy of $<2^{o}$. Care was taken in the site selection to avoid areas susceptible to lightning strikes.

A total of 115 oriented hand samples of IF were collected from pits 1-11 (Figs. 2a-d), the majority being collected by boat from the shoreline exposures of the now flooded pits. Pits 4,6,8 and 9 have been exhausted and are now re-landscaped. The samples were distributed as uniformly as possible from the available outcrops, although problems were encountered particularly along the hanging walls where the grade of iron ore was very low. Hand specimens were collected and oriented in situ using topographic sitings and a modified inclinometer to an accuracy of approximately 3^{o}.

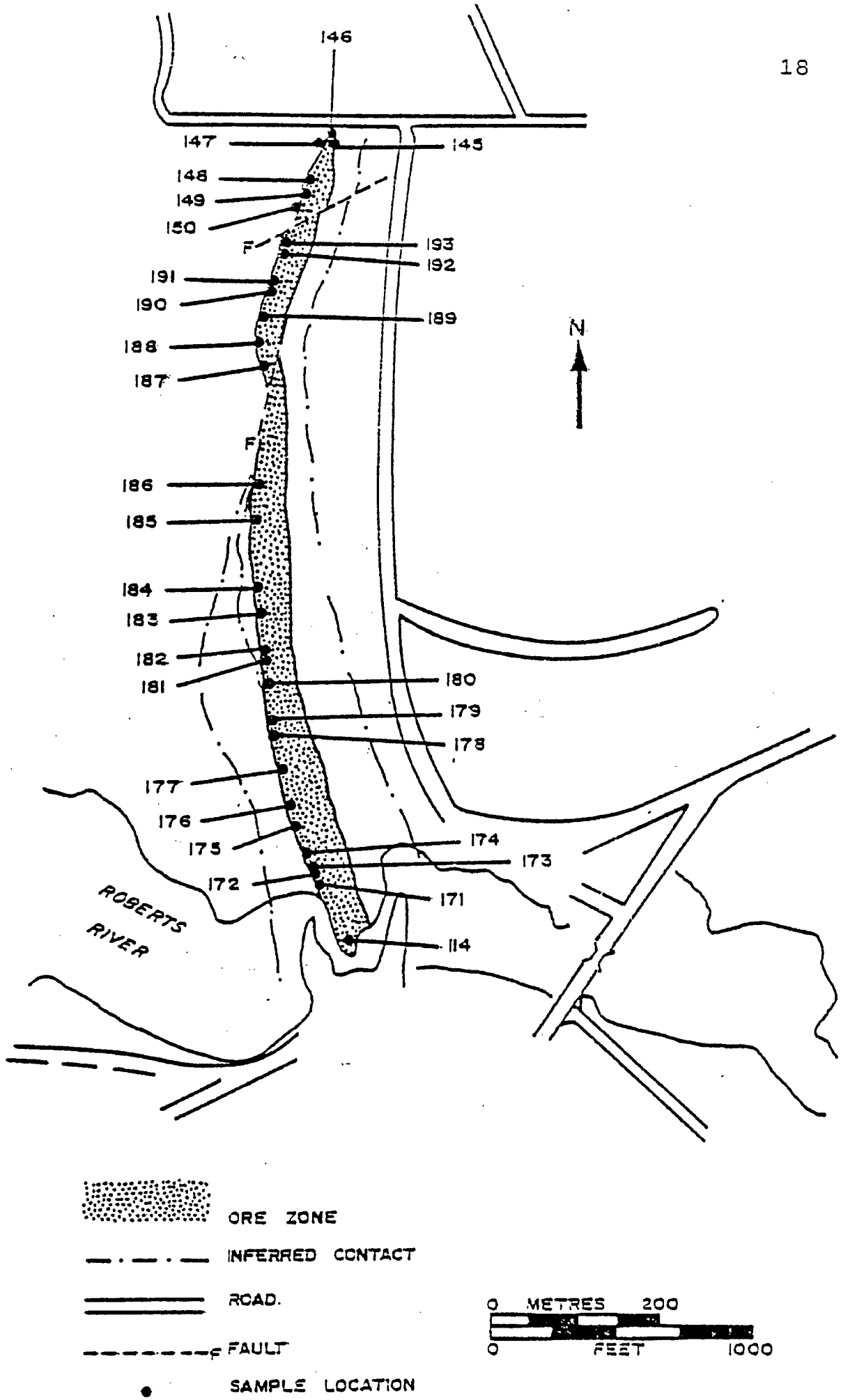

FIG. 2a. Outline of Pit 2N, Moose Mountain mine, showing locations of block samples of iron-formation.

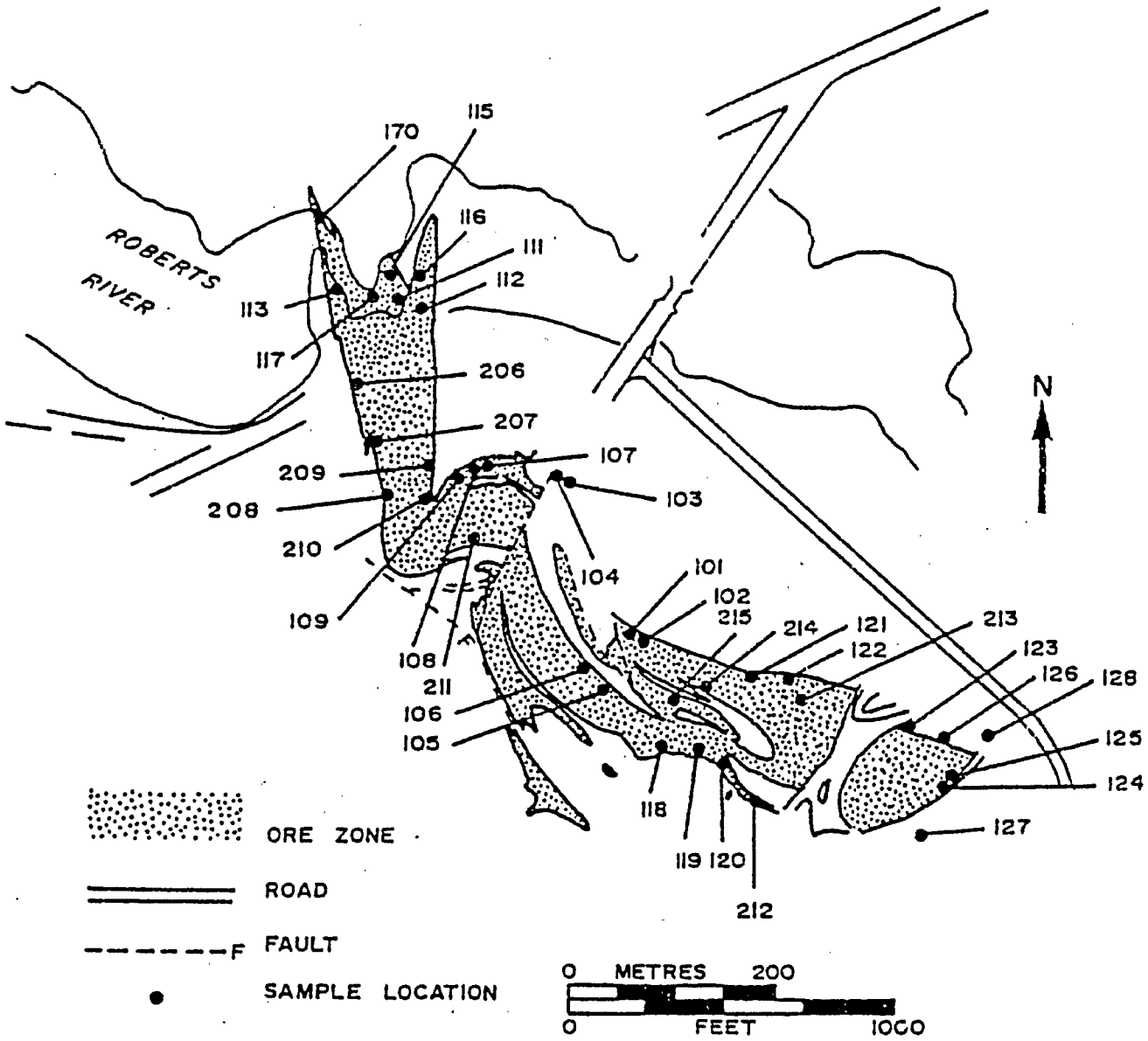

FIG. 2b. Outline of Pit 2S, Moose Mountain mine, showing locations of block samples of iron-formation.

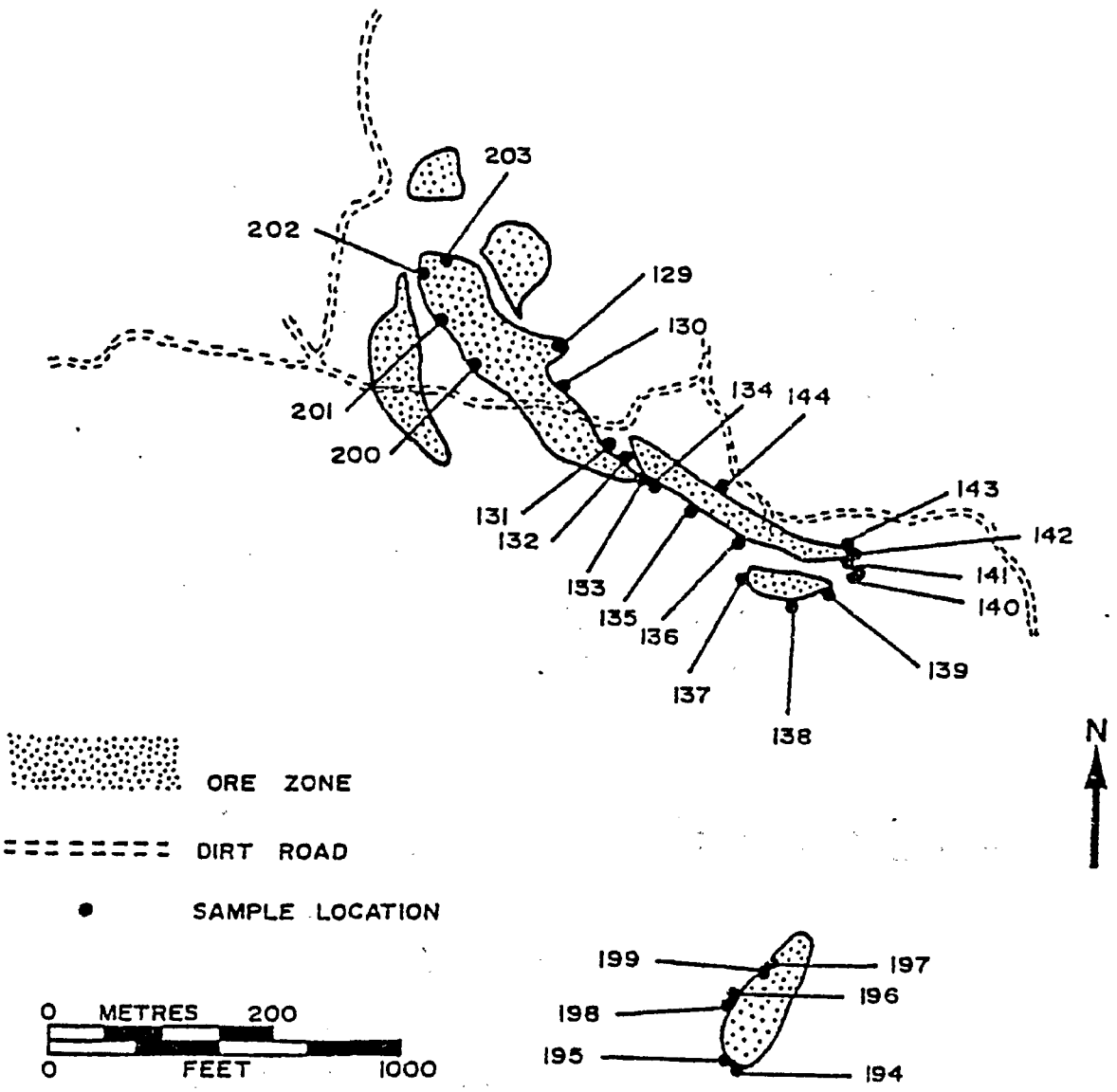

FIG. 2c. Outline of Pits 3 and 3A, Moose Mountain mine, showing locations of block samples of iron-formation.

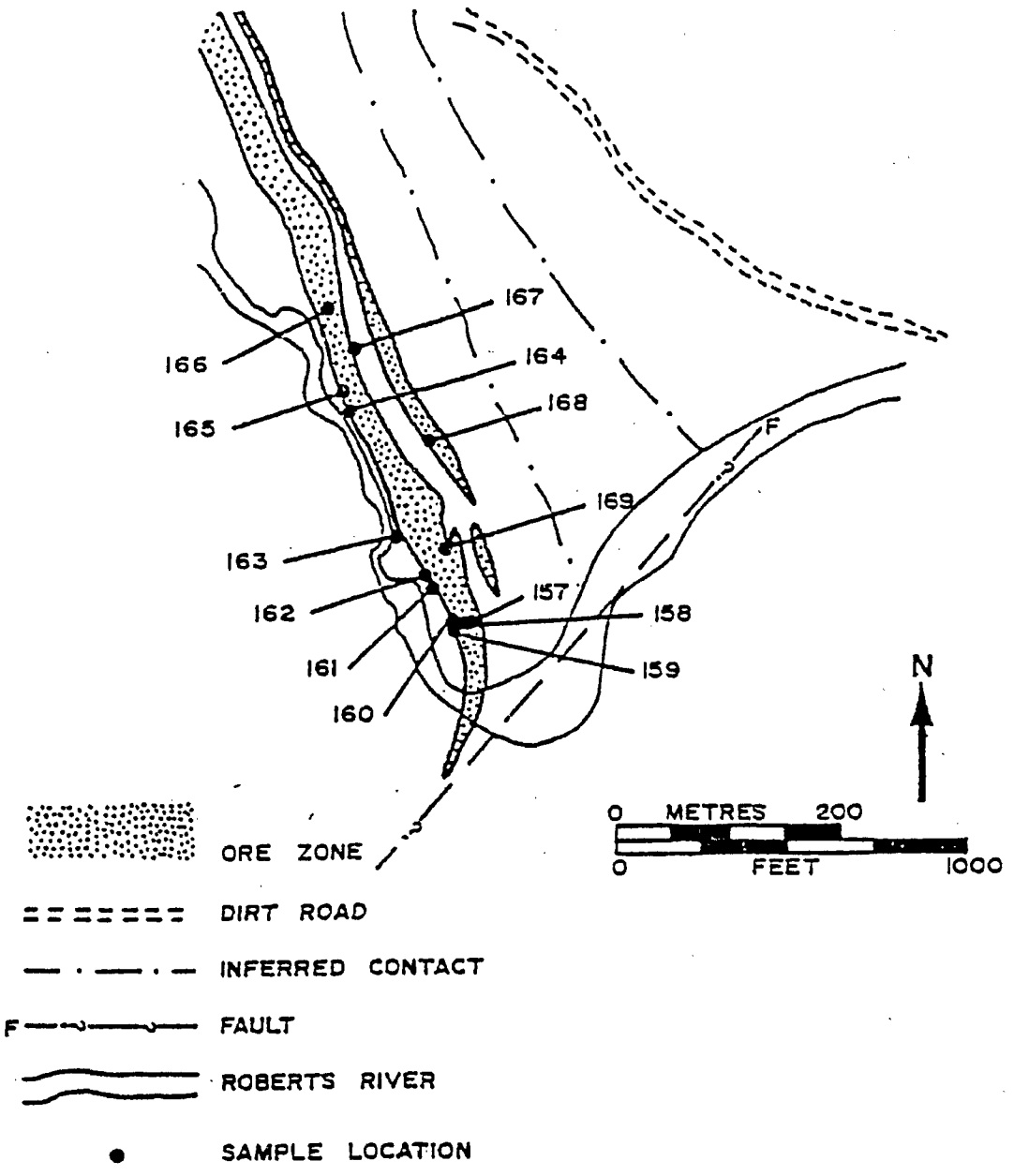

FIG. 2d. Outline of Pit 11, Moose Mountain mine, showing locations of block samples of iron formation.

3.2 SAMPLE PREPARATION

The drilled HR cores were cut into at least two conventional cylindrical specimens of 2.50cm diameter and 2.45cm length, thus yielding ten specimens from each site for AF cleaning; a data base of 370 specimens. A total of 122 additional specimens were cut and put aside for thermal cleaning analysis.

Symons and Stupavsky (1979) after considerable experimentation with a variety of drill bit types and sizes, have found that 1cm right cylindrical IF specimens can be drilled from the IF hand samples despite their hardness using Felker thin-wall bits. At least four such specimens, 1cm in length, were drilled from each block yielding 460 specimens for AF cleaning. Additional specimens were cut for thermal and chemical cleaning yielding a total data base of 680 specimens.

In order to investigate the problem of some of the small cores being confined to one band of IF and hence not being representative of the IF as a whole, 26 specimens of 2.50cm diameter and 2.45cm length were also cut.

3.3 SAMPLE TREATMENT

3.3a Specific Gravity

The specific gravity was measured on the 460 IF specimens using a modified picnometric technique. Results are repeatable to an accuracy of $\pm 0.01 gcm^{-3}$.

3.3b Magnetic Susceptibility

The low-field susceptibility perpendicular to bedding (k_1) was measured on a toroid bridge (Christie and Symons 1969) for 434 HR specimens, 460 small IF specimens and the 26 large IF specimens.

3.3c Anisotropy of Magnetic Susceptibility

Measurements of the low-field susceptibility along 9 directions using a toroid bridge were used to calculate the matrix elements of the susceptibility ellipsoid. The 460 small IF specimens and the 26 large IF specimens were measured in this way. The principal susceptibility axial directions and magnitudes of the ellipsoid were computed from the matrix elements.

3.3d Natural Remanent Magnetization

The Natural Remanent Magnetization (NRM) components of all 1172 specimens were measured using a Schonstedt SSM-1A spinner magnetometer. A '3-spin' technique giving more efficient treatment and yielding reliable measurements was used in the majority of cases. However, for specimens with low magnetic signals, a '6-spin' technique was utilized. The NRM direction and intensity for each specimen were computed from the component measurements.

3.3e AF Cleaning

One pilot specimen per HR site with an average NRM direction and intensity for that site was step demagnetized in alternating fields (AF) with peak intensities of 5,10,15, 20,30,40,60,80 and 100mT using a Schonstedt GSD-1 AF demag-

netizer.

Similarly 37 IF pilot specimens with an average NRM direction and intensity for that sample were selected so as to adequately represent each pit, and step demagnetized in AF fields of 5,10,15,20,30,40,60,80 and 100mT peak intensity.

The paleomagnetic stability index (PSI) method of Symons and Stupavsky (1974) for directional analysis and the intensity decay curves for each pilot specimen were used to select the optimum AF intensity for demagnetizing the remaining specimens from each site and pit (Tables 2 and 3).

3.3f Thermal Cleaning

One HR specimen per site where available, with an average NRM direction and intensity for that site, was thermally demagnetized at temperatures of 100,200,300,400,450,500, 550,600,650 and 700°C using a furnace having a non-inductive heating element, located in a nested series of five 'mu'-metal shields in a shielded room. The introduction of random acquisition of remanence by the specimens during the cooling due to incomplete elimination or shielding of the Earth's field was checked by placing the specimens in opposite directions during successive steps.

Similarly, specimens from 20 representative IF samples have been thermally demagnetized at the same temperatures. A further 60 IF specimens have been thermally cleaned at temperatures of 500°C and 600°C. Spurious coherent magnetizations

TABLE 2. Sampling and remanence data of Iron Formation sites

Sample	Location °W	Location °N	Pit	AF intens mT	Data screening a	b	c	N	Remanent magnetization Length R	Decl. °	Incl. +down	A95 °
101	81.00	46.80	2S	30	1			3	2.924.	6.57	4.61	24.51
102	81.00	46.80	2S	30			1	0				
103	81.00	46.80	2S	60				4	3.832	107.61	2.86	22.34
104	81.00	46.80	2S	60	1			3	2.945	62.87	5.02	20.59
105	81.00	46.80	2S	100		1		2	1.872	165.05	-5.99	72.84+
							1	0				
106	81.00	46.80	2S	100				4	3.762	182.70	16.59	26.91
107	81.00	46.80	2S	40	1			3	2.855	342.01	13.22	34.55
108	81.00	46.80	2S	40	1			3	2.856	316.10	8.70	34.40
109	81.00	46.80	2S	40	1			3	2.872	335.54	-2.96	32.37
110	81.00	46.80	2S	40				4	3.802	143.35	7.35	24.42
111	81.00	46.80	2S	60		1		2	1.988	97.24	6.84	27.76
							1	0				
112	81.00	46.80	2S	60	1			3	2.836	76.45	10.05	36.91
113	81.00	46.80	2S	60	1			3	2.944	90.50	-3.79	20.91
114	81.00	46.80	2S	30		1		2	1.999	101.11	17.84	6.50
							1	0				
115	81.00	46.80	2S	30	1			3	2.887	53.20	11.50	30.26
116	81.00	46.80	2S	30		1		2	1.986	183.20	-8.11	29.68
								2	1.998	104.06	3.20	10.09
117	81.00	46.80	2S	60		1		2	1.999	60.61	6.31	3.69
								2	1.887	184.39	-4.90	82.06+
118	81.00	46.80	2S	60		1		2	1.954	30.05	0.01	56.60+
								2	1.977	116.47	13.97	38.99
119	81.00	46.80	2S	60	1			3	2.859	337.86	10.50	33.99
120	81.00	46.80	2S	60	1			3	2.924	11.45	-1.42	24.53
121	81.00	46.80	2S	60	1		1	0				
122	81.00	46.80	2S	60	4			0				
123	81.00	46.80	2S	60	1			3	2.958	6.17	8.52	18.17
124	81.00	46.80	2S	*								
125	81.00	46.80	2S	*								
126	81.00	46.80	2S	*								
127	81.00	46.80	2S	20			1	0				
128	81.00	46.80	2S	*								
129	81.00	46.80	3	20	1		1	0				
130	81.00	46.80	3	*								
131	81.00	46.80	3	*								
132	81.00	46.80	3	*								
133	81.00	46.80	3	20	1			3	2.834	62.05	12.16	37.15
134	81.00	46.80	3	*								
135	81.00	46.80	3	20	2			2	1.986	292.77	-4.09	30.27
136	81.00	46.80	3	20	1			3	2.855	72.53	2.80	34.60
137	81.00	46.80	3	*								
138	81.00	46.80	3	20	1			3	2.924	11.84	4.94	24.52
139	81.00	46.80	3	*								
140	81.00	46.80	3	80	1			3	2.902	89.10	-17.29	28.04
141	81.00	46.80	3	80		1		2	1.961	12.36	-0.14	51.54+
								2	1.977	306.63	-3.40	39.07

Sample	Location °W	Location °N	Pit	AF intens mT	Data screening a	b	c	N	Remanent magnetization Length R	Decl. °	Incl. +down	A95 °
142	81.00	46.80	3	80				4	3.921	54.70	12.79	15.14
143	81.00	46.80	3	80	1			3	2.923	342.57	6.47	24.67
144	81.00	46.80	3	20		1		2	1.947	181.45	-21.45	60.96+
145	81.00	46.80	2N	30	1			3	2.956	143.25	8.12	18.48
146	81.00	46.80	2N	30			1	0				
147	81.00	46.80	2N	30		1		2	1.932	186.42	-5.53	70.84+
							1	0				
148	81.00	46.80	2N	80	1		1	0				
149	81.00	46.80	2N	80		1		2	1.931	71.24	5.79	71.14+
								0				
150	81.00	46.80	2N	80	1			3	2.891	22.94	7.16	29.63
151	81.00	46.80	10	80	1		1	0				
152	81.00	46.80	10	80	1			3	2.903	267.29	24.53	27.82
153	81.00	46.80	10	80	1		1	0				
154	81.00	46.80	10	80			1	0				
155	81.00	46.80	10	*								
156	81.00	46.80	10	80	1			3	2.901	356.86	5.17	28.21
157	81.00	46.80	11	80	1			3	2.891	266.09	35.79	29.69
158	81.00	46.80	11	80	1		1	0				
159	81.00	46.80	11	80	1			3	2.979	61.34	-25.96	12.65
160	81.00	46.80	11	80				4	3.963	139.79	-7.86	10.20
161	81.00	46.80	11	40			1	0				
162	81.00	46.80	11	40				4	3.985	143.38	-0.79	6.58
163	81.00	46.80	11	40			1	0				
164	81.00	46.80	11	40				4	3.944	37.24	7.09	12.68
165	81.00	46.80	11	40				4	3.914	45.38	9.51	15.82
166	81.00	46.80	11	60	1		1	0				
167	81.00	46.80	11	60				4	3.892	93.53	-0.39	17.75
168	81.00	46.80	11	60	1			3	2.969	53.59	1.47	15.59
169	81.00	46.80	11	60				4	3.947	217.49	-13.12	12.34
170	81.00	46.80	2N	60				4	3.953	193.30	1.29	11.65
171	81.00	46.80	2N	60				4	3.888	34.93	-2.21	18.11
172	81.00	46.80	2N	60				4	3.865	78.92	1.67	19.93
173	81.00	46.80	2N	60				4	3.915	40.14	7.80	15.70
174	81.00	46.80	2N	60				4	3.922	71.84	7.24	15.02
175	81.00	46.80	2N	60				4	3.964	41.02	2.35	10.16
176	81.00	46.80	2N	60	1		1	0				
177	81.00	46.80	2N	40		1		2	1.915	57.71	-2.95	80.95+
								2	1.989	341.97	2.87	26.94
178	81.00	46.80	2N	60	1			3	2.892	20.19	7.70	29.56
179	81.00	46.80	2N	60	1			3	2.990	79.55	-1.10	8.69
180	81.00	46.80	2N	60				4	3.958	69.76	0.45	10.97
181	81.00	46.80	2N	60	1			3	2.904	335.53	-5.88	27.74
182	81.00	46.80	2N	60	2			2	1.974	60.84	5.39	41.82+
183	81.00	46.80	2N	60	1		1	0				
184	81.00	46.80	2N	60		1		2	1.948	266.68	0.19	60.28+
								2	1.976	36.60	15.23	39.85
185	81.00	46.80	2N	60	1			3	2.833	65.05	0.56	37.28

TABLE 2. (contd.)

Sample	Location °W	Location °N	Pit	AF intens mT	Data screening a	b	c	N	Remanent magnetization Length R	Decl. °	Incl. +down	A95 °
186	81.00	46.80	2N	60		1		2	1.975	76.79	11.09	40.74+
								2	1.995	8.02	1.19	17.47
187	81.00	46.80	2N	60				4	3.935	90.53	3.82	13.63
188	81.00	46.80	2N	60	2			2	1.997	102.26	28.89	14.19
189	81.00	46.80	2N	60	1		1	0				
190	81.00	46.80	2N	60		1		2	1.945	84.94	7.38	62.59+
								2	1.997	312.79	-9.27	14.42
191	81.00	46.80	2N	60	1			3	2.946	62.05	7.91	20.63
192	81.00	46.80	2N	60				4	3.930	110.50	9.28	14.18
193	81.00	46.80	2N	60	1			3	2.977	129.95	7.98	13.40
194	81.00	46.80	3A	60	2			2	1.996	103.63	12.79	15.91
195	81.00	46.80	3A	60	1			3	2.849	94.93	6.74	35.30
196	81.00	46.80	3A	60	1			3	2.933	94.62	22.99	23.06
197	81.00	46.80	3A	20	1			3	2.920	70.48	31.09	25.21
198	81.00	46.80	3A	60	1			3	2.985	85.28	-0.26	10.79
199	81.00	46.80	3A	60	1			3	2.980	235.46	1.74	12.38
200	81.00	46.80	3	20		1		2	1.894	85.45	13.65	86.26+
								2	1.988	28.74	18.45	27.95
201	81.00	46.80	3	20	1			3	2.919	28.37	27.29	25.41
202	81.00	46.80	3	20	1			3	2.924	50.75	23.77	24.57
203	81.00	46.80	3	20				4	3.916	28.08	9.15	15.63
204	81.00	46.80	1	60				4	3.964	176.62	-14.20	10.13
205	81.00	46.80	1	60	1			3	2.960	54.23	-3.97	17.65
206	81.00	46.80	2S	60	1			3	2.997	53.31	2.54	4.73
207	81.00	46.80	2S	60				4	3.940	61.61	7.54	13.11
208	81.00	46.80	2S	60		1		2	1.963	142.69	0.40	50.28+
								2	1.995	47.66	11.11	17.81
209	81.00	46.80	2S	60	2			2	1.999	81.97	4.36	8.08
210	81.00	46.80	2S	60	1			3	2.937	141.84	9.94	22.20
211	81.00	46.80	2S	60	1			3	2.922	37.46	11.31	24.81
212	81.00	46.80	2S	60			1	0				
213	81.00	46.80	2S	60				4	3.862	359.40	3.98	20.17
214	81.00	46.80	2S	60	1			3	2.927	42.60	8.03	24.09
215	81.00	46.80	2S	60			1	0				

NOTES: Location by longitude (°W) and latitude (° N).
Data Screening: (a) core rejected as anomalous with respect to remaining cores from the sample, (b) sample considered to contain two direction populations, (c) sample rejected as specimen directions diverge from sample mean direction by more than 20°.
* is a sample considered to have too low intensity for demagnetization.
R is the length of vector resultant.
A95 is the radius of the cone of 95% confidence (Fisher 1953) in degrees.
+ is a stable site with A95 > 40°.

TABLE 3. Sampling and remanence data of Host Rock sites

Site	Location °W	Location °N	Pit & Phase	AF intens mT	Data screening a	b	c	N	Remanent magnetization Length R	Decl.	Incl. +down	A95
1	81.00	46.80	2N-T	60	4	1		0				
2	81.00	46.80	2N-V	30	1		2	2	1.904	98.78	11.86	87.41+
3	81.00	46.80	2N-V	15	1			4	3.769	96.47	22.62	26.48
4	81.00	46.80	V	10	1		2	2	1.968	94.92	16.91	46.65+
5	81.00	46.80	2N-V	40	4	1		0				
6	81.00	46.80	2N-T	30	3		2	0				
7	81.00	46.80	V	60	1		2	2	1.999	98.59	10.16	5.04
8	81.00	46.80	2S-D	60			1	4	3.657	23.05	-2.07	32.93
9	81.00	46.80	2S-T	40	5			0				
10	81.00	46.80	2S-T	40	3		2	0				
11	81.00	46.80	2S-T	30	1		1	3	2.834	76.37	47.31	37.15
12	81.00	46.80	2S-T	30	5			0				
13	81.00	46.80	3A-V	15	1		1	3	2.853	246.05	27.51	34.75
14	81.00	46.80	3A-V	60	3			2	1.847	269.55	19.88	55.23+
15	81.00	46.80	3 -V	30	2			3	2.998	12.97	-10.00	3.75
16	81.00	46.80	3 -T	30	1		2	2	1.912	78.43	-3.41	82.66+
17	81.00	46.80	3 -T	10	5			0				
18	81.00	46.80	11-V	30	1		2	2	1.987	142.63	29.65	28.63
19	81.00	46.80	11-V	60	3			2	1.837	102.83	34.48	46.79+
20	81.00	46.80	11-D	40	3			2	1.930	40.83	21.58	71.67+
21	81.00	46.80	11-V	30	1		2	2	1.960	230.17	25.46	51.91+
22	81.00	46.80	11-V	40	3			2	1.903	148.77	-21.75	88.46+
23	81.00	46.80	1 -V	30	2	1	2	0				
24	81.00	46.80	1 -V	20	3			2	1.960	291.76	66.64	52.05+
25	81.00	46.80	4 -V	60	4	1		0				
26	81.00	46.80	4 -V	60	2			3	2.946	344.17	-3.30	20.64
27	81.00	46.80	V	10	1			4	3.758	60.62	23.50	27.15
28	81.00	46.80	2N-V	60	3		2	0				
29	81.00	46.80	6 -V	30	1		1	3	2.943	82.47	-15.79	21.09
30	81.00	46.80	V	20	3			2	1.950	276.95	-17.32	59.21+
31	81.00	46.80	V	20			3	2	1.982	91.42	-43.97	33.94
32	81.00	46.80	V	40	3		2	0				
33	81.00	46.80	10-V	15	1			4	3.935	31.78	20.50	13.64
34	81.00	46.80	10-V	15	2		1	2	1.979	355.59	55.24	37.29
35	81.00	46.80	10-V	40	3		2	0				
36	81.00	46.80	8 -V	40	4		1	0				
37	81.00	46.80	V	80	2			3	2.680	296.86	-2.46	54.18+

NOTES: Location by longitude (°W) and latitude (° N).
Phase: V-volcanics, T-tuff, D-diabase.
Data Screening: (a) core rejected because the 2 specimen directions diverged by more than 25°, (b) core rejected as sole remaining direction to inadequately represent site, and (c) core rejected as anomalous with respect to remaining cores from the site.
R is the length of vector resultant.
A95 is the radius of the cone of 95% confidence (Fisher 1953) in degrees.
+ is a stable site with A95 > 40°.

acquired by the IF specimens during heating were statistically eliminated by positioning the specimens randomly in the oven.

3.3g Chemical Cleaning

A pilot study using 6 IF specimens was performed to assess the relative merit of chemical cleaning. Previous studies mainly on red beds and using conventional cores (Park 1970; Roy and Lapointe 1975) have found it necessary to use slotted or multi-cored cores. For optimum results, Henry (1979) advocates the use of acid at a temperature of 105°C.

In this study, promising results were obtained using the 1cm IF cores immersed in 6N HCl at room temperature. Specimens were stored in a 'mu'-metal shielded can between measurements. Cores were washed in water, allowed to dry and their remanence re-measured before re-storing in fresh acid.

Two further experiments were set up using 80 and 40 IF specimens. Their remanence was measured after 96,252 and 1656 hours for the former and after 50,96,256,312,410,506, 626 and 962 hours for the latter.

3.3h Stability Tests

In order to assess the viscous remanence (VRM) component of the anomaly and the stability of the remanence, a number of storage tests have been performed.

The NRM of 14 representative HR specimens and 20 representative IF specimens, stored so that their NRM direction opposed the Earth's magnetic field (EMF) direction, were

measured after 1,2,3 and 4 weeks. The IF specimens were stored so that 10 specimens lay with the banding perpendicular to the EMF and 10 specimens lay with the banding parallel to the EMF direction.

To assess the effect of blasting operations on the NRM response of the IF, a shock test involving 5 specimens was performed. The initial NRM's were measured and then re-measured after hitting the specimens sharply 20 times on an aluminium block such that their NRM directions oppose the EMF direction. This procedure was repeated with the IF NRM along the EMF direction.

Ten IF pilot specimens after AF cleaning in a field of 100mT were stored such that 5 lay with the banding parallel to, and 5 lay with the banding perpendicular to the EMF direction. Their remanence was measured after 1,10,100,1000, 10000,25000 and 100000 minutes.

3.4 COMPUTATIONS

Existing laboratory computer programs were used to calculate and plot the declination, inclination and intensity of the remanence, and the declination, inclination and magnitudes of the axes of the anisotropy of susceptibility ellipsoids as well as their means and confidence limits.

Other input data include specimen identification, location (longitude and latitude), k_1 susceptibility and specific gravity. In order to handle the $\sim$20 quantitative

variables for each of the 1172 specimens, it is necessary to use the computer extensively for computations and analysis. The BMDP5D program (BMDP-77) has been adopted to calculate the means and confidence limits using both normal and lognormal statistics of all data set quantities and to plot the output in histogram form.

The BMDP6D program has been adopted to do regression fits with the correlation statistics between any two data set quantities and to plot the data. Many combinations including subsets have been examined to compare different mine pits. The objects of these statistical tests is to closely define the limits of each of the parameters that are required for the magnetic model to be proposed.

3.5 MAGNETIC MODEL

Existing computer programs for interpreting magnetic anomalies over a magnetic sheet (dike, sill, slate, etc.) usually calculate only the induced magnetic component for a variety of thicknesses, strikes and dips relative to the Earth's varying geomagnetic field. Some programs incorporate the remanence and/or the demagnetizing factor, but none the very significant anisotropy effect. The model used here was compiled and tested in the study of the Sherman mine (Symons and Stupavsky 1979) and incorporates all of these factors. It follows standard theoretical equations for the induced component. The demagnetizing factor and anisotropy

of susceptibility equations follow Gay (1963) and the remanence equations follow Strangway (1965). See Appendix I for the model computations.

The model assumes infinite strike length and depth extent. A modification for IF of finite depth extent was found necessary. The program was adjusted accordingly (Appendix II; 4.12b).

CHAPTER IV

DISCUSSION OF RESULTS

4.1 SPECIFIC GRAVITY

The histogram of IF specific gravity (S.G.)(Fig. 4) shows a normal distribution with a complete spectrum from HR values of $\sim 2.75 gcm^{-3}$, reflecting high silica content (S.G. = $2.65 gcm^{-3}$) up to massive iron ore values of $\sim 5.00 gcm^{-3}$, reflecting $\sim$93% magnetite (S.G.=$5.20 gcm^{-3}$) or hematite (S.G.=$5.26 gcm^{-3}$).

The normal mean S.G. for various pits are similar (Table 4). The overall mean value from 403 specimens is 3.56 (Standard Deviation=0.42). This value is less than ore values because the pit sampling includes low grade and barren wall-rock samples: i.e. mixed ore and lean IF.

4.2 MAGNETIC SUSCEPTIBILITY

The HR k_1 values show a lognormal distribution (Fig. 5) with a lognormal mean of 5.00×10^{-5} $cgscm^{-3}$ for 454 specimens.

After rejection of 67 barren specimens having susceptibilities below the limit of instrumental sensitivity, the IF k_1 values show a similar lognormal distribution with a lognormal mean of 6210×10^{-5} $cgscm^{-3}$ (Fig. 6). Mean values for various pits are once again similar (Table 4).

Because the ratio of k_{1IF}/k_{1HR} is $\sim$1200 it is reasonable to neglect k_{1HR} in calculating the IF anomaly above background.

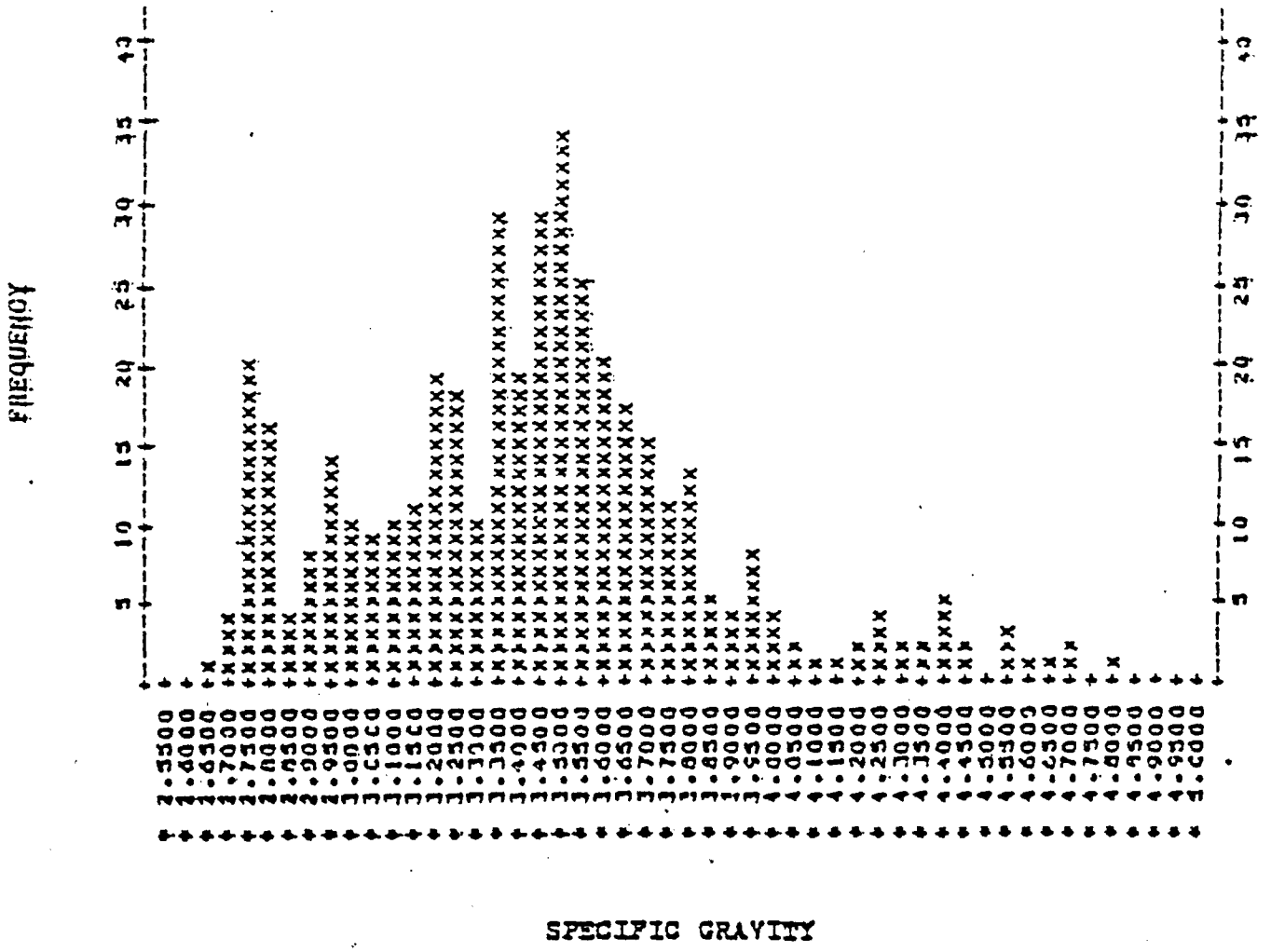

FIG. 4. Histogram of the specific gravities of 403 iron formation specimens.

TABLE 4. Summary of regression fit between S.G. and k_1

Pit	Number of specimens N	S.G. g/cc	Mag. susc. cgs/cc×10^{-2}	Regression Fit: $k_1 = mS.G. + c$ m	c	r
1	4	4.63	16.56	0.0699	-0.1561	0.31
2S	128	3.30	5.12	0.0959	-0.2618	0.82
2N	112	3.49	5.21	0.0812	-0.2201	0.78
3	46	3.25	6.32	0.1160	-0.3306	0.95
3A	20	3.68	7.40	0.1133	-0.3317	0.88
10	4	3.30	6.92	0.1559	-0.4986	0.91
11	36	3.59	7.14	0.0912	-0.2478	0.88
Overall	350	3.56	6.21	0.0912	-0.2492	0.84

NOTES: Barren specimens with low Specific Gravity (S.G.) or low Magnetic Susceptibility have been rejected.
Regression fit calculated by BMDP6D program.
r is the correlation coefficient.

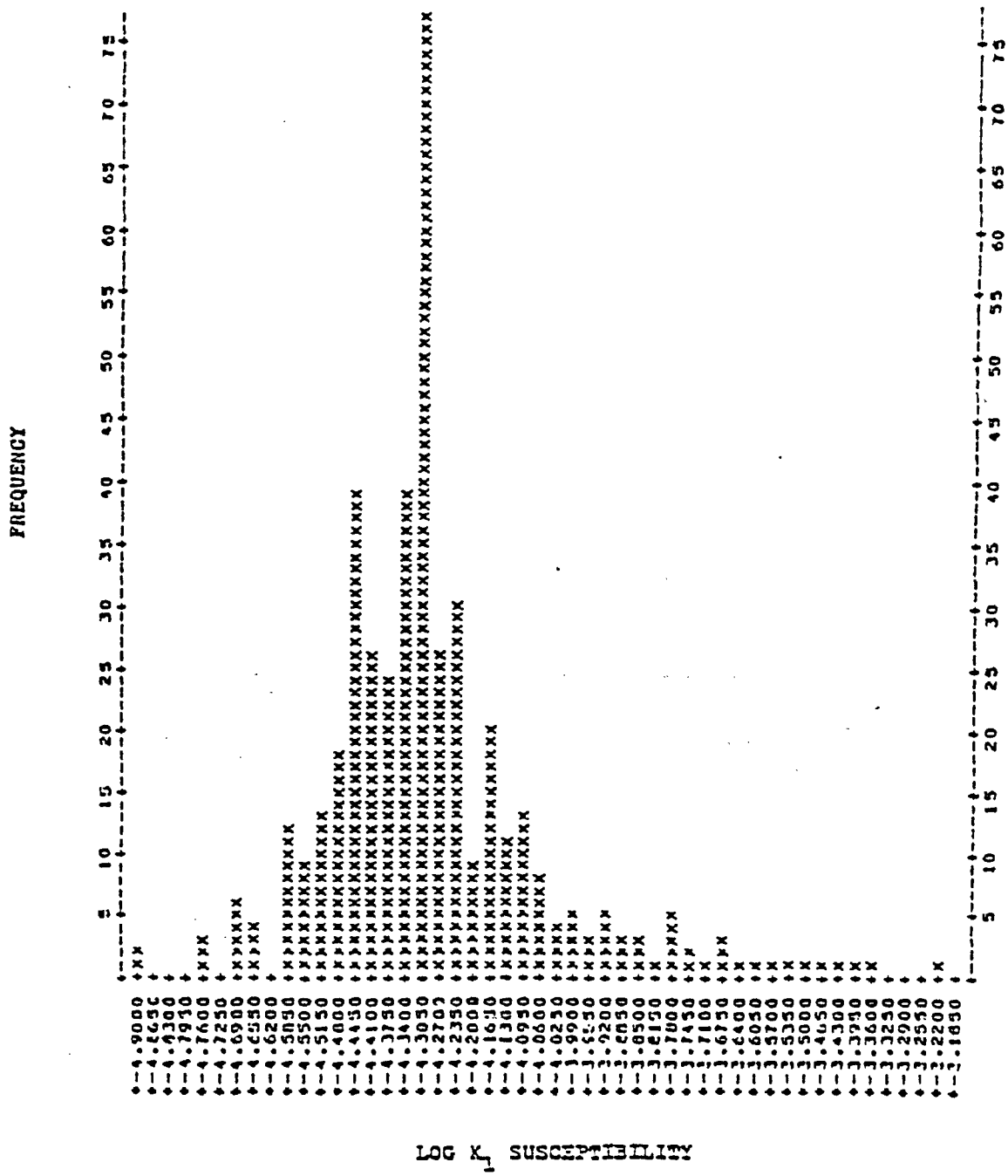

FIG. 5. Lognormal histogram of k_1 susceptibility for 454 specimens of host rock.

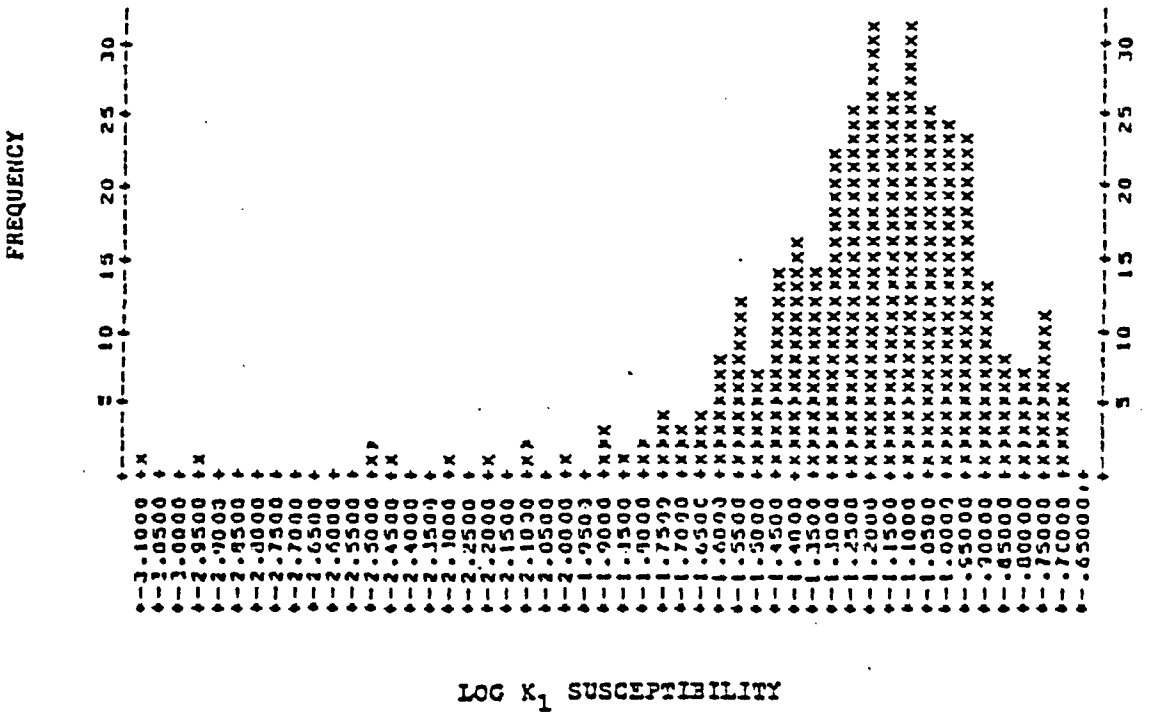

FIG. 6. Lognormal histogram of k_1 susceptibility for 393 specimens of iron formation.

The regression fit between S.G. and k_1 of IF shows an excellent fit (Fig. 7) with a correlation coefficient of +0.838 for 350 specimens. Table 4 summarizes the regression fits obtained from the individual pits. Thus the relationship:

$$k_1 = 0.0912 S.G. - 0.249$$

is very valid for the Moose Mountain IF. This compares closely to the relationship:

$$k_1 = 0.0906 S.G. - 0.245$$

obtained from the Temagami IF at the Sherman mine (Symons and Stupavsky 1979).

Economic ore for the Moose Mountain mine contains 28.4% total Fe with ∿20.6% Fe in magnetite, ∿7.8% Fe in hematite, and only ∿0.1% Fe in iron silicates and carbonates (Markland 1966). Thus, the S.G. of economic ore can be calculated from the equation:

$$S.G._{ore} = \frac{\%Fe \text{ in magnetite} \times S.G. \text{ magnetite}}{\%Fe \text{ in 1 formula weight magnetite}} + \frac{\%Fe \text{ in hematite} \times S.G. \text{ hematite}}{\%Fe \text{ in 1 formula weight hematite}} + \%Silica \times S.G. \text{ silica}$$

The S.G. of economic ore is thus $3.93 gcm^{-3}$ giving a mean value of 0.11 $cgscm^{-3}$ for k_1 for iron ore.

4.3 ANISOTROPY OF SUSCEPTIBILITY

After correction for IF tilt by rotating the IF to horizontal, the principal susceptibility axes show the expected pattern for banded IF. The minimum susceptibility (k_{min})

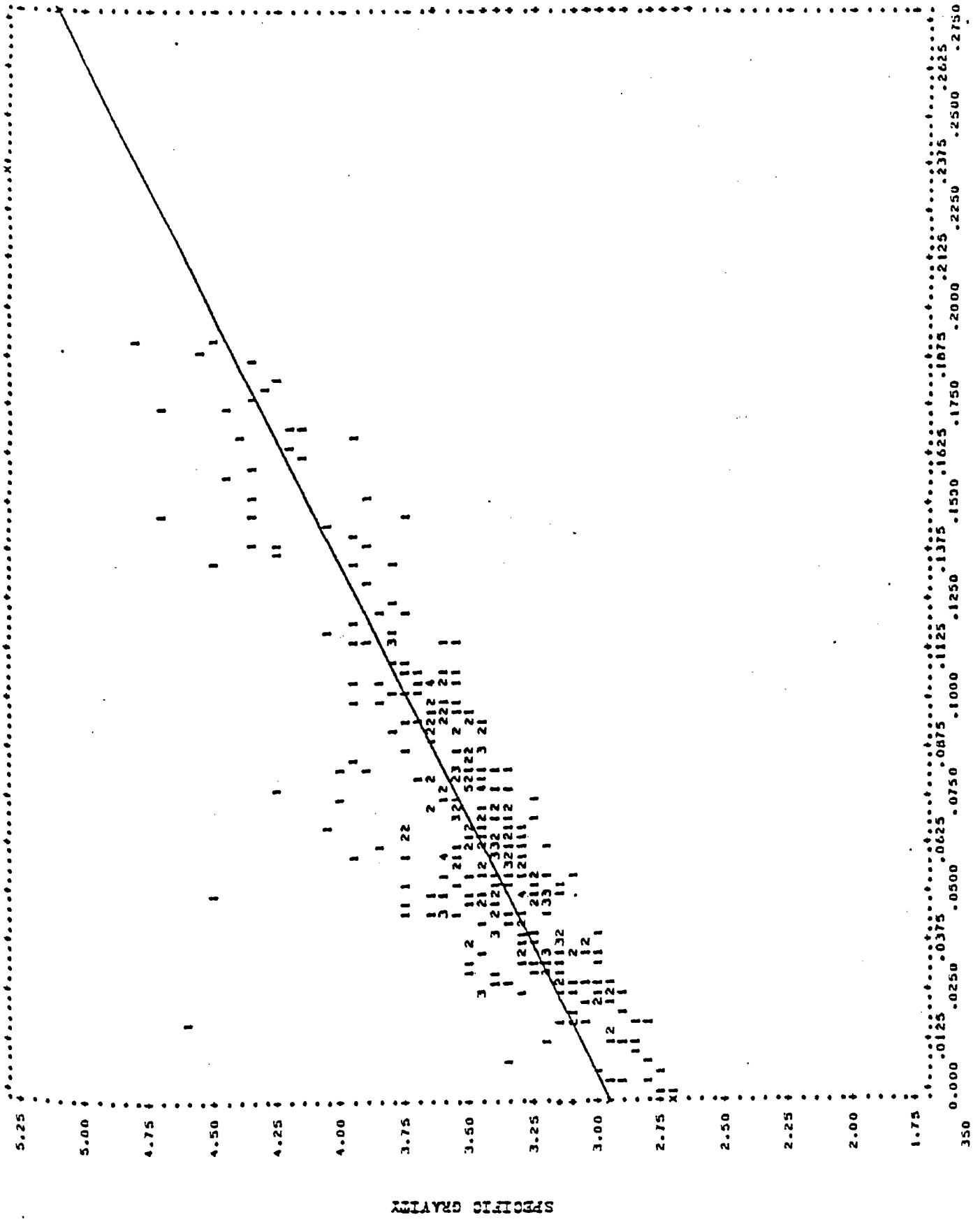

FIG. 7. Regression line of specific gravity versus k_1 susceptibility for 350 iron formation specimens.

direction is perpendicular to bedding, i.e. k_1 (Figs. 8a and 8b) with the intermediate (k_{int}) and maximum (k_{max}) directions in the bedding plane (Figs. 9a and 9b). The mean magnitude ratio of k_{int}/k_{min} is 1.6 (Fig. 10) and of k_{max}/k_{min} is 1.7 (Fig. 11). Thus the mean bedding plane susceptibility is:

$$k_{11} = ((k_{int} + k_{max})/2)\, k_{min}$$
$$= 1.65k_1$$

This ratio may be slightly lower than reality because some of the small cores may be confined to one band of IF and hence appear more isotropic than the IF as a whole. There is however an opposing effect due to the probable slight bias in sampling toward more banded IF. Analysis of the anisotropy of susceptibility for the 26 large 2.45cm right cylindrical specimens gives a mean magnitude ratio of $k_{int}/k_{min} = 1.7$ and of $k_{max}/k_{min} = 1.8$. Thus the mean bedding plane susceptibility is:

$$k_{11} = 1.75k_1$$

This anisotropy value compares with a value of $1.60k_1$ obtained at the Sherman mine (Symons and Stupavsky 1979) which is considered reasonable for an IF that has been subjected to low-grade regional metamorphism. Thus the higher anisotropy value of $1.7k_1$ for Moose Mountain is consistent with the rather higher regional metamorphic grade. In both cases, the anisotropy leads to significant differences in the computed anomaly.

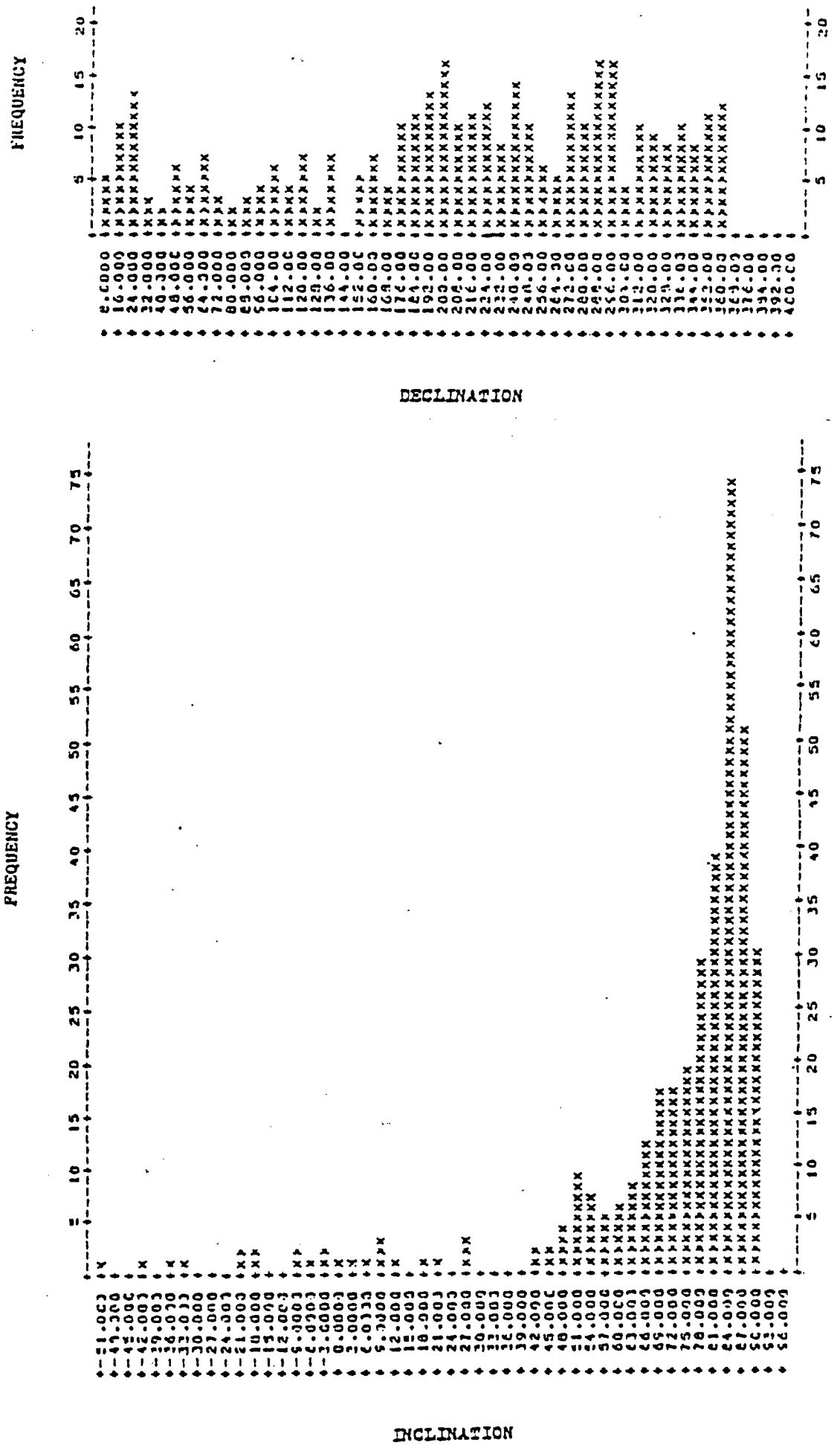

FIG. 8. Histogram of k_{min} (k_1) directions for 356 specimens of IF.

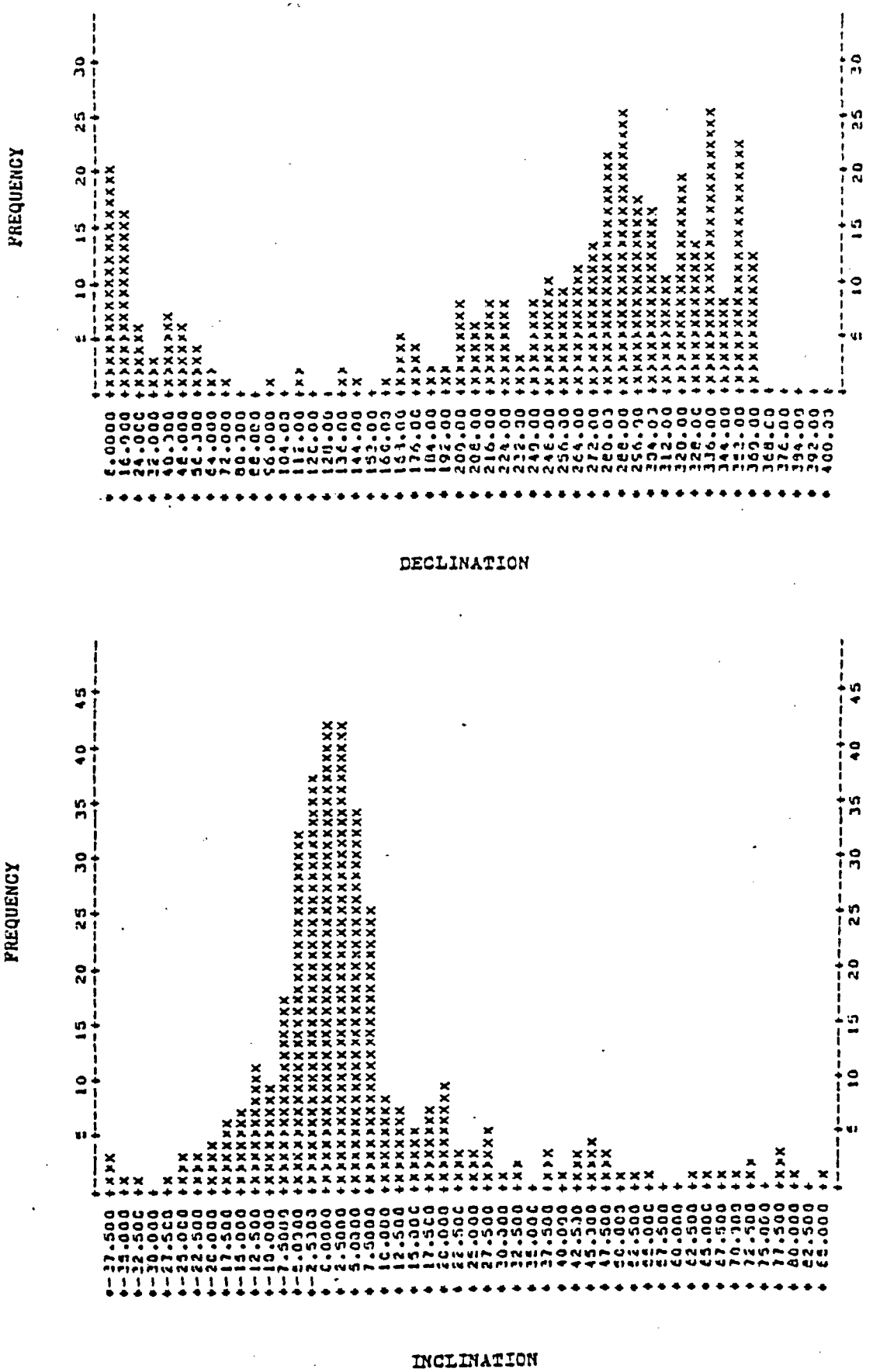

FIG. 9. Histograms of k_{max} directions for 356 specimens of IF.

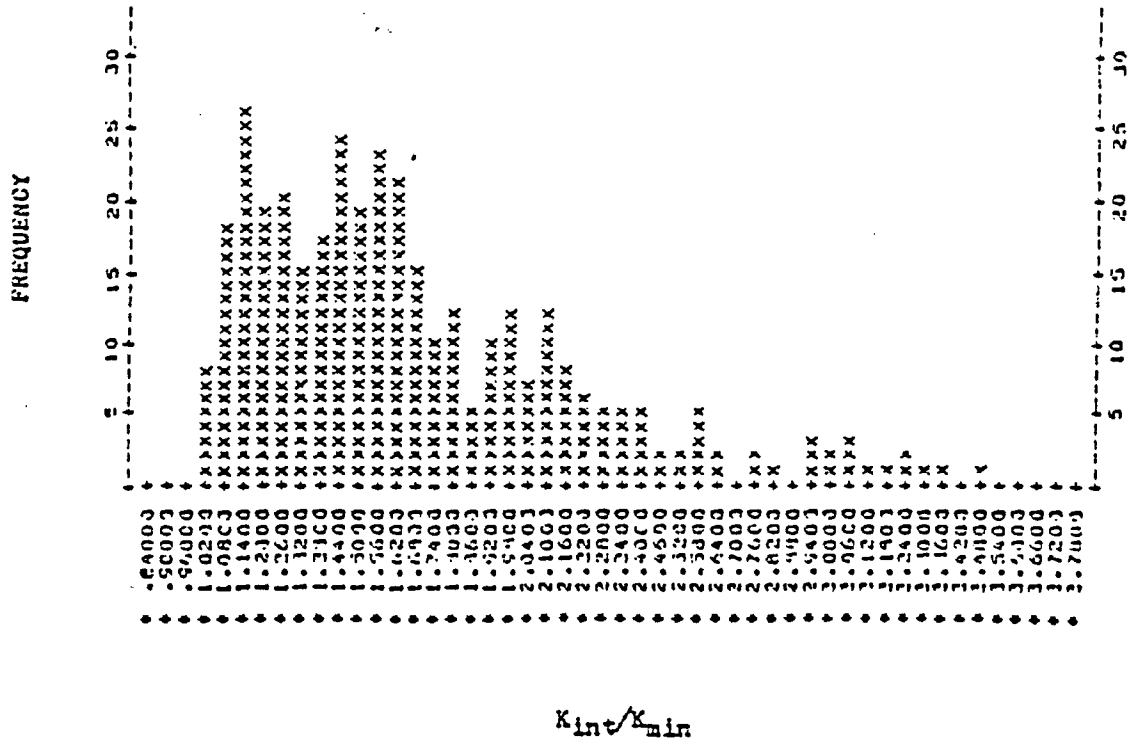

FIG. 10. Histogram of k_{int}/k_{min} for 356 specimens of IF.

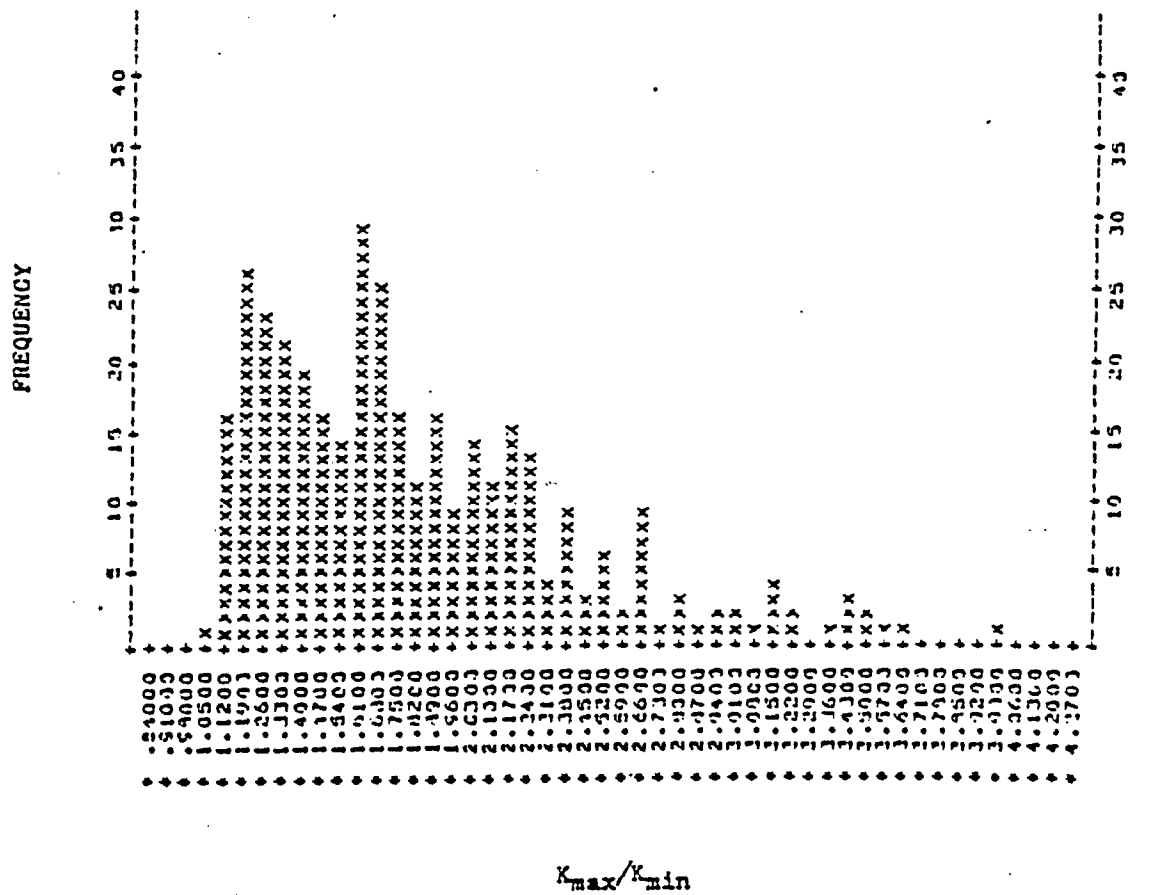

FIG. 11. Histogram of k_{max}/k_{min} for 356 specimens of IF.

When the directions of k_{min} and k_{max} are analyzed for the various limbs of Pit 2 (north limb, centre limb, south limb), good correlation exists between the pole to the bedding plane and the direction of k_{min} (Fig. 12). However, the direction of k_{max} shows no close parallelism to the strike as found in the Sherman mine. Here, k_{max} is $\sim 30^{o}$ from the strike direction while k_{int} is $\sim 30^{o}$ from the dip direction. This again may reflect the effect of a combination of two dynamic metamorphic stresses from the two stages of folding reported by Markland (1966) and/or of primary paleocurrent directions. A strain determination investigation using the susceptibility ellipsoids as strain markers after the methods of Dunnet (1969) and Elliot (1970) would perhaps help to clarify the situation.

4.4 NATURAL REMANENT MAGNETIZATION

4.4a Host Rock NRM

The NRM intensities (J_o) of the HR specimens exhibit a lognormal distribution with a broad spectrum of values from 2.09×10^{-8} emucm^{-3} to 1.20×10^{-2} emucm^{-3} with a log-normal mean from 443 specimens of 1.99×10^{-6} emucm^{-3} (Fig. 13). Thus their Koenigsberger ratio (Q) of the remanent to induced magnetization also has a lognormal distribution with values ranging from 5×10^{-4} to 400 with a lognormal mean of 0.063 (Fig. 14). Although there are a number of localized areas where the NRM contribution is important, the mean induced

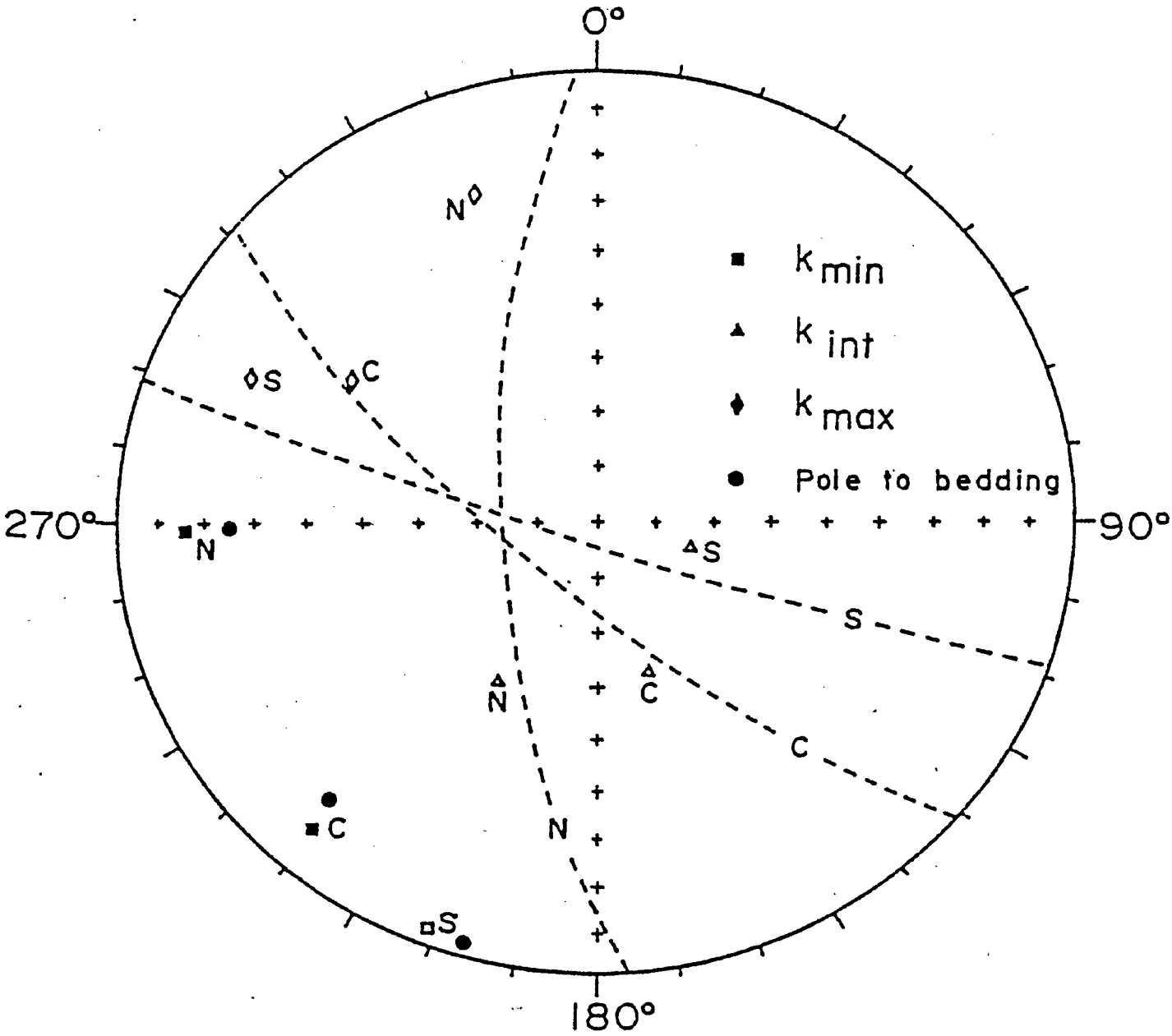

FIG. 12. Relation between directions of k and limbs of Pit 2.

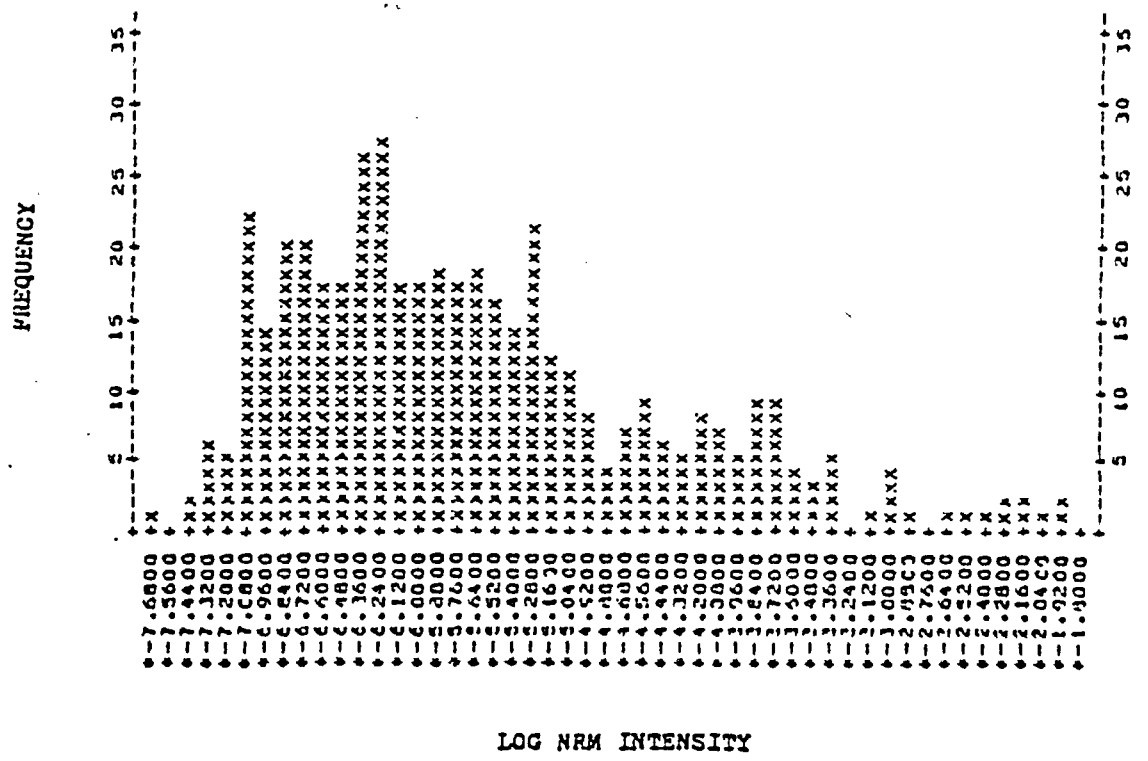

FIG. 13. Lognormal histogram of NRM intensity for 443 HR specimens.

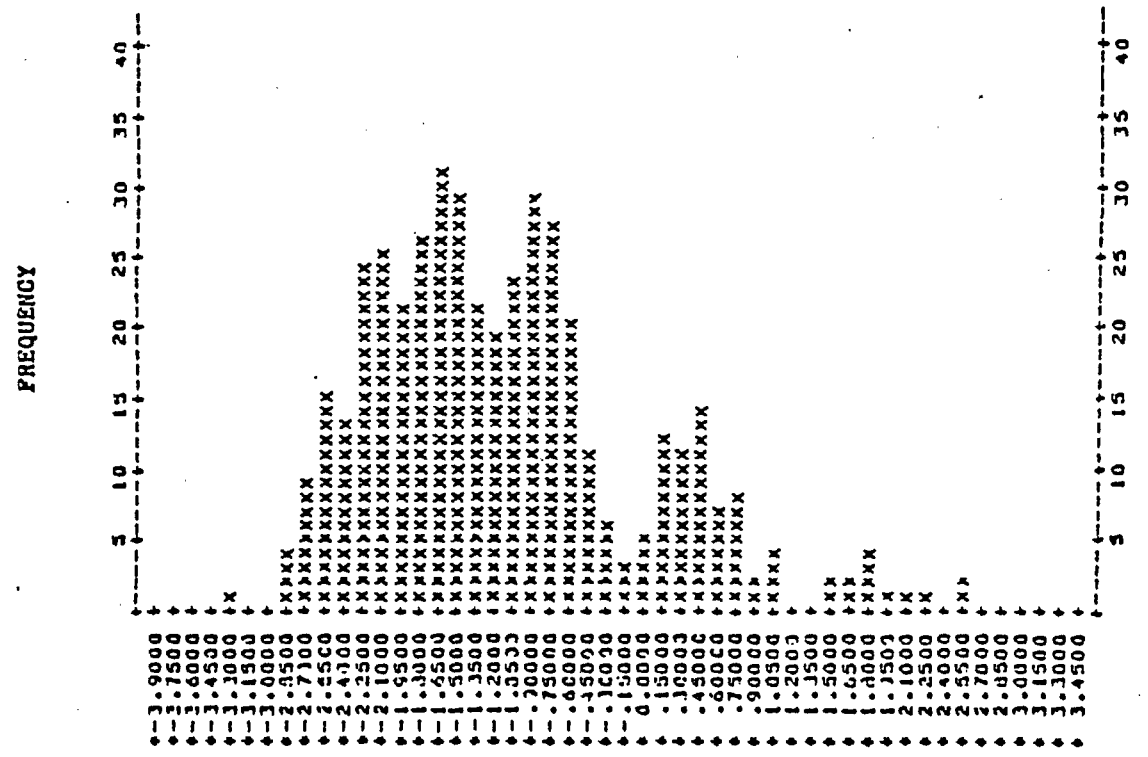

FIG. 14. Lognormal histogram of the Koenigsberger ratio for 443 HR specimens.

magnetization of the IF is ~18,000 times greater than the mean HR NRM, suggesting that the HR NRM can clearly be omitted from the anomaly calculation.

The 37 HR NRM site mean directions were calculated and grouped. Populations of the data corrected for bedding 'tilt' and the uncorrected data were compared using the angular variance ratio test (Larochelle 1969). The test shows that the NRM is post-folding at the 95% level because the variance ratio of 2.20 is greater than the theoretical statistic at the 95% level and the precision parameters are significantly greater for the uncorrected population (Table 5). Thus the NRM is dominantly either secondary metamorphic or viscous in origin.

A storage test run on 14 HR specimens of varying NRM intensities showed less than a 3% change in intensity over a four week period (Fig. 15a) with practically no change in direction (Fig. 15b). This suggests that the NRM stability is high and that the viscous (VRM) component is relatively small.

4.4b Iron Formation NRM

The NRM intensities of the IF specimens show a bimodal lognormal distribution (Fig. 16). Barren and hematite-rich specimens give rise to the lower intensity distribution having a mean of 3.9×10^{-6} emucm^{-3}. Magnetite-rich specimens give rise to the higher intensity population having a log-normal mean of 4.8×10^{-2} emucm^{-3}. For anomaly interpretation purposes therefore, only the magnetite remanence is important

TABLE 5. Angular variance ratio analysis for HR and IF NRM's

Group	Number of samples N	Mean remanence direction: Length R	Decl. °	Incl. +down	K	A_{95} °	V	$F_{0.05}$	Result
1. Host rock									
Corrected	37	13.363	43.2	33.8	1.5	32.2	2.20	1.51	Negative
Uncorrected	37	26.269	217.9	79.5	3.4	15.3			
2. Iron formation									
Corrected	132	54.968	57.3	53.3	1.7	14.6	1.02	1.20	Positive
Uncorrected	132	57.089	263.5	69.1	1.7	14.2			

NOTES: R is the length of vector resultant.
K is Fisher's (1953) precision parameter.
A_{95} is the radius of 95% confidence (Fisher 1953) in degrees.
V is the variance ratio $\delta_{corr}/\delta_{uncorr}$ of the two populations.
$F_{0.05}$ is the theoretical statistic $F_{2(N_{corr}-1),2(N_{uncorr}-1),0.05}$ thereby setting the test at the 95% confidence level.

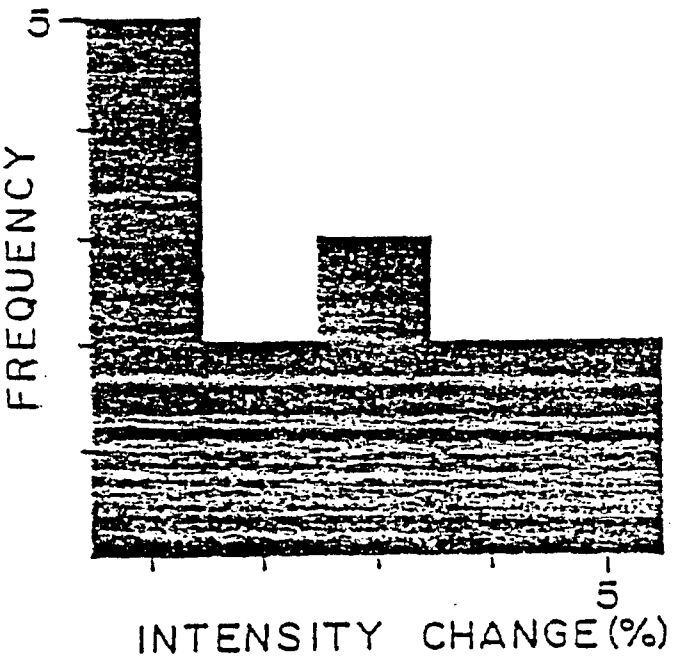

FIG. 15a. Histogram of NRM intensity change of HR specimens over four weeks.

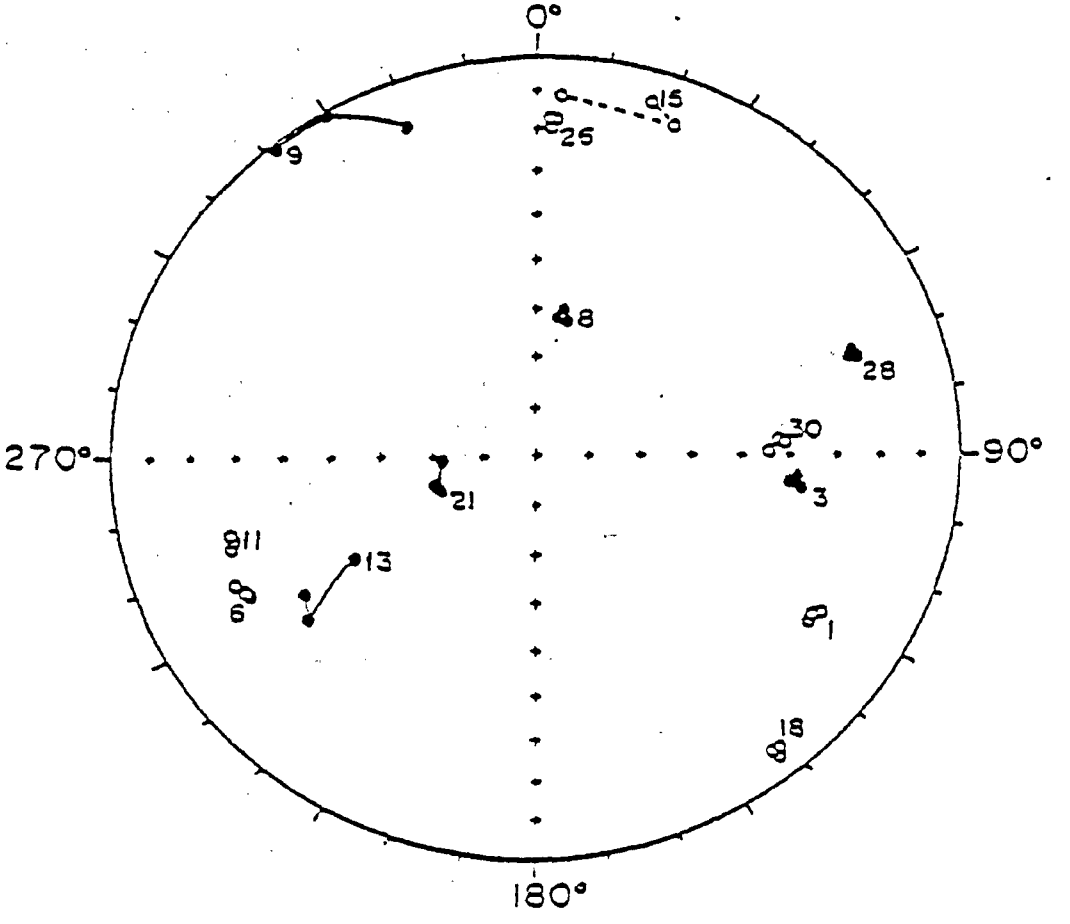

FIG. 15b. Directional changes of NRM vectors of HR specimens over a four week period.

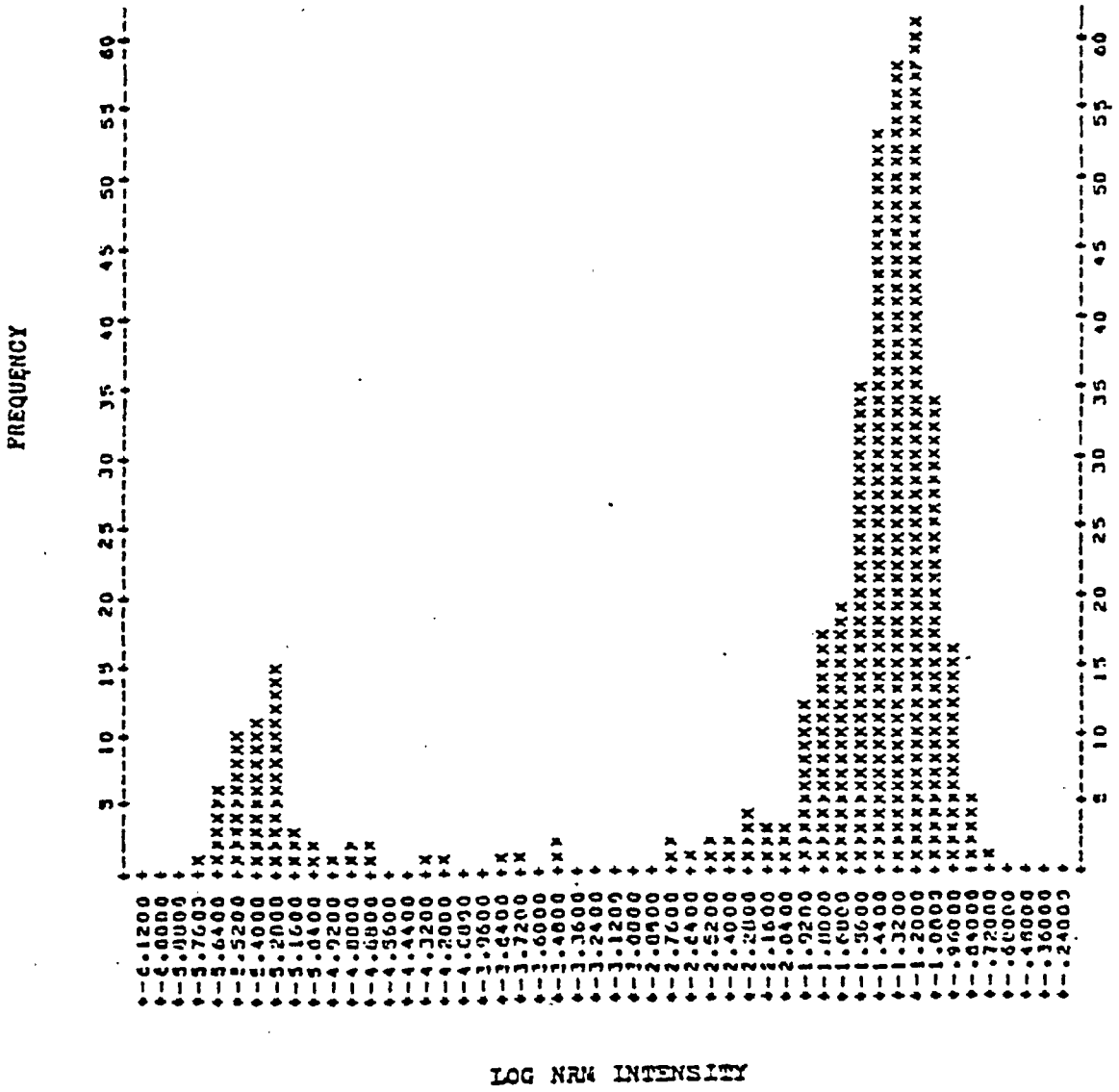

FIG. 16. Lognormal histogram of NRM intensity for 460 IF specimens.

because it is ~12,000 times more intense. The overall log-normal mean from 423 specimens, after rejection of the barren specimens, is 1.1×10^{-2} emucm^{-3}.

The Q ratio for the magnetite population has a lognormal distribution with a mean of 0.63 (Fig. 17). Thus, if the IF NRM directions were entirely aligned with the Earth's field, then the remanence would increase the induced anomaly by 63%. In fact, the mean NRM direction for the IF has a declination of 263.5° and an inclination of 69.1° which is ~26°(θ) from the EMF direction of (8.3°W,76.1°). The ratio of the vector resultant (R) to the number of block mean directions (N) gives an effective Koenigsberger ratio (Q_e) of $Q_e = (R/N) \times Q$. Thus the remanence augments the vertical induced magnetic component (J_i) by $(Q_e \times \cos\theta)J_i$, i.e. $((57.1/133) \times 0.63 \times \cos 26^\circ)J_i = 0.24J_i$. This compares closely to the augmenting factor of $0.22J_i$ obtained at the Sherman mine (Symons and Stupavsky 1979).

A 'fold test' run on the IF NRM sample means shows that the uncorrected directions and the directions corrected for bedding attitude have similar populations of directions (Table 5; Section 4.6d for the nature of the test). The variance ratio of 1.02 is less than the theoretical statistic of 1.20 at the 95% confidence level. Thus, the test is inconclusive at the 95% level.

A storage test run on 20 representative IF specimens shows less than a 2% change in NRM intensity over a four week

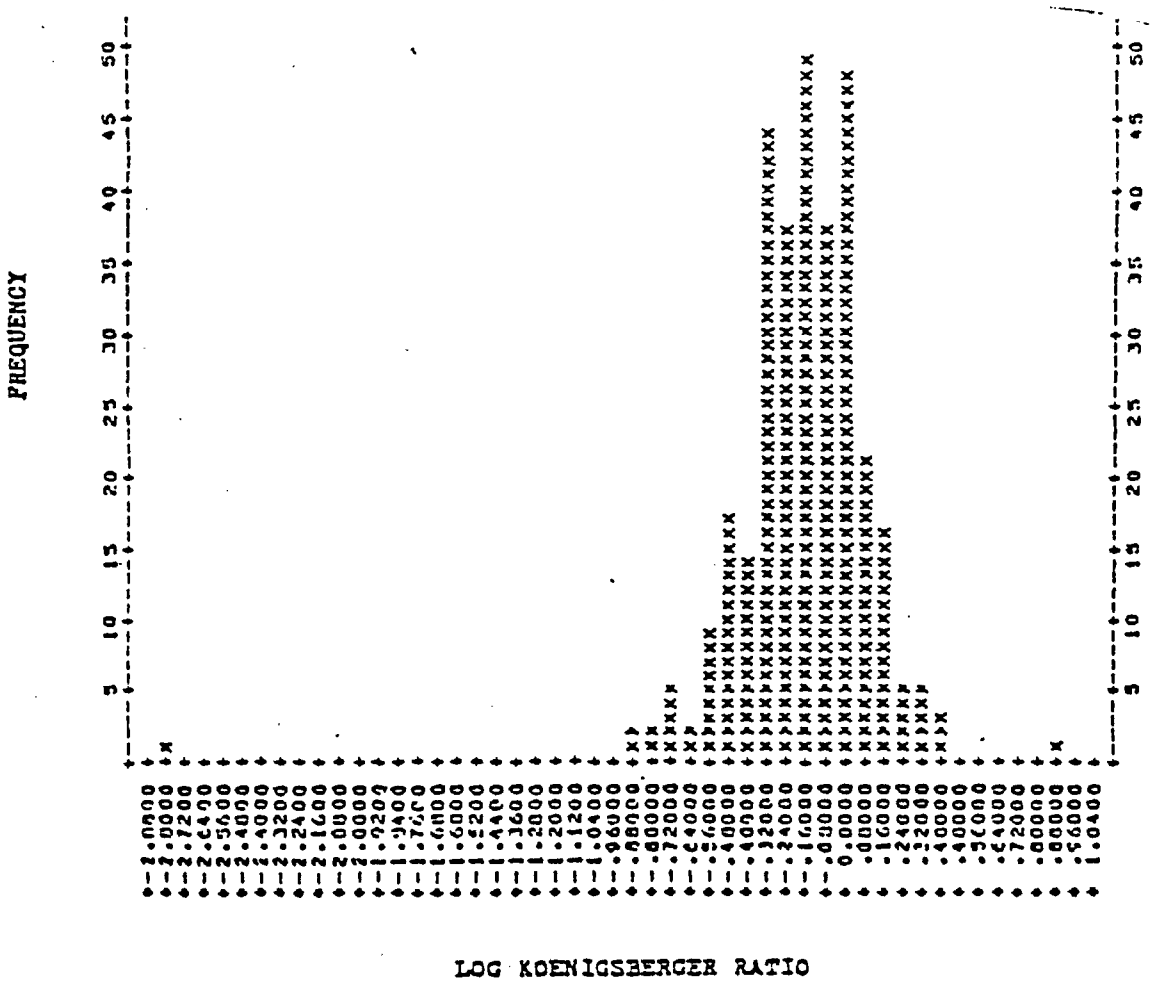

FIG. 17. Lognormal histogram of the Koenigsberger ratio (Q) for 423 IF specimens.

period with no change in direction (Figs. 18a and b). Thus the IF NRM's are extremely stable with small viscous (VRM) components.

The shock test results show a significant reduction in NRM intensity of up to 60% after 40 shocks (Fig. 19a). However, there is no measureable change in direction of the NRM (Fig. 19b) A possible explanation for the intensity decrease is that during the shock the magnetically soft domains become remagnetized in the 'demagnetizing field' of the harder domains. Since this internal field is $\gg$ EMF this results in a remanence decrease.

The magnetite-rich IF NRM intensity is approximately linearly related to k_1 (Fig. 20.). The correlation coefficient is 0.55 for 323 specimens. Individual pits give slightly better fits (Table 6). Thus the similar relationships:

NRM = 0.439 k_1 + 0.023 for the Moose Mountain IF,

and NRM = 0.434 k_1 + 0.0051 with a 0.64 correlation coefficient for the Sherman IF, suggest similar IF genesis at the two mines. The somewhat higher NRM intensities at the Moose Mountain deposit are most likely a result of the higher ore grade and the higher metamorphic grade.

4.5 STATISTICAL ANALYSIS

4.5a Host Rock Statistical Analysis

The HR paleomagnetic remanence directions show a high degree of scatter. Thus screening of the data at the core level and at the site level was necessary to eliminate unstable

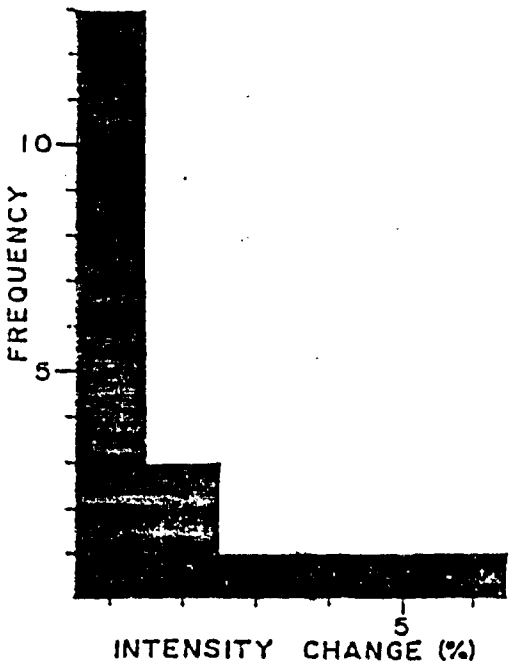

FIG. 18a. Histogram of NRM intensity change of IF specimens over four weeks.

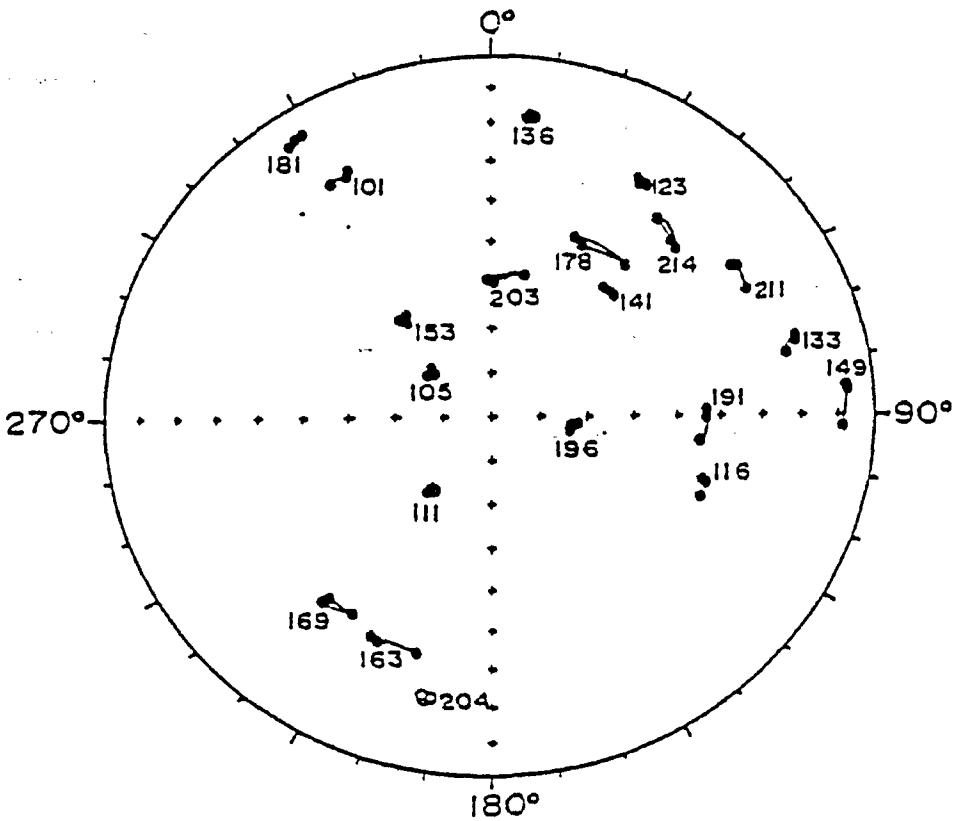

FIG. 18b. Directional changes of NRM vectors of IF specimens over a four week period.

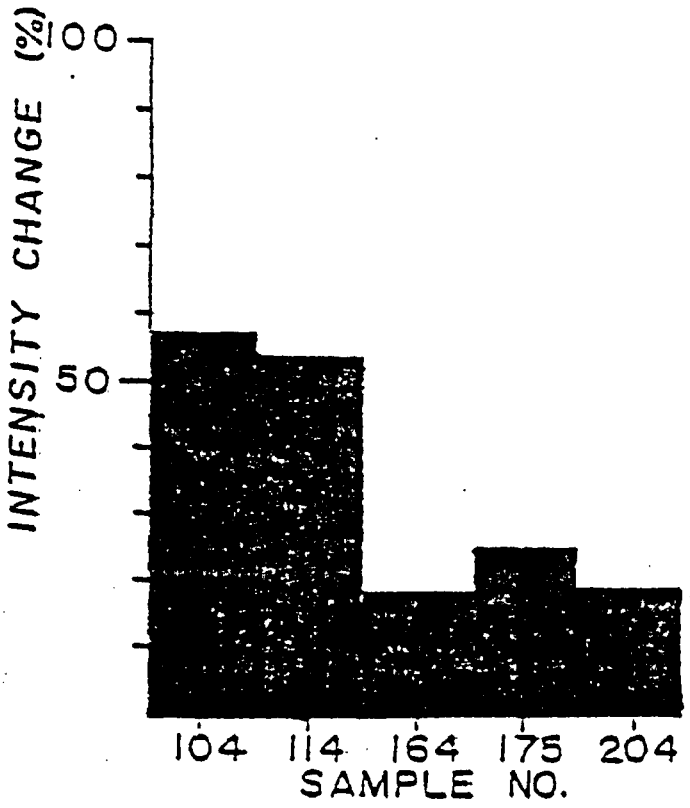

FIG. 19a. Histogram of NRM intensity change of IF specimens after induced shock.

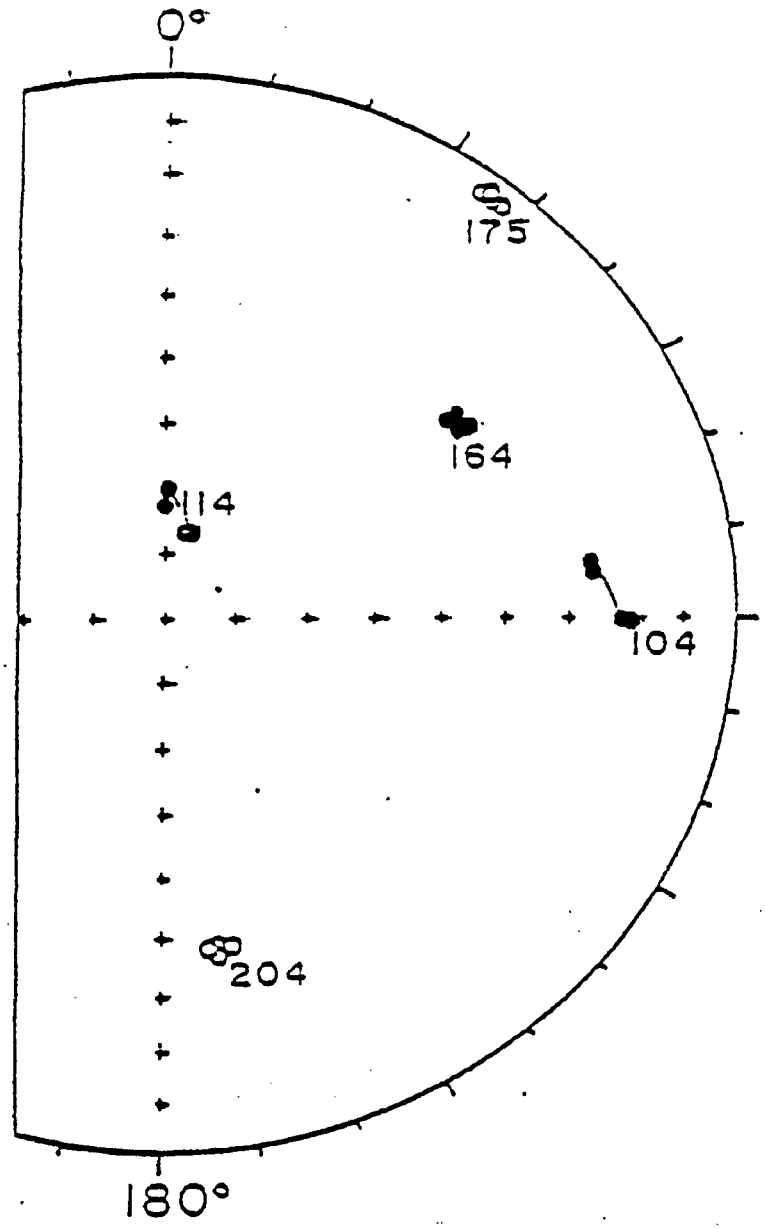

FIG. 19b. Directional changes of NRM vectors after induced shock.

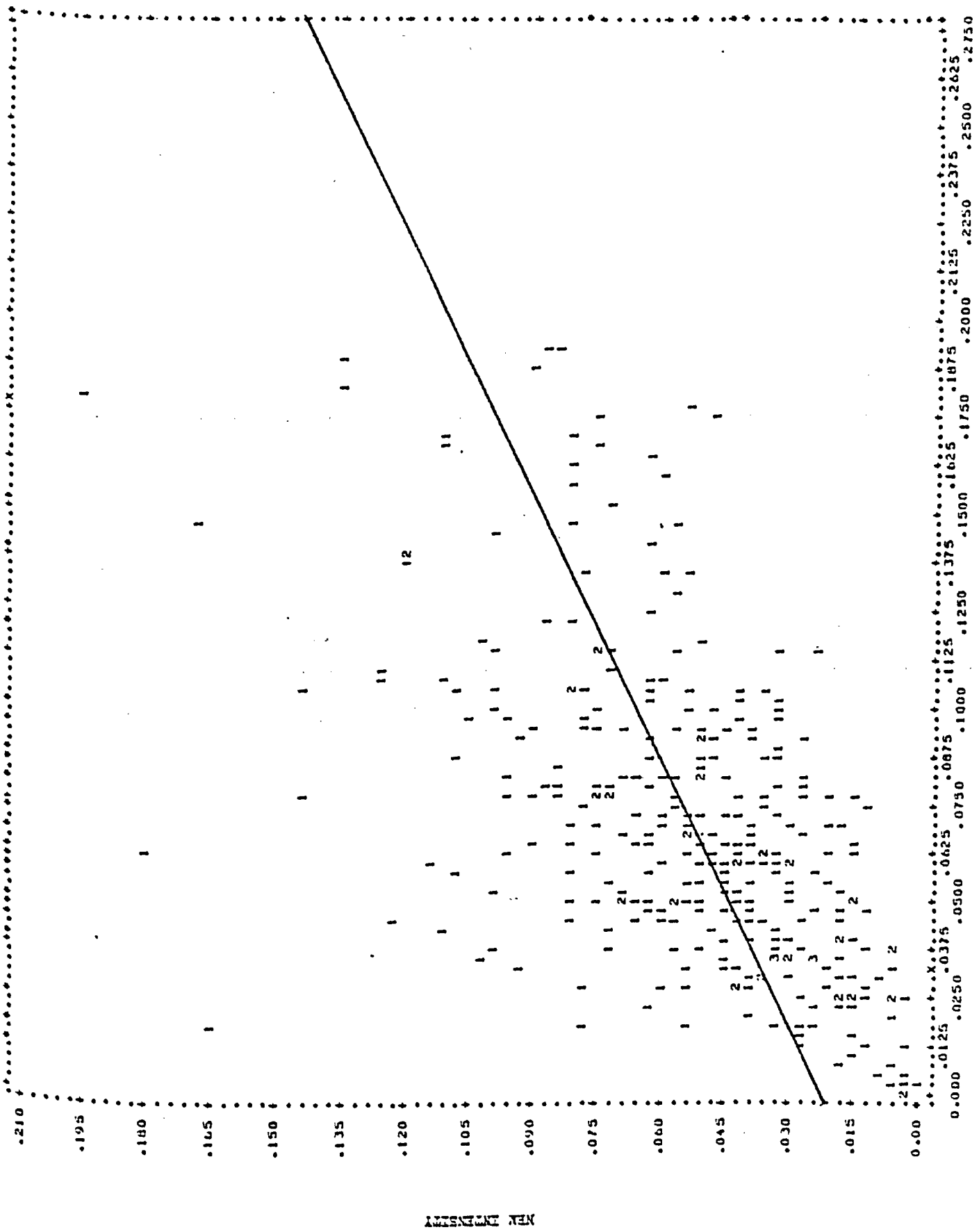

FIG. 20. Regression line of NBM intensity versus K_1 susceptibility for 323 IF specimens.

TABLE 6. Summary of regression fit between k_1 and NRM

Pit	Number of specimens N	NRM emu	Mag. susc. cgs/cc×10^{-2}	Regression Fit; NRM=mk_1 + c		
				m	c	r
1	4	0.071	16.56	0.5853	-0.0270	0.99
2S	125	0.045	5.12	0.6394	+0.0124	0.66
2N	105	0.054	5.21	0.4078	+0.0274	0.55
3	46	0.029	6.32	0.5570	+0.0050	0.72
3A	15	0.053	7.40	0.4461	+0.0114	0.81
10	4	0.027	6.92	0.2582	+0.0343	0.29
11	24	0.064	7.14	0.1376	+0.0743	0.13
Overall	323	0.048	6.21	0.4386	+0.0230	0.55

NOTES: Barren specimens with low NRM or Magnetic Susceptibility have been rejected.
Regression fit calculated by BMDP6D program.
r is the correlation coefficient.

and inhomogeneous directions.

The following tests were used to select reliable remanence directions from the HR after AF cleaning (Table 3). In 33 of 185 cores the directions for the two specimens diverged by more than 20°. These cores were considered to be inhomogeneously magnetized and their data rejected.

Four sites then had only one acceptable core and so they were rejected as being insufficiently represented. The specimen directions were then combined to give the core mean directions which were then averaged to give the site mean directions.

In 18 sites, the direction of one or two cores deviated by >40° from the site mean direction. Data from these anomalous cores were rejected. Site mean directions with a radius of 95% confidence (A95; Fisher 1953) exceeding 40° were regarded as insufficiently homogeneously magnetized and rejected.

A total of 13 of the original 37 sites (35%) survived the screening tests and yielded acceptable site mean directions. The 24 rejected sites show some petrological bias in that 16 are from the 27 mafic volcanic sites (60%), 7 are from the 8 tuff sites (88%), and 1 is from the 2 diabase sites (50%). Thus there seems to be a bias toward the more basic phases suggesting the acidic phases are less stable.

4.5b Iron Formation Statistical Analysis

The stable sample mean remanence directions for IF (Table 2) were identified in a similar manner. In 11 of the

115 samples the intensity of magnetization was considered to be too low for reliable remanence measurement and so their data was rejected. In 57 of the 104 remaining samples, one or two specimen directions diverged by more than 40^{o} from the remaining specimen directions. These specimens were rejected as being anomalous with respect to the remaining specimens. In 17 samples, two direction populations were recognized and their respective specimen directions grouped together as a single sample.

One sample then had only one acceptable specimen and so it was rejected as being insufficiently represented. The specimen directions were then averaged to give the sample mean directions. Fisher (1953) statistics were used to determine the degree of dispersion about the sample mean direction. In 22 samples, the specimen directions diverged by more than 20^{o} from the sample mean direction; i.e. R, the length of the vector resultant, $<N\cos\theta$ where N is the number of cores and $\theta = 20^{o}$. These samples were regarded as insufficiently homogeneously magnetized and rejected. Sample mean directions with a radius of 95% confidence exceeding 40^{o} were similarly rejected.

Of the original 115 samples, a total of 81 (70%) samples yielding acceptable sample mean directions resulted from the screening tests. This high acceptability rate is partly a consequence of the 16 extra samples generated due to two

direction populations being present. The survival rates for the various pits are as follows: 1(100%), 2S(74%), 2N(74%), 3(50%), 3A(100%), 10(33%), and 11(69%).

4.6 AF CLEANING OF IRON FORMATION

4.6a Pilot Specimens - Conventional Analysis

In order to define the nature of the IF remanence, 37 pilot specimens were AF step demagnetized to 100mT. Examination of the various isolated directions showed that they could be grouped into four populations. These pilot specimen results were statistically treated by computing at each AF demagnetization field, the mean direction and confidence statistics for each population.

Figure 21a shows the directional changes for the specimens representing the different stable components along with the circles of 95% confidence about the mean direction at the optimum AF field. The PSI curves are shown in Figure 21b. They both clearly illustrate the removal of unstable viscous remanence (VRM) components in the present steeply inclined Earth's field direction in the 5-15mT steps. High initial rates of directional change in the order of 20deg/T decrease noticeably to less than 4deg/T between 20mT and 60mT as the stable direction is isolated. Above 60mT the curves record an increasing rate of directional change from step to step as larger random anhysteritic remanence (ARM) components are progressively added in the demagnetization process. The

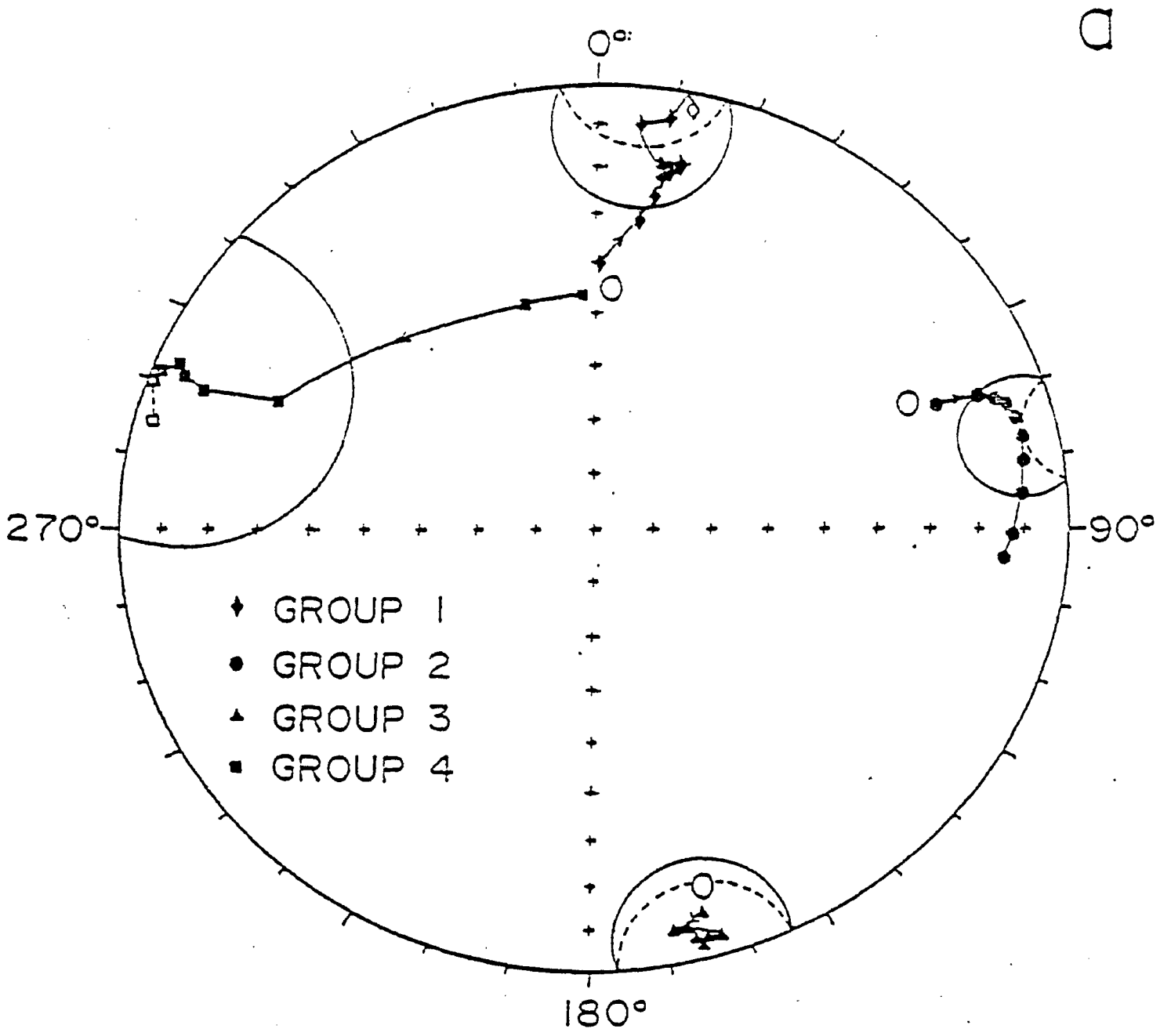

FIG. 21. Demagnetization Curves - AF

a)Equal area projection showing the change in direction onprogressive AF demagnetizatio in fields of 0,5,10,15,20,30,40,60,80 and 100mT, for IF pilot specimens isolating; a N directed component (diamond,Group 1), a E directed component (circle,Group 2), a S directed component (triangle,Group 3),and a W directed component (square,Group 4) Solid(open) symbols indicate normal(reverse) or down(up) directions.
b)Paleomagnetic Stability Index for above directional changes.
c)Remanence Intensity is plotted as a ratio of the NRM intensity against the demagnetic field.
d)Radius of 95% confidence (Fisher 1953),A95 of mean direction at each demagnetization step. The number of specimens(rejects) in each group is shown.

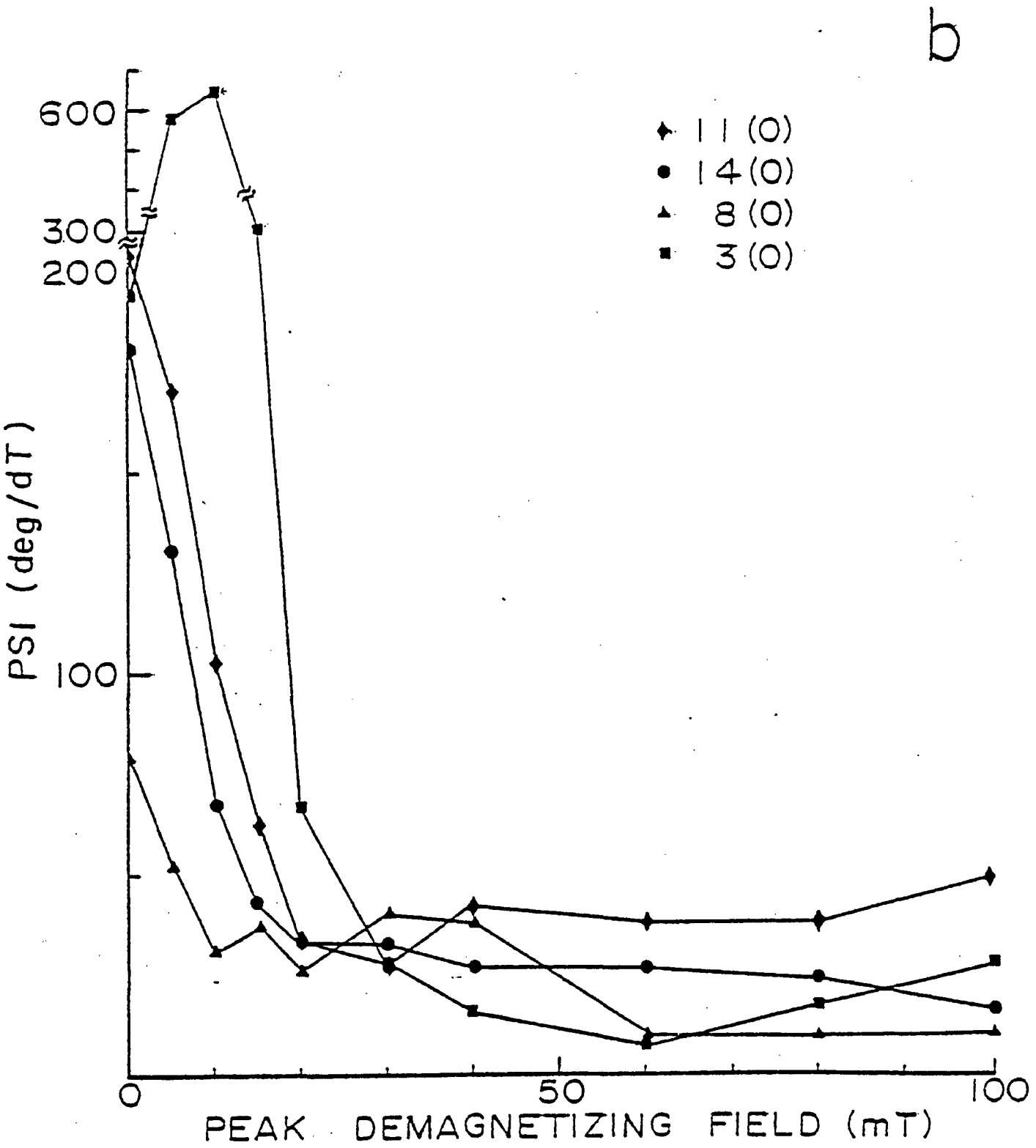

FIG. 21. contd.

intensity decay curves (Fig. 21c) support this interpretation. All components show the same rapid exponential intensity decay up to 20-30mT as significant viscous components are removed and thereafter a linear intensity decay throughout the demagnetization process. If the radii for the circles of 95% confidence for each mean direction are plotted, the curves show mimima in the 30-60mT range as the stable components are isolated (Fig. 21d). The marked increases in the radius of confidence above 70mT suggest the introduction of random directional changes due to the addition of ARM components. However, the lack of any random intensity increases above 70mT and the fact that PSI increases are minimal above 70mT suggests that ARM components when treated statistically in this manner are insignificant.

Progressive demagnetizations is a valuable tool in paleomagnetic research. The total magnetic composition of a rock sample can be revealed by a stepwise demagnetization. However, the quantities illustrated so far are of little use in identifying the magnetizations present, their directions and size ratios. The intensity decay curves show the magnitude of the vector sum of the different magnetizations, which is altogether an implicit quantity and should never be used (Zijderveld 1967). Also, depicting only the stereographic projection of the changing magnetization vector gives but a poor insight into the result of the progressive demagnetization

C

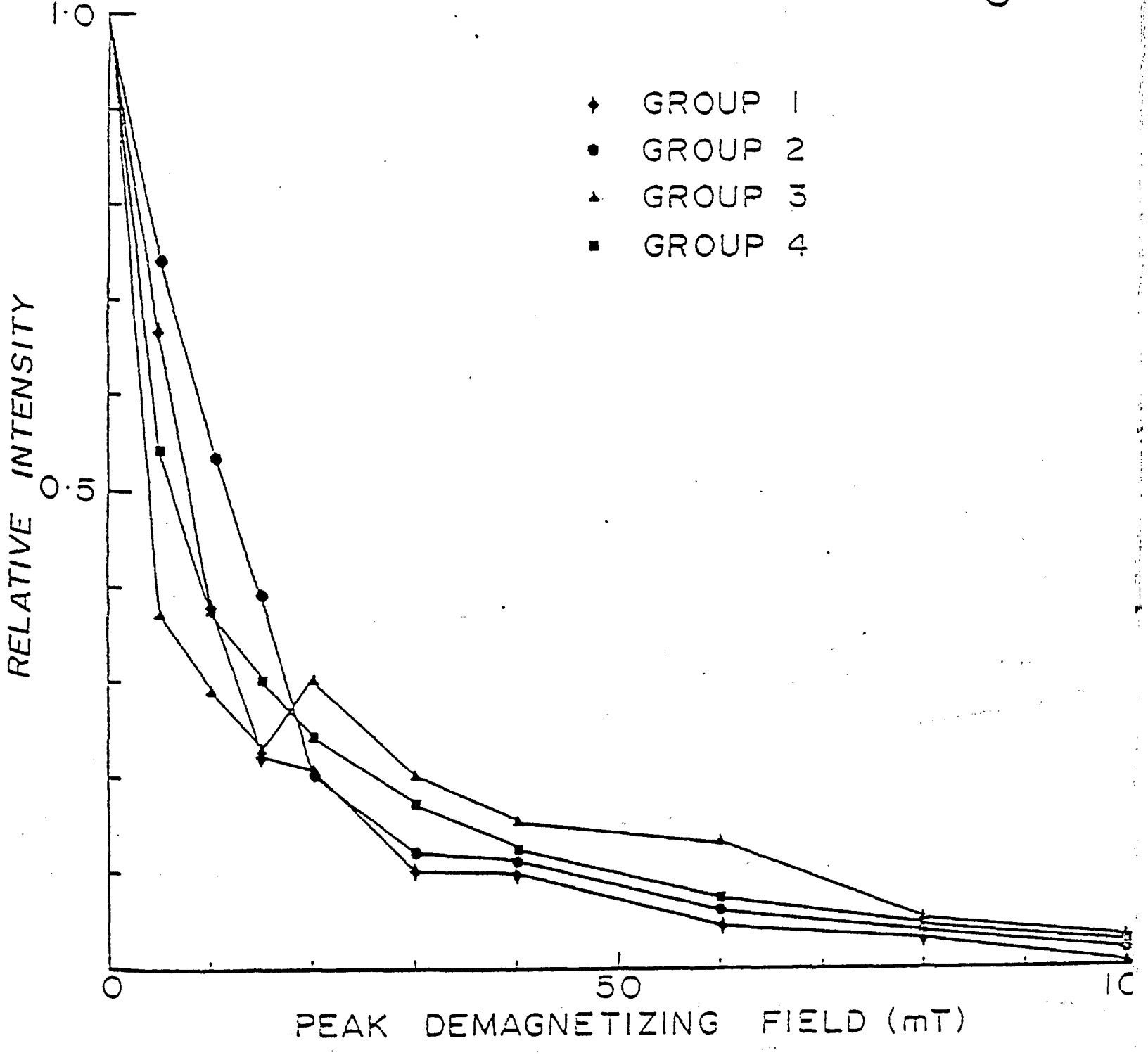

FIG. 21. contd.

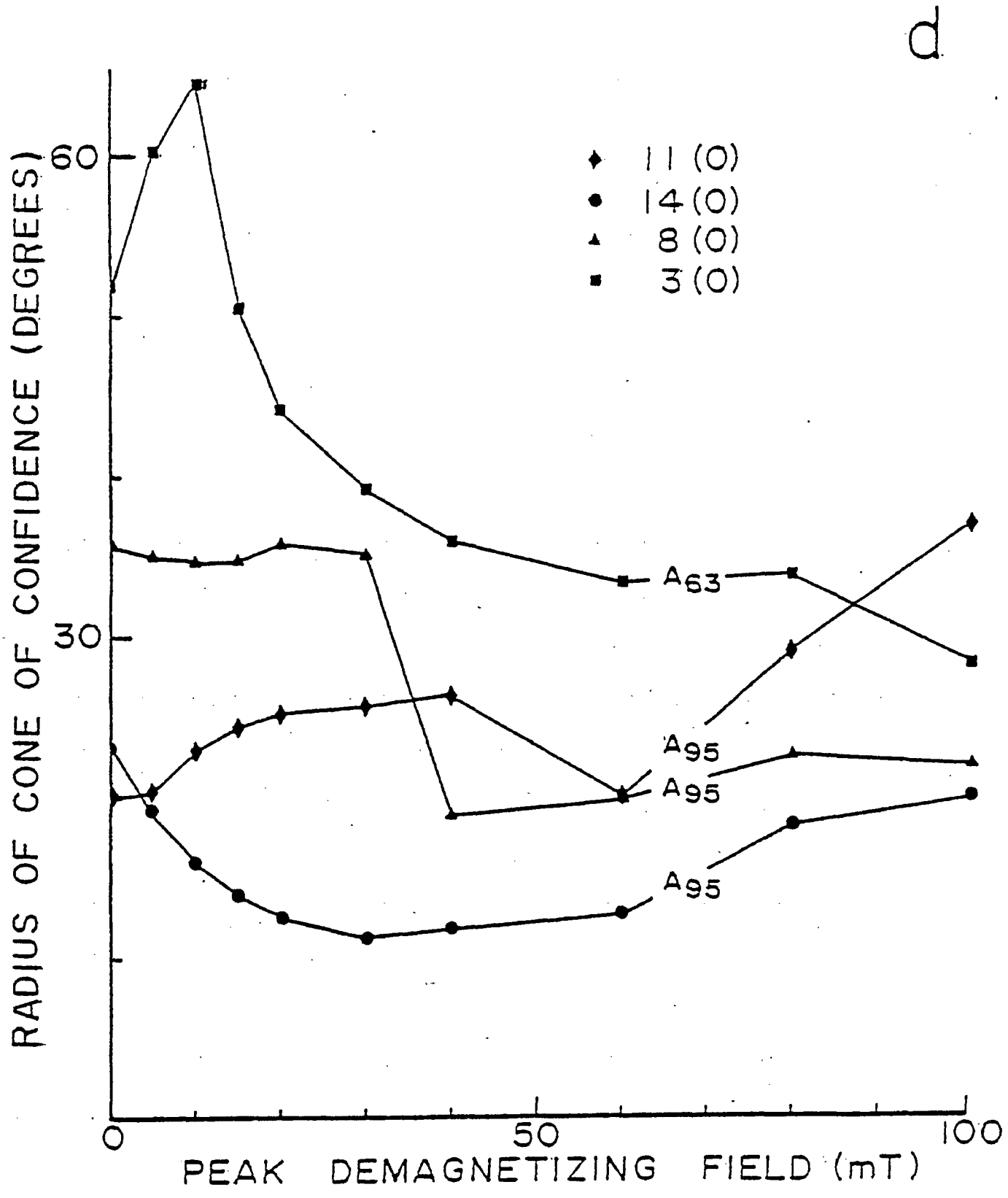

FIG. 21. contd.

Figure 22a-d shows Zijderveld diagrams of the progressive AF demagnetization from the pilot specimens, showing the N-S component, the E-W component and the vertical component of the population means at each demagnetization step. In each case a large vertical component of magnetization is removed in the 5-15mT steps. Thereafter, the resultant magnetization vectors no longer change their direction appreciably, but decrease along a straight line exactly to the centre of the co-ordinate system, inferring that the magnetization must be one single component.

The preceeding discussion illustrates the isolation of four stable components in AF fields between 30mT and 60mT. The histogram in Figure 23 supports this interpretation. The optimum cleaning field has been selected on the basis of PSI mimima and agreement between the vector removed and the measured vector between successive demagnetization steps. Every magnetization has not a single hardness, but is eliminated over a large trajectory of increasing alternating field. An alternating field coercivity spectrum is defined in part by its' median destructive field which is the alternating field coercive force required to demagnetize one-half of the magnetization. This H_c may be used as a characteristic value for the magnetization. Figure 21c shows that for each of the magnetizations present here, H_c = 5-10mT, illustrating the 'softness' of the viscous or secondary magnetization. At the

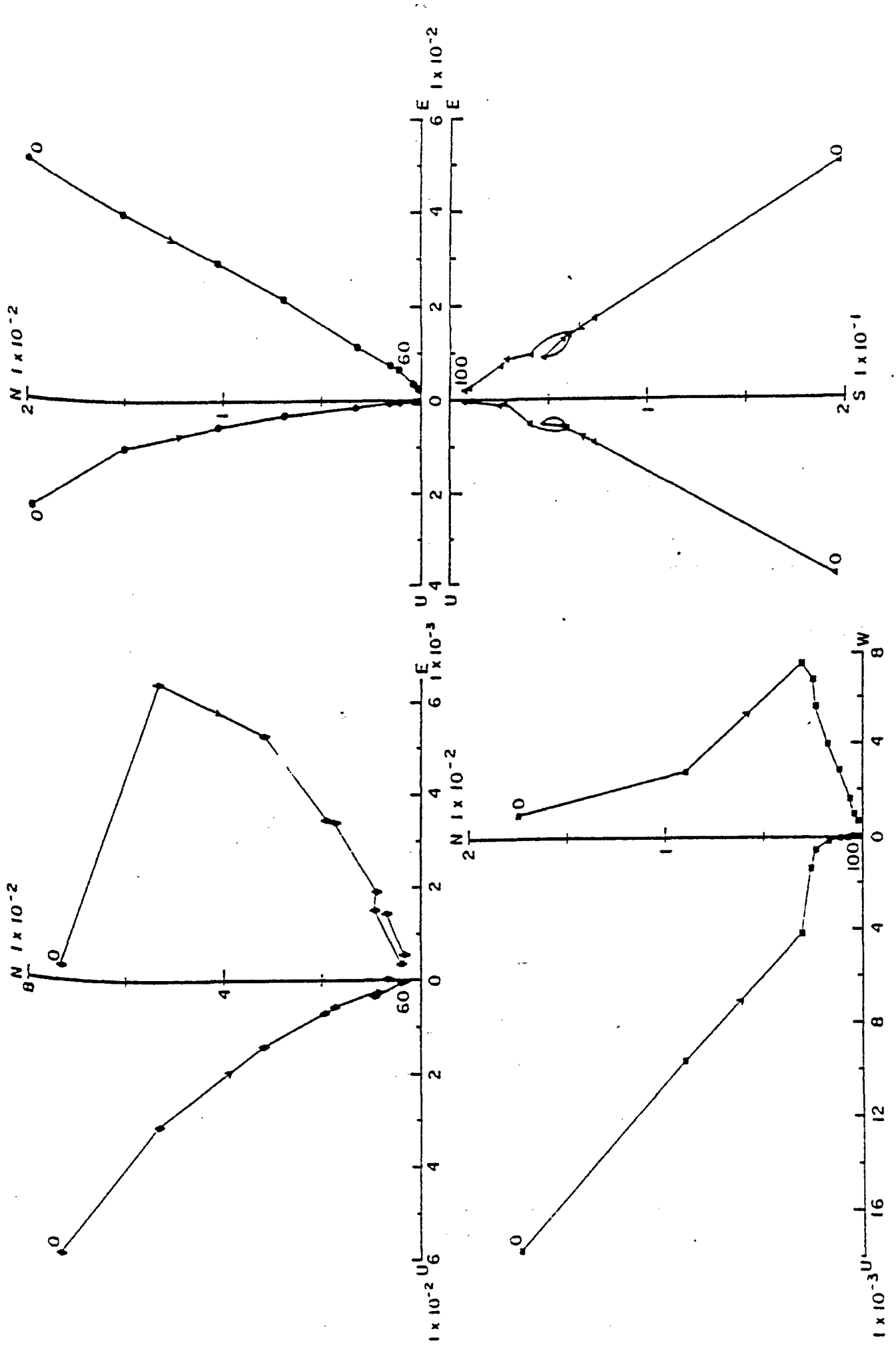

FIG. 22. Demagnetization vector diagrams - AF.

Showing the successive end points of the mean magnetization vector for the 1F pilot specimens during AF demagnetization. Intensity in emucm^{-3} units on the geographic axes; north(N)-south(S); east(E)-west(W); down(D)-up(U). Numbers represent demagnetization step in mT. Symbols and conventions as used in Figure 21.

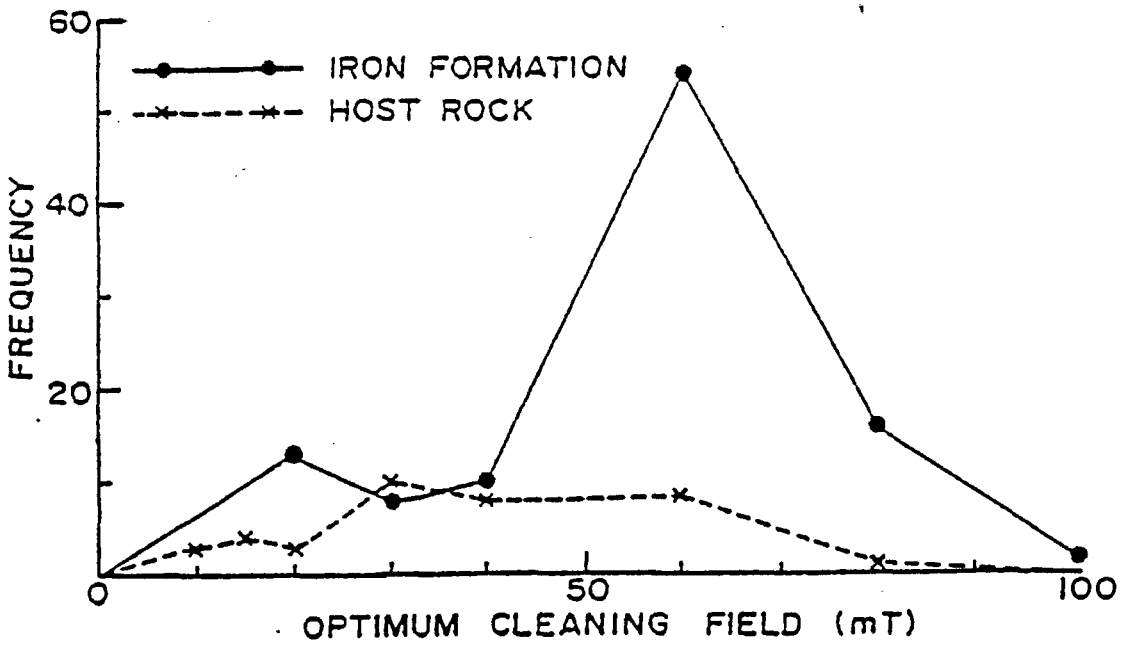

FIG. 23. Plot of optimum AF cleaning field for HR and IF specimens.

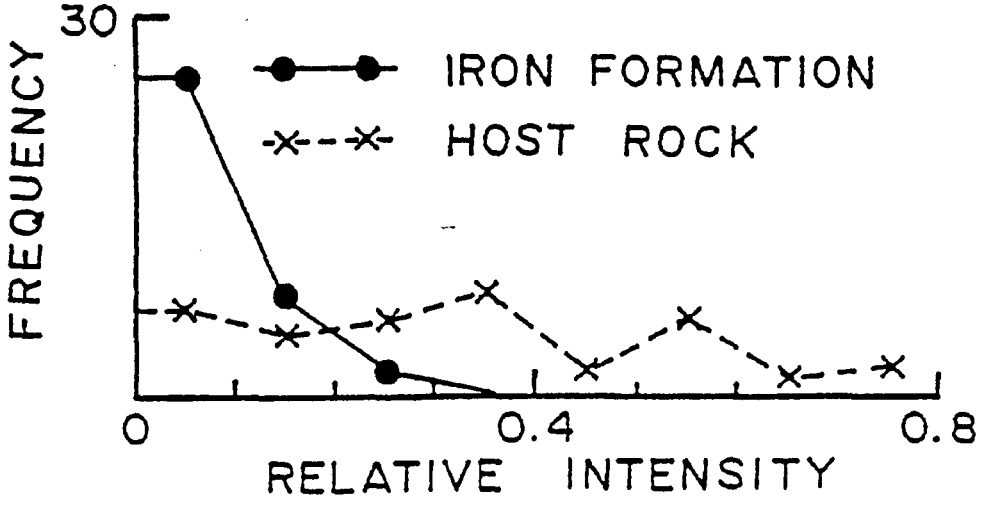

FIG. 24. Relative intensity of NRM after cleaning at optimum AF field.

optimum cleaning field it can be seen from Figure 24 that in all cases the relative intensity (J_n/J_o) has been reduced to less than 25% of the original intensity (J_o).

4.6b Pilot Specimens - Least Squares Model Analysis

The techniques used above for analyzing AF step demagnetization data to show the degree of isolation of characteristic remanence directions are the conventional methods. They are successful in separating components only if their coercivity spectra exhibit significantly wide windows free of overlap. These techniques do not indicate the complete isolation of characteristic directions for two common types of rock magnetizations. One of these shows a continuous change in direction at low AF intensities followed by increasingly large erratic directional changes with increasing AF intensities. Thus the primary direction is masked at low AF intensities by secondary magnetization components and at higher fields by induced laboratory viscous or anhysteritic components. From the discussion so far it is apparent that such a situation exists here. It was therefore decided to use the least squares model technique as described by Stupavsky and Symons (1978). This technique is applicable to all AF demagnetization data to analyze the directions, intensities and decay rates of the individual magnetization components in a rock specimen whether or not their coercivity spectra overlap. Advantages over conventional methods include:

1) Directions, magnitudes and decay rates of the inherent magnetization components are given quantitatively,

2) An estimate of the uncertainty in the directions and magnitudes is computed,

3) Components hitherto unrevealed by conventional methods are computed, and

4) Only the pilot specimens need be analyzed, thus saving time.

Thus the 37 AF pilot specimens were analyzed using the Least Squares Models computer program with two different weighting functions (Stupavsky and Symons 1978). The first, where $W(H) = 1.0$ has the effect that the influence of each measured vector on the object function is proportional to its' intensity whereas the second, where W(H) = 1.0/(remanent magnetization magnitude), ensures that each measured vector has equal influence on the object function that is being minimized. The results were inspected and the best model selected on the basis of the goodness of fit parameters as specified by Stupavsky and Symons (1978); the most important being the mean angular deviation (M.A.D.) of the computed directions from the measured directions.

Model 5 invariably gives the best-fit model for each specimen. This model isolates three exponential components; 'primary'(1^{o}),'secondary'(2^{o}),'tertiary'(3^{o}), the decay rates for which provide useful information. Rapid decay rates with

$H_{1/2} \sim 5mT$ are commonly associated with secondary VRM components in large domain titano-magnetite or magnetite, or may simply reflect temporary magnetization components acquired in the laboratory. Similarly, moderate decay rates ($H_{1/2} \sim 15mT$) tend to be associated with a primary remanence residing in small domain titano-magnetite or magnetite. Finally, very slow decay rates ($H_{1/2} \sim 150mT$) are normally associated with hematite and may be either primary or secondary.

Figure 25 shows examples of the three isolated components for four typical specimens. Table 7 summarizes the results of this analysis listing the directions of the various components isolated, their median AF coercivity ($H_{1/2}$) and the M.A.D. Stereographic analysis of the components (Fig. 26) leads to the grouping of the components into five populations. The 'primary' and 'secondary' components fall into four groups in the N,E,S and W directions as seen previously. Also apparent are the steeply inclined directions consistently given by the 'tertiary' components. The directions were grouped and their mean statistics evaluated. Approximately 10% of directions were rejected as having anomalous directions falling much greater than two times the angular standard deviation, A63 (Fisher 1953) from the mean. The surviving specimens were re-averaged.

The 'A' component magnetizations were chosen on the basis of their directions and include 'primary' and 'secondary'

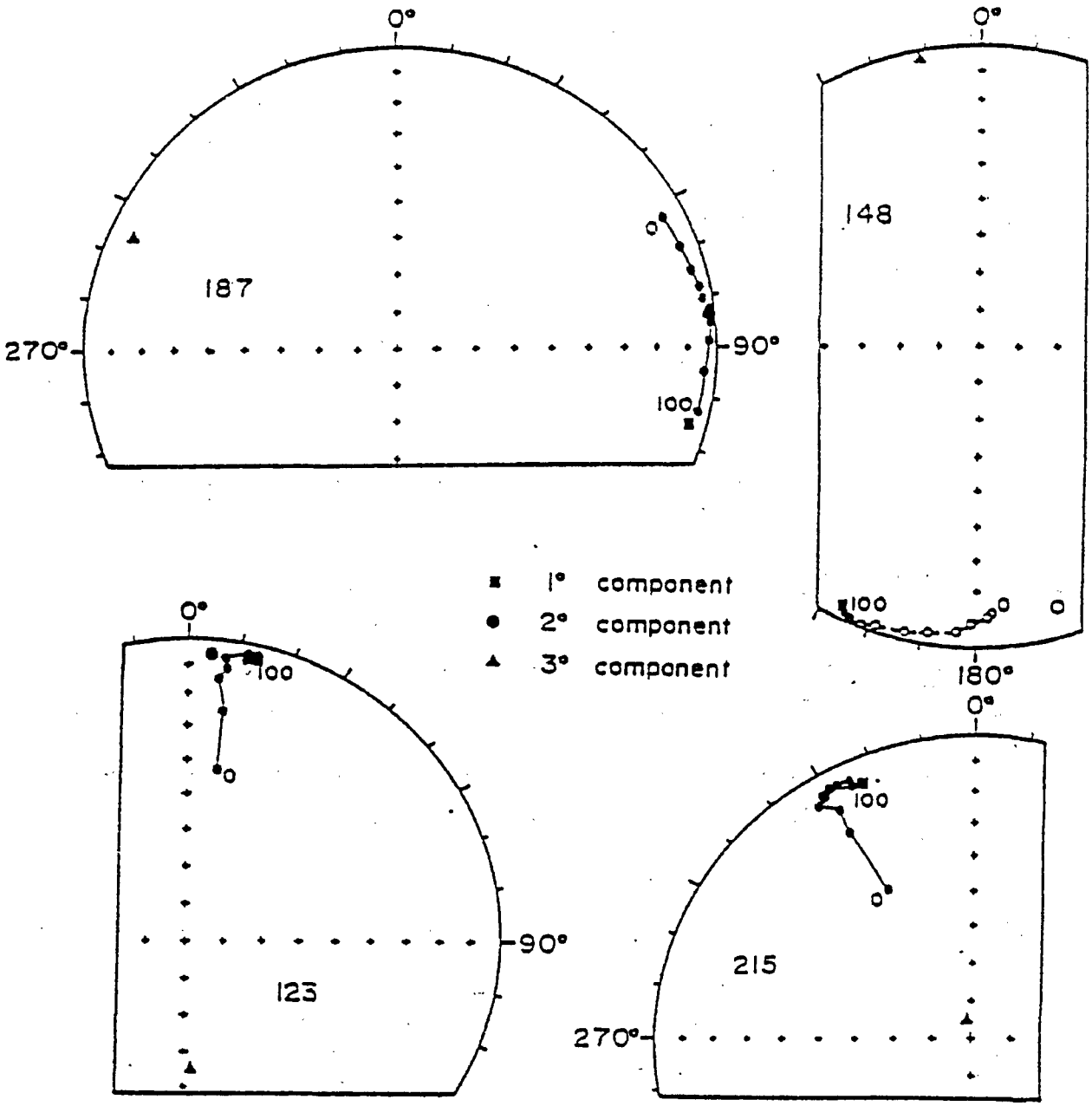

FIG. 25. Examples of least squares isolated components.

Directional changes of IF pilots during AF step demagnetization, showing components isolated by least squares. High coercivity 'primary',(1°) component (square); medium coercivity 'secondary',(2°) component (large circle); and low coercivity 'tertiary',(3°) component (triangle). Sample numbers are shown. Numbers represent demagnetization field in mT.

TABLE 7. Summary of 1°,2° and 3° magnetization components isolated by least squares methods

Specimen	Primary Component				Secondary Component				Tertiary Component				Model	M.A.D.	W(I
	Degl.	Incl. +down	Magn.	Coerc. mT	Decl. °	Incl. +down	Magn.	Coerc. mT	Decl. °	Incl. +down	Magn.	Coerc. mT			
101	342.00	5.73	0.051	35	12.62	4.88	1.11	12	245.27	15.75	0.41	3	5	1.19	I
103	107.55	-3.17	0.146	51	99.81	-4.85	1.24	15	282.52	28.17	0.43	4	5	0.88	I
106	165.07	16.91	0.004	108	357.59	-14.48	0.10	7	288.56	66.12	0.81	4	5	8.02	I
109	150.49	-13.94	0.016	59	322.77	3.57	1.27	15	184.52	30.17	0.93	6	5	2.46	I
112	135.02	6.88	0.012	81	39.33	15.54	0.17	13	352.74	65.33	0.94	3	5	5.18	I
115	107.14	-49.35	0.004	211	358.67	-7.75	0.47	13	8.86	45.21	0.69	5	5	4.58	I
117	165.65	8.61	0.048	46	164.14	-18.61	0.91	10	69.55	64.52	0.68	6	5	2.55	I
120	28.47	-9.39	0.336	23	7.87	0.46	0.76	11	208.08	70.92	0.33	4	5	2.40	II
123	12.69	3.43	0.182	21	4.02	4.28	1.01	6	176.10	54.00	0.71	3	5	1.16	I
138	342.07	39.05	0.029	38	19.78	-0.81	0.38	8	18.51	61.35	0.75	3	5	5.36	I
142	300.33	-2.34	0.180	31	350.94	5.07	0.67	8	13.53	72.32	0.43	3	5	1.25	I
145	142.62	71.71	0.017	32	137.03	-1.07	0.49	10	170.87	63.28	0.78	4	5	4.61	I
148	206.35	3.10	0.373	40	164.48	-10.65	1.40	8	348.63	2.20	0.69	4	5	1.64	II
151	347.64	-14.56	0.007		168.52	24.71	0.01	47	186.66	78.36	1.19	2	4	8.45	I
159	56.58	-30.64	0.202	54	53.91	-10.01	1.67	61	232.85	-12.23	1.02	4	5	0.74	I
162	141.60	0.57	0.161	35	133.72	3.62	0.92	11	342.87	66.23	0.23	4	5	0.33	I
165	36.79	16.99	0.039	25	33.19	7.98	0.84	7	293.08	52.16	0.63	4	5	2.18	I
167	94.53	1.67	0.004	107	78.56	-8.17	8.30	4	260.87	7.67	7.40	3	5	4.11	I
170	167.31	6.62	0.828	28	202.50	-3.55	1.34	17	9.93	0.11	1.07	9	5	0.49	II
173	92.46	10.79	0.147	29	38.20	4.45	1.44	14	233.93	-12.96	0.55	3	5	1.16	I
177	326.77	-54.23	0.008		58.07	-15.50	3.40	12	253.17	23.79	2.77	10	4	1.94	I
180	62.24	2.90	0.050	67	62.43	3.69	1.13	17	256.52	38.59	0.29	4	5	0.63	I
183	132.69	8.53	0.286	25	166.02	-17.21	3.49	7	338.16	24.04	2.86	6	5	1.23	I
187	116.40	4.79	0.034	376	83.77	0.40	1.56	16	290.40	8.03	0.76	7	5	0.58	I
191	131.05	40.23	0.012	42	51.80	-0.72	0.28	10	313.79	28.98	0.98	4	5	6.43	I
194	102.30	20.15	0.018	63	98.44	9.75	0.71	9	154.18	69.97	0.52	3	5	2.17	I
197	187.22	40.04	0.005	80	65.19	32.00	0.17	10	81.72	64.15	0.89	3	5	7.67	I
198	88.57	-2.59	0.031	236	79.75	-10.32	1.20	3					3	2.07	I
199	236.60	-2.62	0.188	58	207.38	0.73	0.83	7	53.31	11.33	1.87	4	5	2.04	I
202	227.05	10.63	0.014	55	41.24	25.17	0.27	13	62.89	72.28	0.91	4	5	8.14	I
204	170.17	-18.06	0.094		352.33	16.44	0.21	4	157.30	-39.75	1.10	1	4	3.09	II
207	70.58	15.56	0.181	26	80.54	4.52	0.81	13	172.32	37.67	0.27	3	5	1.64	I
209	87.72	4.65	0.452	26	56.69	-2.84	0.94	10	269.93	20.26	0.43	4	5	1.20	II
212	67.32	12.24	0.150	19	62.82	5.61	0.73	6	186.32	66.93	0.58	1	5	4.01	II
215	336.81	8.13	0.039	39	329.15	5.60	0.68	13	347.65	84.75	0.61	3	5	1.92	I

NOTES: Optimum Model selected from goodness of fit parameters (Stupavsky and Symons 1978).
M.A.D. is the mean angular deviation.
W(I) is the weighting function: I where W(I)=1.0/remanent magnetization magnitude, II where W(I)=1.0

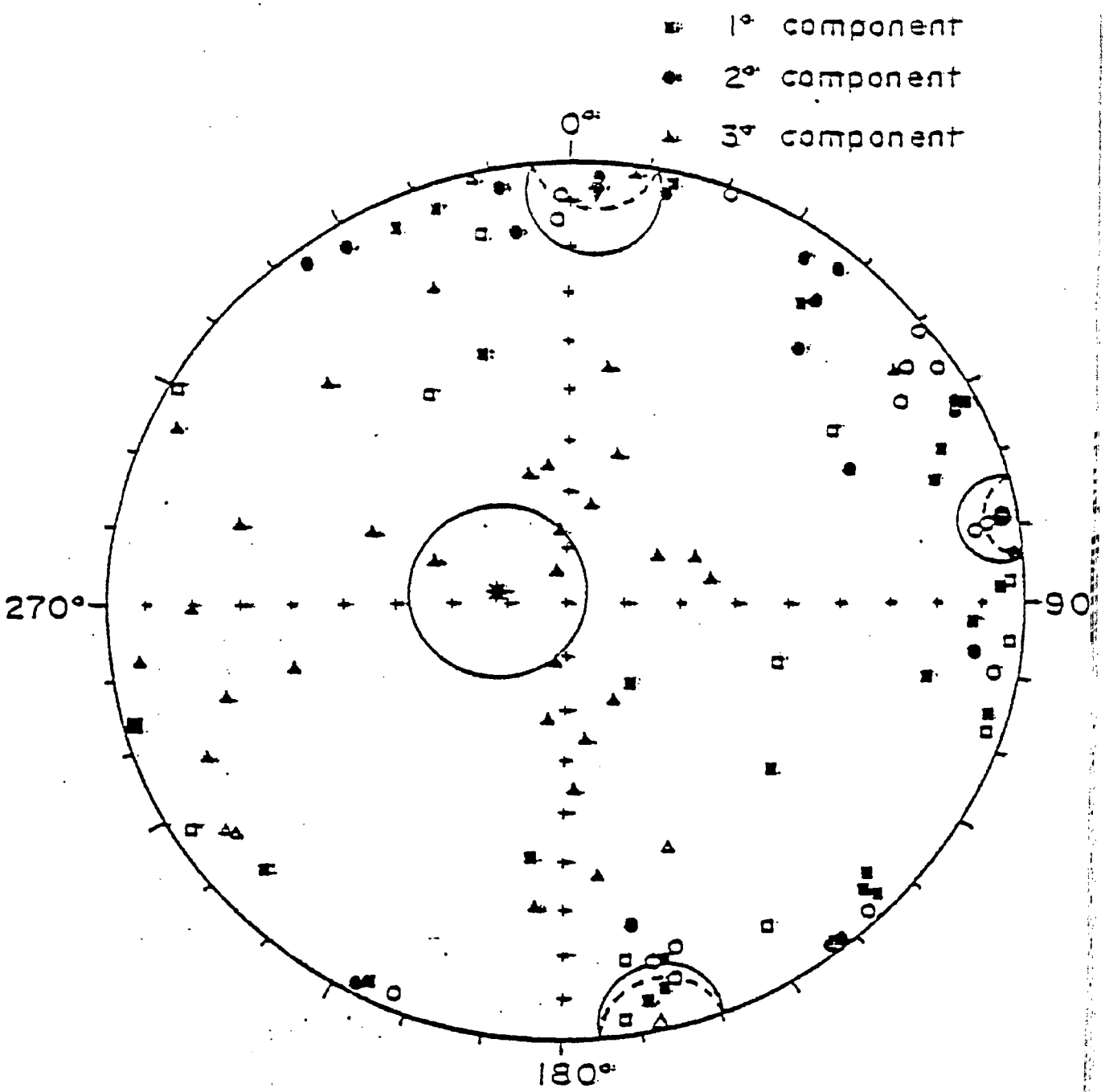

FIG. 26. Equal area projection showing all least squares isolated components.

Symbols and conventions as used in Figure 25. Mean directions of the four component directio
isolated are shown with the same symbols as used in Figure 21, together with their circles o
95% confidence. The mean low coercivity direction is shown by an asterisk.

isolated components. After combining 'normal' and 'reversed' components they form a cluster about a mean of (354.3°, 2.9°), (A95 = 8.4°). Site differences in the magnetic mineralogy give a coercivity range ($H_{1/2}$) from 4mT to 180mT. The 'B' components form a cluster about a mean of (79.1°, 1.4°), (A95 = 8.4°) and give a coercivity range from 4mT to 375mT.

Table 8 summarizes the remanence data. It is apparent from visual inspection alone that these directions are not significantly different from those revealed by conventional methods.

Of greater interest is the isolation of a very 'soft' steeply inclined component with a median AF coercivity of ∿4mT. Suspecting that this may represent a secondary metamorphic or viscous component the angular variance ratio test was performed on the corrected and uncorrected directions. The variance ratio of 1.72 is greater than the theoretical statistic of 1.61 at the 95% confidence level showing that there is a significant difference between the dispersion characteristics of the two populations (Table 9). The precision parameter, K (Fisher 1953) is greater for the corrected data suggesting that the remanence isolated predates the regional folding.

TABLE 8. Summary of remanence directions from least squares isolated components

Group	Number of specimens N	Mean remanence direction Length R	Decl.	Incl. +down	A95
A component	38	33.742	354.3	2.9	8.4
B component	25	23.146	79.1	1.4	8.4
C component	27	20.074	278.4	77.7	16.7

NOTES: R is the length of vector resultant.
A95 is the radius of 95% confidence (Fisher 1953) in degrees.
A component refers to directions centred on (360°,0°); B component refers to directions centred on (90°,0°). In both cases, normal and reversed components have been combined.
C component refers to a population of steeply inclined directions.

TABLE 9. Angular variance ratio analysis for 'C' component fold test

Group	Number of specimens N	Mean remanence direction Length R	Decl.	Incl. +down	K	A95	V	$F_{0.05}$
Corrected	27	20.074	278.4	77.7	3.8	16.7	1.72	1.61
Uncorrected	27	15.075	249.7	14.2	2.2	25.4		

NOTES: R is the length of vector resultant.
K is Fisher's (1953) precision parameter. A95 is the radius of 95% confidence (Fisher 1953).
V is the variance ratio $\delta_{corr}/\delta_{uncorr}$ of the two populations.
$F_{0.05}$ is the theoretical statistic $F_{2(N_{corr}-1),2(N_{uncorr}-1),0.05}$ thereby setting the test at the 95% confidence level.

TABLE 10. Summary of ungrouped remanence directions by pit

Group	Number of samples N	Mean remanence direction Length R	Decl.	Incl. +down	K	A95
Pit 1	1		176.6	-14.2		
Pit 2S	32	17.228	67.7	10.2	2.0	24.5
Pit 2N	29	17.048	61.6	7.2	2.3	23.0
Pit 3	15	9.052	33.8	9.3	2.4	32.5
Pit 3A	6	4.083	98.7	18.2	2.6	52.1
Pit 10	2	1.445	314.6	20.5	1.8	>99.9
Pit 11	9	3.729	89.1	1.2	1.5	69.0
Overall	94	48.001	63.2	9.9	2.0	14.5

NOTES: R is the length of the vector resultant.
K is Fisher's (1953) precision parameter.
A95 is the radius of 95% confidence (Fisher 1953) in degrees.
Sample means have been calculated without isolation of different components.

4.6c Remaining Specimens

The remaining specimens were demagnetized using the optimum AF intensity selected for each sample (Table 2). The specimen directions were then combined after appropriate data screening (5.4b) to give the sample mean directions, which were then averaged to give the mean direction for each pit. Each pit has a poorly defined cluster of sample mean directions because of the presence of the four stable component directions (Table 10).

4.6d Fold Test - Pit 2

Pit 2 has three limbs (Figs. 2a and 2b). The north limb (2N) trends north-south and contains the samples 111-117, 145-150, 170-193 and 206-210. The centre limb (2C) trends east-west and contains samples 103-104, 107-110 and 211. The south limb (2S) trends WNW-ENE and contains samples 101-102, 105-106, 118-128 and 212-215.

The sample means were grouped on these structural grounds and the populations of the three limbs compared using a series of variance tests (Larochelle 1969; Watson 1956; Table 11).

For each pair of limbs, the ratio of the variances in dispersion ($V = \delta_A^2 / \delta_S^2$) was calculated and compared to the corresponding theoretical statistic:

$$F_{2(N_A-1),2(N_S-1),0.05}$$

If $V > F$, then the two populations have significantly different distributions and hence probably reflect different conditions of remanence acquisition or removal.

The second test is more powerful. It follows the method of Watson (1956) and computes the statistic:

$$F_c = N-2\left(\frac{R_1 + R_2 - R}{N - R_1 - R_2}\right)$$

R is the length of the vector sum of the resultants of the separate populations, and $N = (N_1 + N_2)$ is the total number of samples in the two populations. This is compared to the theoretical statistic:

$$F_{2,2(N-2),0.05}$$

If $F_c > F$, then the two populations define significantly different directions possibly as a result of the folding.

The results of these tests are shown in Table 11. The consistent positive result for the first test shows that the three limbs have similar dispersions of directions and

TABLE 11a. Mean remanence directions for groups of sites - Pit 2

Group	Samples	Number of samples	Strike	Mean remanence direction			
				Length R	Decl. °	Incl. +down	A_{95} °
By structural limb							
(2N)North limb	110,111,112,113,114 115,116*,117*,145,147 149,150,170,171,172 173,174,175,177*,178 179,180,181,182,184* 185,186*,187,188,190 191,192,193,206,207 208*,209,210	45	327	27.412	76.6	7.5	17.3
(2C)Centre limb	103,104,107,108,109 211	6	288	3.688	16.6	10.3	60.9
(2S)South limb	101,105,106,118*,119 120,123,213,214	10	311	4.809	29.1	12.2	55.0

NOTES: * is a sample considered to contain two stable directions.
R is the length of vector resultant.
A95 is the radius of the cone of 95% confidence (Fisher 1953) in degrees.

TABLE 11b. Angular variance ratio analysis for the pit 2 fold test

Test units compared	Number of samples N	V	$F^*_{0.05}$	Result	F_c	$F_{0.05}$	Result
North vs. Centre	51	1.16	2.60	Positive	4.02	3.10	Negativ
South vs. Centre	16	1.25	2.80	Positive	0.09	3.34	Positiv
South vs. North	55	1.44	1.75	Positive	3.09	3.08	Negativ

NOTES: N is the combined number of samples from the two test units ($N_A + N_S$).
V is the variance ratio σ_A^2/σ_S^2 of the two populations.
F_c is the statistic defined by Watson (1956).
$F^*_{0.05}$ is the theoretical statistic $F_{2(N_A-1),2(N_S-1),0.05}$ thereby setting the test at the 95% confidence level.
$F_{0.05}$ is the theoretical statistic $F_{2,2(N-2),0.05}$ also setting the test at the 95% level.

thus justifies the comparison of these similar remanences.

The negative results for the comparison of limbs 2N vs. 2C and 2N vs. 2S indicates that these limbs have significantly different remanence directions. The strong positive result for the 2S vs. 2C limbs is not suprising because of the similarity of the strike of these two limbs. One would therefore expect their remanence directions to be significantly similar. It is clear therefore that the remanence isolated in Pit 2 predates the folding.

4.6e Correlation of Normal and Reversed Components

An examination of the directions of the four stable components suggests that those in groups 1 and 3 are anti-parallel as are those in groups 2 and 4. Next, it was decided to compare these 'normally' (N) and 'reversely' (R) polarized components using the variance tests as described above. Since the data from a few progressively demagnetized samples are more suitable than those of many partially demagnetized samples it was decided to use the pilot specimen data obtained at the optimum AF cleaning field.

The variance tests between the components after conversion of the reversed sites to normal polarity shows that they do not have either significantly different dispersion statistics or significantly different directions (Table 12). This provides strong evidence indicating that most of the VRM has been removed, that the measured rem-

TABLE 12a. Variance tests between normal and reversed components from AF data

Components compared	Number of specimens N	V	$F^{*}_{0.05}$	Result	F_c	$F_{0.05}$	Result
Group 1 vs. Group 3+	17	2.05	2.77	Positive	1.08	3.32	Positive
Group 2 vs. Group 4+	19	1.84	2.69	Positive	1.39	3.30	Positive

NOTES: N is the number of pilot specimens isolating the two components compared, $(N_A + N_S)$.
V is the variance ratio δ_A^2/δ_S^2 of the two populations.
F_c is the statistic defined by Watson (1956).
$F^{*}_{0.05}$ is the theoretical statistic $F_{2(N_A-1),2(N_S-1),0.05}$ thereby setting the test at the 95% confidence level.
$F_{0.05}$ is the theoretical statistic $F_{2,2(N-2),0.05}$ also setting the test at the 95% level.
+ refers to reversed vectors in anti-parallel position.
Normal and reverse statistics are given in Table 12b.

TABLE 12b. Mean remanence directions for optimum AF cleaned pilot specimens

Group	Number of specimens N	Mean remanence direction				
		Length R	Decl.	Incl. +down	K	A95
A component						
Normal samples(Group 1)	11	9.391	4.9	9.4	6.2	19.9
Reversed samples(Group 3)	6	5.608	171.9	0.8	12.7	19.5
All samples*	17	14.854	0.0	5.7	7.5	14.0
B component						
Normal samples(Group 2)	16	14.077	80.7	7.2	7.8	14.1
Reversed samples(Group 4)	3	2.528	285.3	-4.4	4.2	69.4
All samples*	19	16.409	84.4	6.8	6.9	13.7

NOTES: R is the length of vector resultant.
K is Fisher's (1953) precision parameter.
A95 is the radius of 95% confidence (Fisher 1953) in degrees.
* Reversed vectors in antiparallel position.

anences are primary and that the normal and reversed paleofields were truly antiparallel. Therefore all the data can be validly combined to form two component directions: an A component and a B component (Table 13).

4.6f Fold Test - Entire Grouped Data

The high dispersion in the directions within each limb in the previous fold test is a consequence of the four stable components present. A more meaningful fold test was performed by grouping the site means into populations based on their isolated component directions. The site mean directions corrected for bedding attitude were compared with the uncorrected site mean directions using the same angular variance test as described above (Table 14).

The first test compares the corrected and uncorrected directions for the normally polarized A component, A_N i.e. the population centred on (360°, 0°). The test is negative indicating that there is a significant difference in dispersion of directions because the variance ratio of 1.98 is greater than the theoretical statistic at the 95% confidence level. The second test compares the corrected and uncorrected directions for the normally polarized B component, B_N, i.e. the population centred on (90°, 0°). The variance ratio of 2.09 is greater than the theoretical statistic of 1.48 indicating that the directions from the

TABLE 13. Summary of remanence directions after AF demagnetization

Group	Number of blocks N	Mean remanence direction Length R	Decl. °	Incl. +down	K	A95 °
A component						
Pit 1	1		356.6	14.2		
Pit 2S	18	16.138	354.7	3.1	9.1	12.1
Pit 2N	12	10.820	12.5	3.0	9.3	15.0
Pit 3	7	6.658	13.3	13.0	17.6	14.8
Pit 10	1		356.9	5.2		
Pit 11	4	3.162	359.2	9.1	3.6	56.9
All blocks	43	36.267	3.7	5.4	8.5	8.2
B component						
Pit 1	1		54.2	4.0		
Pit 2S	14	12.916	79.5	7.7	11.9	12.0
Pit 2N	17	15.686	83.5	6.5	12.2	10.7
Pit 3	8	7.102	81.7	7.7	7.8	21.2
Pit 3A	6	5.640	84.3	12.4	13.9	18.6
Pit 10	1		87.3	24.5		
Pit 11	5	4.524	67.4	-10.7	8.4	28.0
All blocks	52	45.482	80.6	6.1	10.8	6.4

TABLE 14. Group mean remanence directions and variance tests of AF data

Group	Number of sites N	Mean remanence direction Length R	Decl. °	Incl. +down	K	A95 °	V	$F_{0.05}$
1.Centred on (360°,0°)								
Corrected	29	26.272	12.6	7.1	10.3	8.8	1.98	1.58
Uncorrected	29	23.597	347.7	56.1	5.2	13.1		
2.Centred on (90°,0°)								
Corrected	44	40.795	78.3	6.9	13.4	6.1	2.09	1.48
Uncorrected	44	37.306	80.9	72.6	6.4	9.2		
3.Centred on (180°,0°)								
Corrected	14	13.563	168.0	-2.8	9.7	12.9	2.64	1.94
Uncorrected	14	10.473	162.6	5.8	3.7	24.1		
4.Centred on (270°,0°)								
Corrected	7	6.102	278.8	7.0	6.7	25.2	3.45	2.69
Uncorrected	7	3.903	282.0	-38.7	1.9	60.9		

NOTES:R is the length of vector resultant.
K is Fisher's (1953) precision parameter.
A95 is the radius of 95% confidence (Fisher 1953) in degrees.
V is the variance ratio $\delta_{corr}/\delta_{uncorr}$ of the two populations.
$F_{0.05}$ is the theoretical statistic $F_{2(N_{corr}-1),2(N_{uncorr}-1),0.05}$ thereby setting the test at the 95% confidence level.

two subsets have different populations of directions. Thirdly, the variance ratio of 2.64 is again significantly greater than the theoretical statistic of 1.94 indicating that the directions from the corrected subset showing the reversed A component, A_R (i.e. the population centred on (180^o, 0^o)) form a different population from the uncorrected directions. Finally, the directions showing the reversed B component, B_R, centred on (270^o, 0^o), give the same highly negative test result. The variance ratio of 3.45 greatly exceeds the theoretical statistic of 2.69. It is clear therefore that there is a significant difference between the corrected and the uncorrected direction populations. The histograms of declination and inclination for the A_N component (Fig. 27) illustrate how the standard deviation for the corrected directions is far less than that for the uncorrected directions. The other components give similar results. In addition, in all cases, the precision parameter, K (Fisher 1953) is greater for the corrected directions population. It is clear therefore that the remanence isolated in the IF predates the folding.

The highly significant results of these tests may be a result of the combination of the prefolding nature of the remanence and the deflection of the remanence into the plane of the bedding due to the anisotropy of magnetic susceptibility as discussed earlier (4.6b).

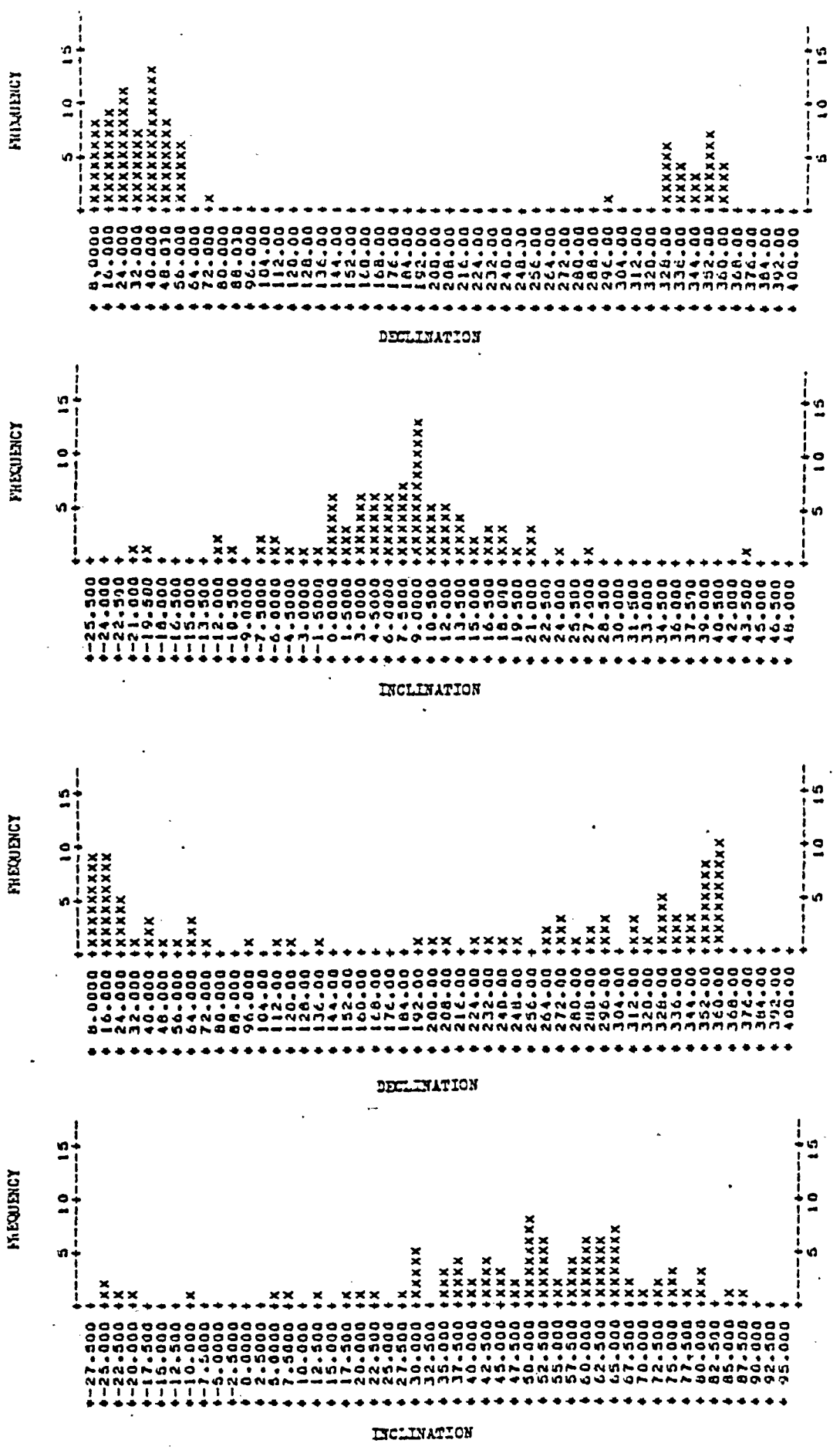

FIG. 27. Histograms of declination and inclination for Group 1.
a) and b) corrected for bedding attitude
c) and d) uncorrected for bedding attitude.

4.7 THERMAL CLEANING OF IRON FORMATION

4.7a Pilot Specimens

The pilot specimens show the same multicomponent nature of the magnetization during thermal step cleaning. When present, initial viscous or 'soft' secondary components are removed below 200°C or 300°C. All specimens show isolation of a single stable component either to temperatures above 500°C or 550°C. All specimens at higher temperatures show weak randomly directed components. It should be noted that due to a crack in the furnace, that moved the temperature sensor away from the furnace tube, that the measured temperatures are perhaps too low by up to 40°C. It is not known at what stage of the experiment this crack occurred.

Once again, the stable directions fall into four populations. After combining the specimens isolating the same component, the directional changes during thermal step demagnetization are illustrated in Figure 28a. The pilot specimens all exhibit a common behaviour on thermal step demagnetization. Figure 28c shows the thermal intensity decay curves for each component. They show an initial rapid drop in intensity up to 300°C as viscous remanent magnetization components and unstable components are removed, leaving the stable directions. The curves then take on a more typical knee shaped form, showing that the blockage temperature of some grains is ~425°C above which the magnetization carried by such grains is destroyed.

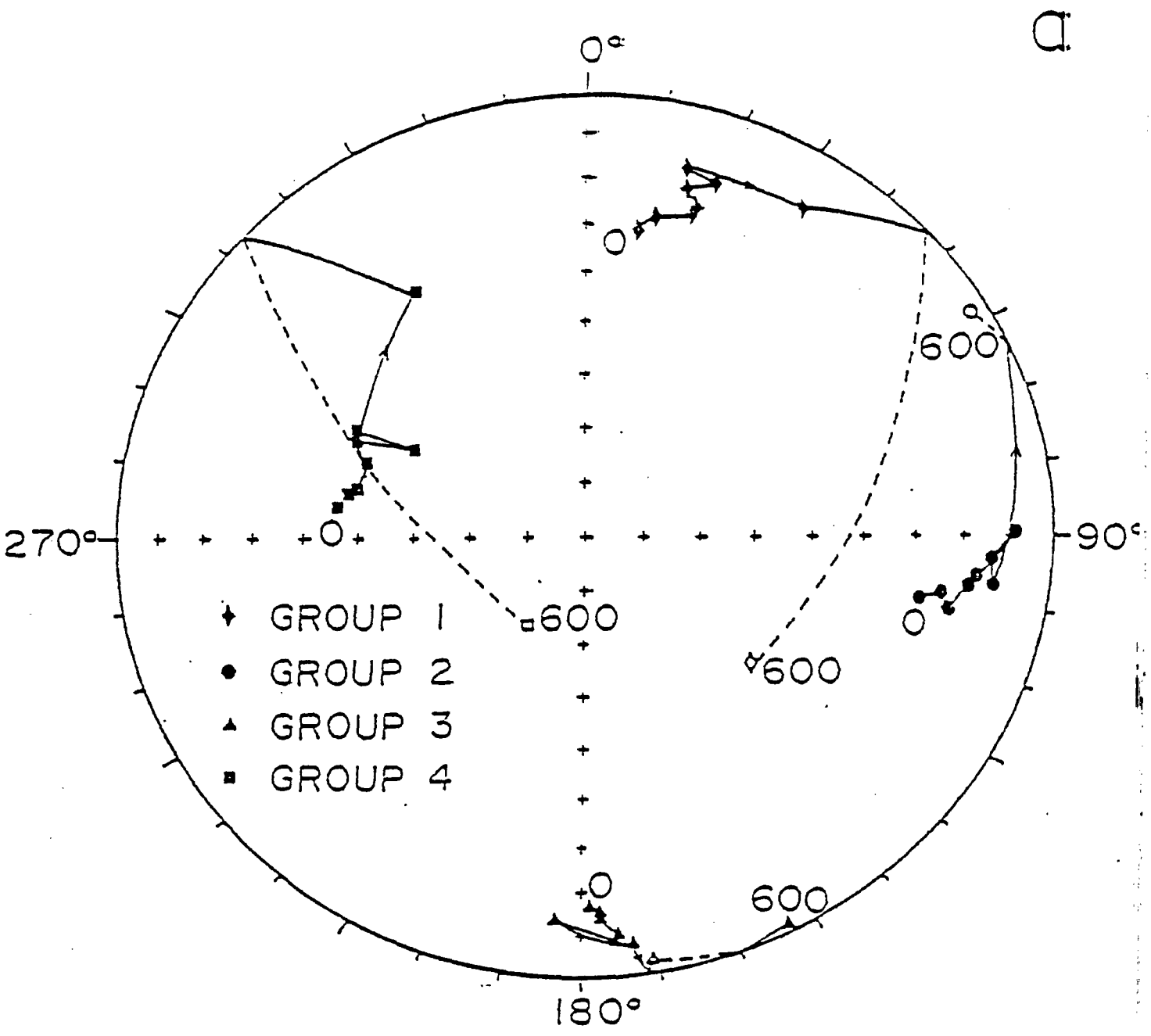

FIG. 28. Demagnetization Curves - Thermal

a) Equal area projection showing the change in direction on progressive thermal demagnetization at temperatures of 0,100,200,300,400,450,500,550,600,650 and 700 C for IF pilot specimens. Symbols and conventions as in Figure 21.
b) Paleomagnetic stability index. c) Remanence intensity is plotted as a ratio of the NRM intens against the demagnetization temperature,
d) Radius of 63% confidence (Fisher 1953), A63 of the mean directions.

C

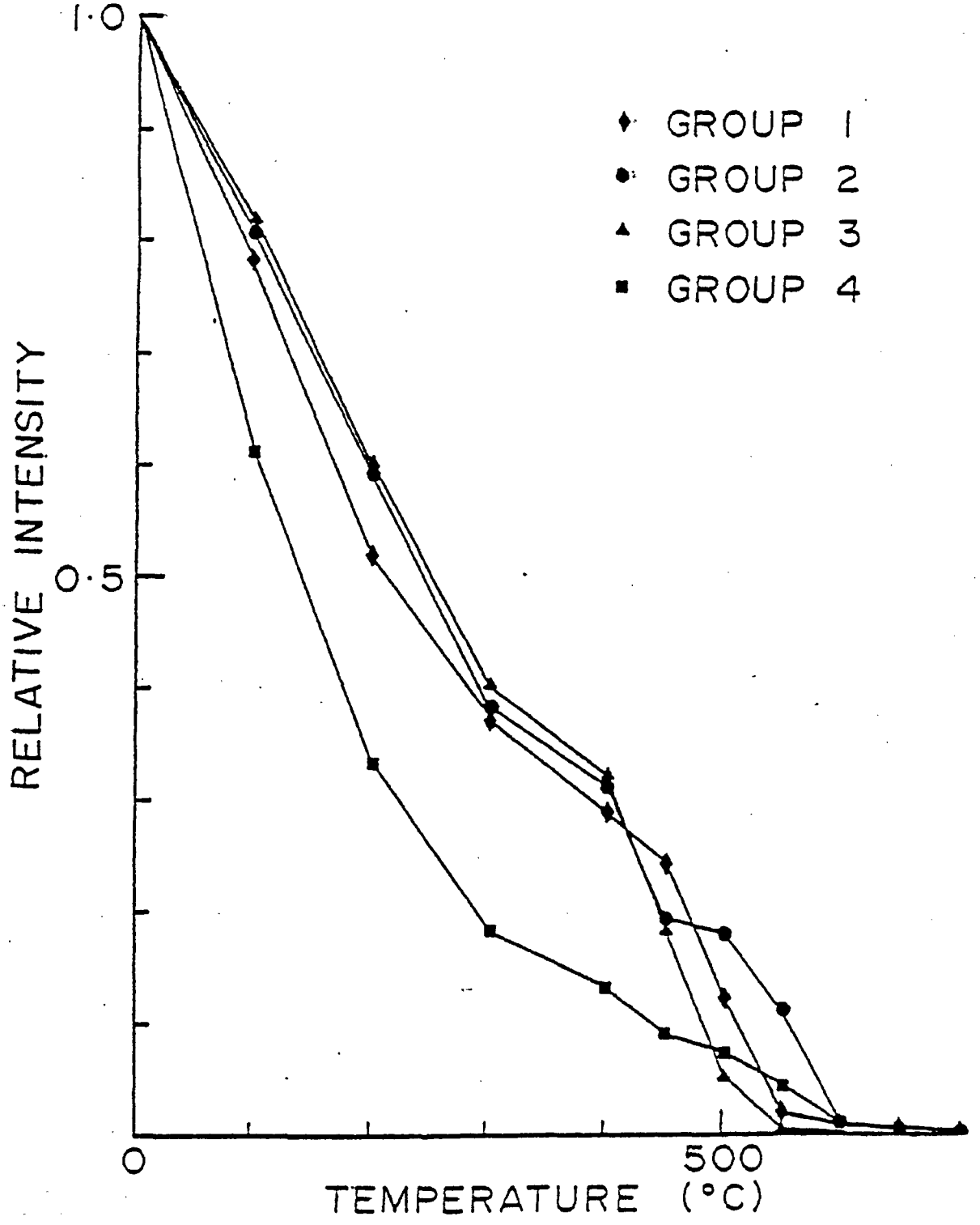

FIG. 28. contd.

The thermal coercivity spectrum of the stable direction is probably carried by magnetite (T_c = 580°C) and is blocked dominately above 450°C. A further drop in intensity indicates that the thermal coercivity spectrum of the stable direction is probably carried by magnetite grains of a different size which is blocked dominately above 550°C.

The PSI curves (Fig. 28b) support this interpretation. High initial rates of directional change in the order of 50 mdeg/°C decrease slightly as the stable direction is isolated. Thereafter the curves record an increasing rate of directional change up to values of ∿2000 mdeg/°C above 550°C as the randomly directed thermoremanent (TRM) components dominate the specimen response. The randomness of these components is illustrated in Figure 28d by the large cones of confidence at temperatures above 550°C.

The Zijderveld diagrams (Fig. 29) take the same form as those for AF cleaning, showing the removal of large vertical components in temperatures of 100°C - 300°C. Above 300°C, in most cases a moderately straight line is definable. Of significance, is the fact that the line segment at 450°C is in the same direction at 550°C suggesting that the two carriers are carrying the same direction of magnetization.

4.7b Comparison of AF and Thermally Isolated Components

The above discussion shows the isolation of four stable components. With reference to Figure 28a, five specimens in

b

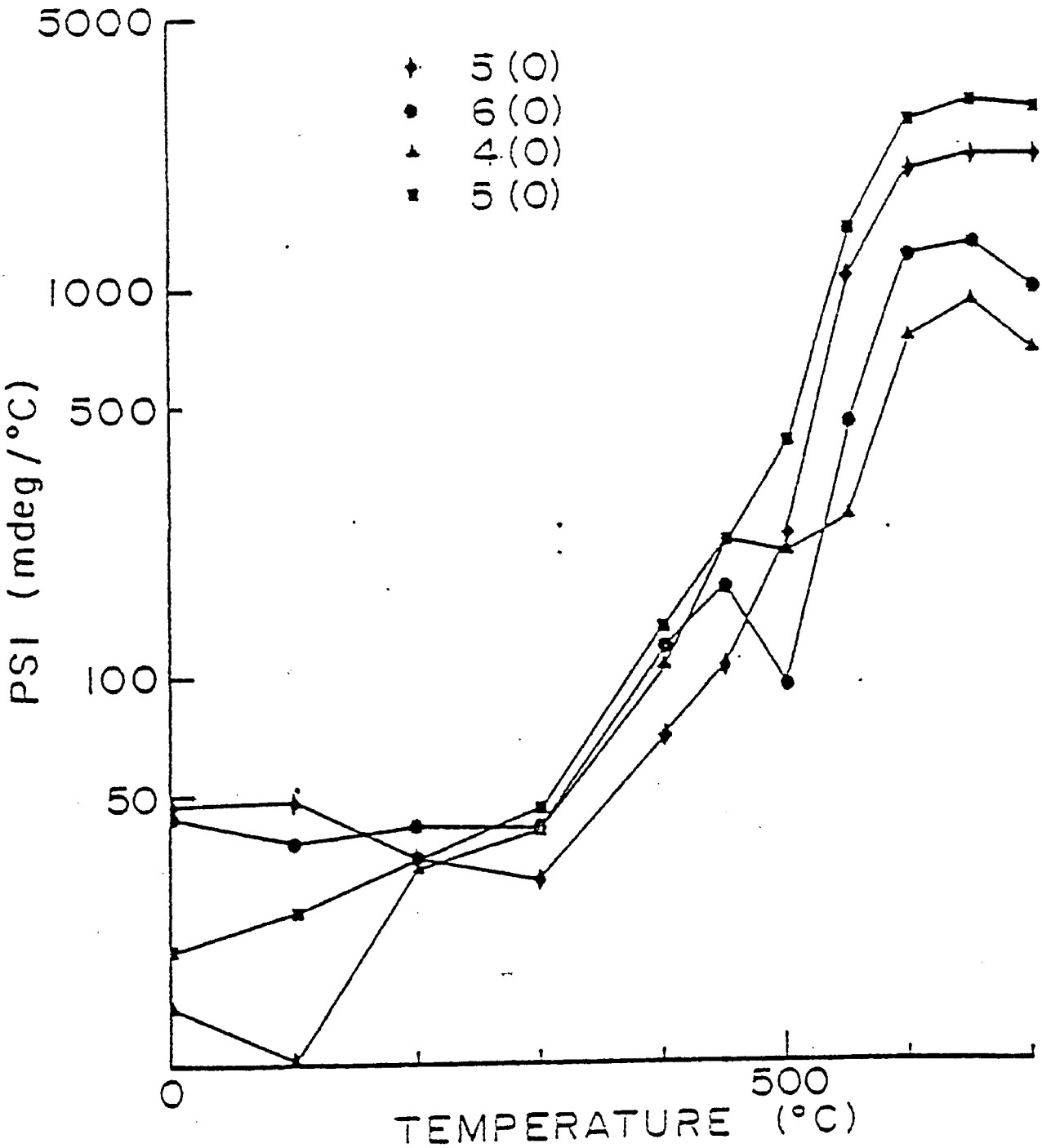

FIG. 28. contd.

d

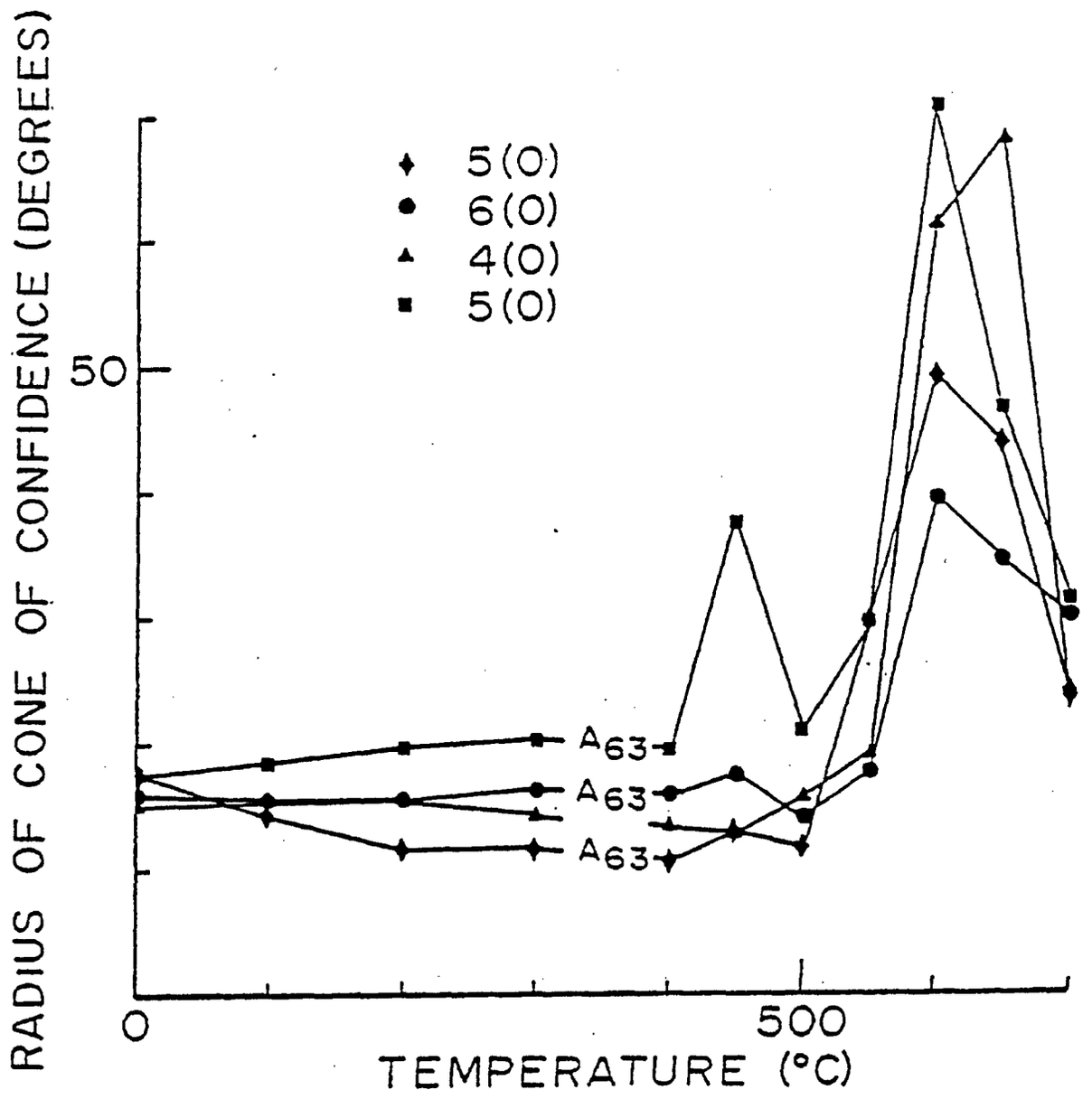

FIG. 28. contd.

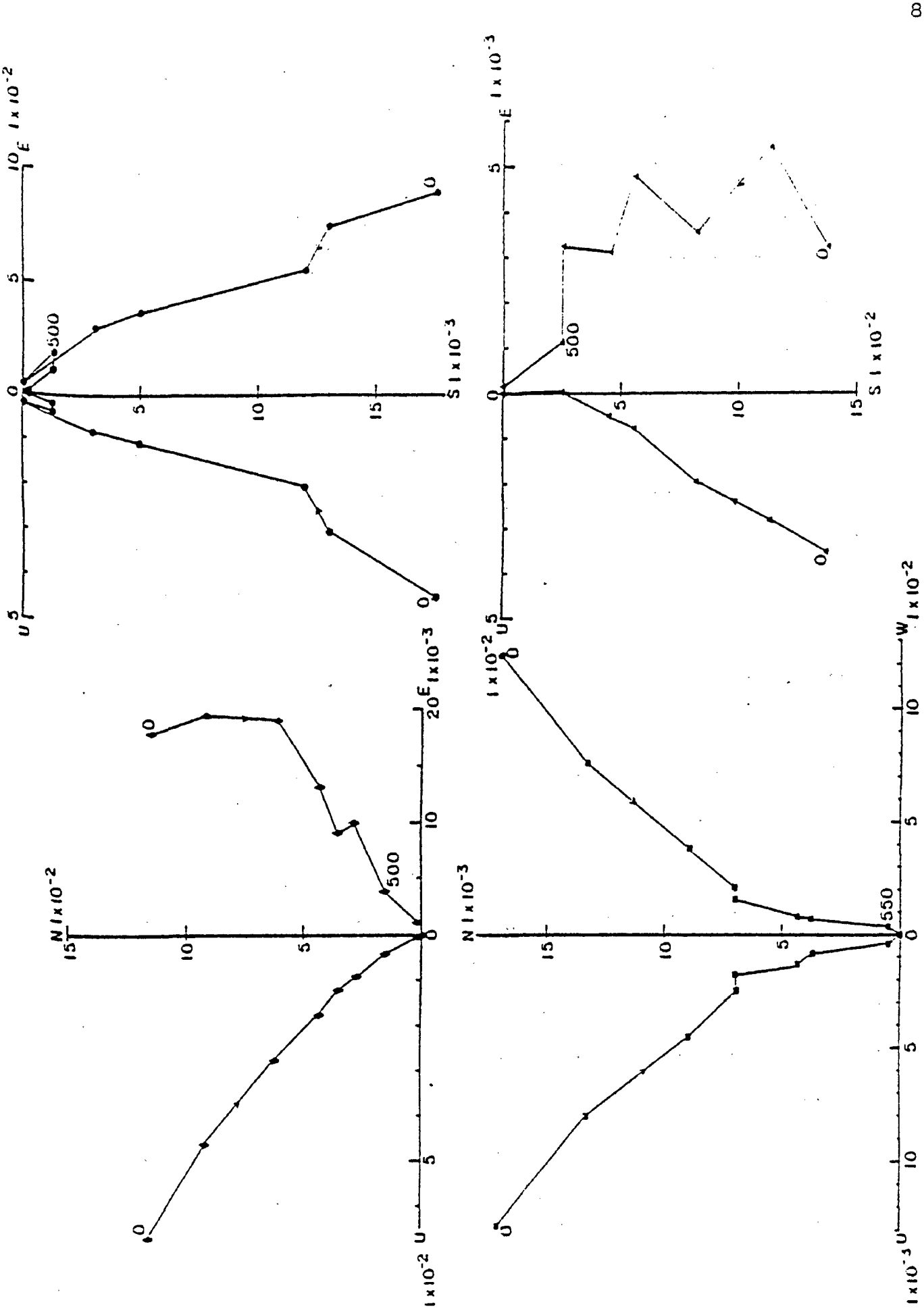

FIG. 29. Demagnetization vector diagrams - Thermal

Symbols and conventions as used in Figure 22. Numbers represent demagnetization temperature. Intensity in emucm^{-3}.

the quadrant centred on (360°,0°) show the isolation of a single stable component to a temperature above 500°C in the same direction as the population mean isolated by AF demagnetization. Six specimens centred on (90°,0°) and four specimens centred on (180°,0°) show the isolation of single stable components to temperatures above 550°C in the same direction as the mean isolated by AF demagnetization. The five specimens centred on (270°,0°) show the isolation of a single stable component to a temperature above 500°C. Once again, although here the agreement for individual specimen cores is poor, the stable components isolated by thermal and AF demagnetization have similar directions.

The angular variance ratio tests described previously were used to test the agreement between the components isolated by the two cleaning techniques (Table 15). The tests show that the components have significantly similar dispersion statistics and do not have significantly different directions at the 95% confidence level.

4.7c Correlation of Normal and Reversed Components

As before, the antiparallel components were compared using the angular variance test. Table 16 summarizes the results The test results are not very reliable because the populations are small. However, it seems the normal and reversed components do not have significantly different dispersion statistics. The variance test between group 1 and group 3 components after

TABLE 15. Variance tests between AF and thermally isolated components

Components compared	Number of specimens N	V	$F^{*}_{0.05}$	Result	F_c	$F_{0.05}$	Result
AF vs. Thermal							
Group 1	16	2.22	3.15	Positive	0.58	3.34	Positive
Group 2	21	1.31	2.19	Positive	1.45	3.24	Positive
Group 3	11	1.17	4.00	Positive	0.46	3.55	Positive
Group 4	8	1.12	3.84	Positive	2.78	3.89	Positive

NOTES: N is the number of pilot specimens isolating the component from AF and Thermal data
V is the variance ratio of the two populations.
F_c is the statistic defined by Watson (1956).
$F_{0.05}$, and $F^{*}_{0.05}$ are the theoretical statistics defined earlier and set the test at the 95% confidence level.

TABLE 16. Variance tests between normal and reversed components from thermal d

Components compared	Number of specimens N	V	$F^{*}_{0.05}$	Result	F_c	$F_{0.05}$	Result
Group 1 vs. Group 3^{+}	9	1.17	3.58	Positive	3.86	3.74	Negative
Group 2 vs. Group 4^{+}	11	1.47	3.07	Positive	7.32	3.55	Negative

NOTES: As above.
+ refers to reversed vectors in antiparallel position.

reversal of the latter is positive at the 97.5% confidence level, indicating that the directions are not significantly different and can validly be combined to give the stable A component. However, the variance ratio of 7.32 is greater than the theoretical statistic of 6.01 at the 99% confidence level, indicating that the directions from group 2 and those from the reversed group 4 are significantly different.

Visual inspection of the group 4 directions show that four of the five specimens have retained a high inclination, possibly as a result of incomplete cleaning, or perhaps indicative of a true stable component in this direction. It was decided to group these four specimens together, to give a third component in a similar direction to that isolated by least squares (4.6b). The fifth specimen in the group 4 population, considered as truly antiparallel to the normal B_N component represented by group 2, was grouped with those specimens, to give the stable B component (Table 17).

4.7d Demagnetization at 500°C and 600°C.

After grouping and averaging the directions isolated from the 80 specimens demagnetized at 500°C and 600°C into appropriate populations, four components; A_N, A_R, B_N and B_R, are once again evident. Inspection of individual specimens shows that in many cases (38%), the direction isolated at 500°C reverts to its' antiparallel direction when demagnetized to 600°C. After reversal of the antiparallel components A_R and

TABLE 17. Mean remanence directions for thermally isolated components

Group	Number of specimens N	Mean remanence direction				
		Length R	Decl. °	Incl. +down	K	A95 °
Pilot specimens:						
A component						
Normal specs.(Group 1)	5	4.710	14.4	18.3	13.8	21.4
Reversed specs.(Group 3)	4	3.746	176.1	6.7	11.8	27.9
All specimens*	9	8.157	6.1	7.4	9.5	17.6
B component						
Normal specs.(Group 2)	6	5.283	94.1	11.9	6.9	27.3
Reversed specs.(Group 4)	1		269.7	-11.4		
All specimens*	7	6.152	92.3	11.6	7.2	27.2
C component	4	3.787	311.8	54.8	14.1	25.3
Remaining specimens:						
A component						
Demag. @ 500°C	38	29.060	356.8	11.2	4.1	13.1
Demag. @ 600°C	38	28.077	358.1	6.2	3.7	14.0
B component						
Demag. @ 500°C	42	35.671	79.2	11.3	6.5	9.4
Demag. @ 600°C	42	32.452	88.1	-3.3	4.3	12.1

NOTES: R is the length of vector resultant.
K is Fisher's (1953) precision parameter.
A95 is the radius of 95% confidence (Fisher 1953) in degrees.
* Reversed vectors in antiparallel position.

B_R the directions were re-grouped and averaged. Table 17 illustrates the remanence directions obtained from which it is readily apparent that there is no significant difference between the directions at 500°C and those at 600°C presumably carried by two grain size populations of magnetite, or perhaps by magnetite and hematite given the furnace temperature errors.

The presence of antiparallel components may either represent true paleofield reversals or the acquisition by a small percentage of carriers of the internal field set up within the IF. Low temperature analysis (Fuller and Kobayashi 1967) may hold some promise for investigation of this form of multicomponent magnetization.

4.8 CHEMICAL CLEANING OF IRON FORMATION

4.8a Pilot Specimens

The pilot specimens exhibit a common behaviour on chemical leaching. Figure 30 shows the directional changes for four specimens. Disintegration of the remaining two specimens prevented their measurement. The three northerly magnetized specimens; 101,123,142 clearly show the removal of unstable VRM components in the present steeply inclined Earth's field direction and the isolation of a stable component in a similar direction to the A component obtained by AF and thermal cleaning. The fourth specimen, 211, with an easterly directed NRM also appears to isolate a northerly directed component perhaps indicative of two carriers with different

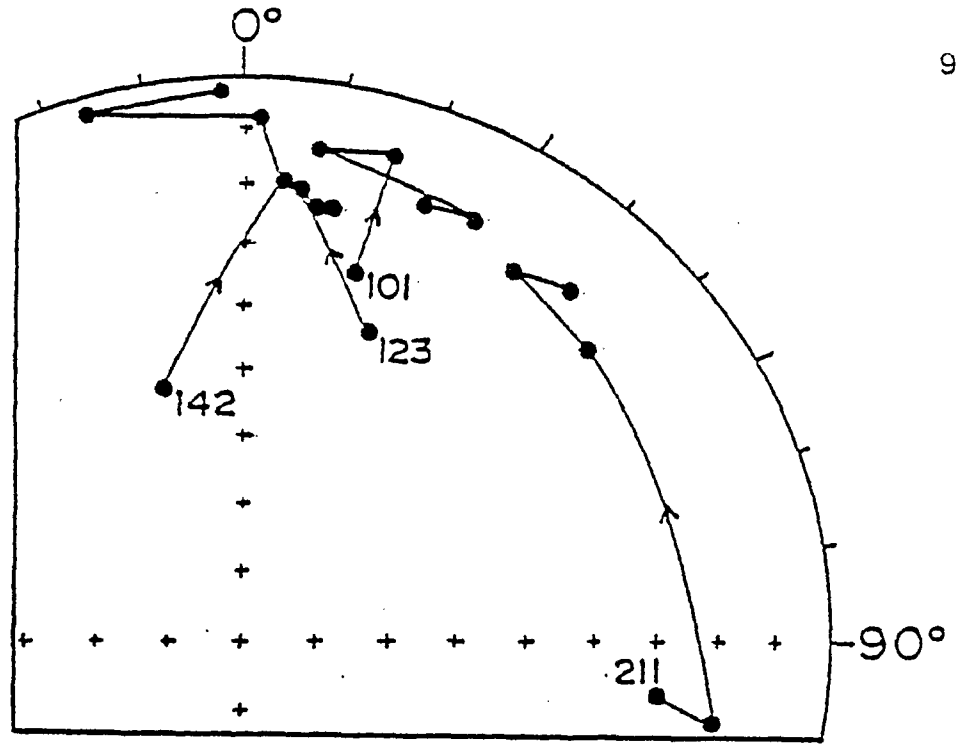

FIG. 30. Equal area projection showing the change in direction on progressive chemical leaching of pilot specimens.

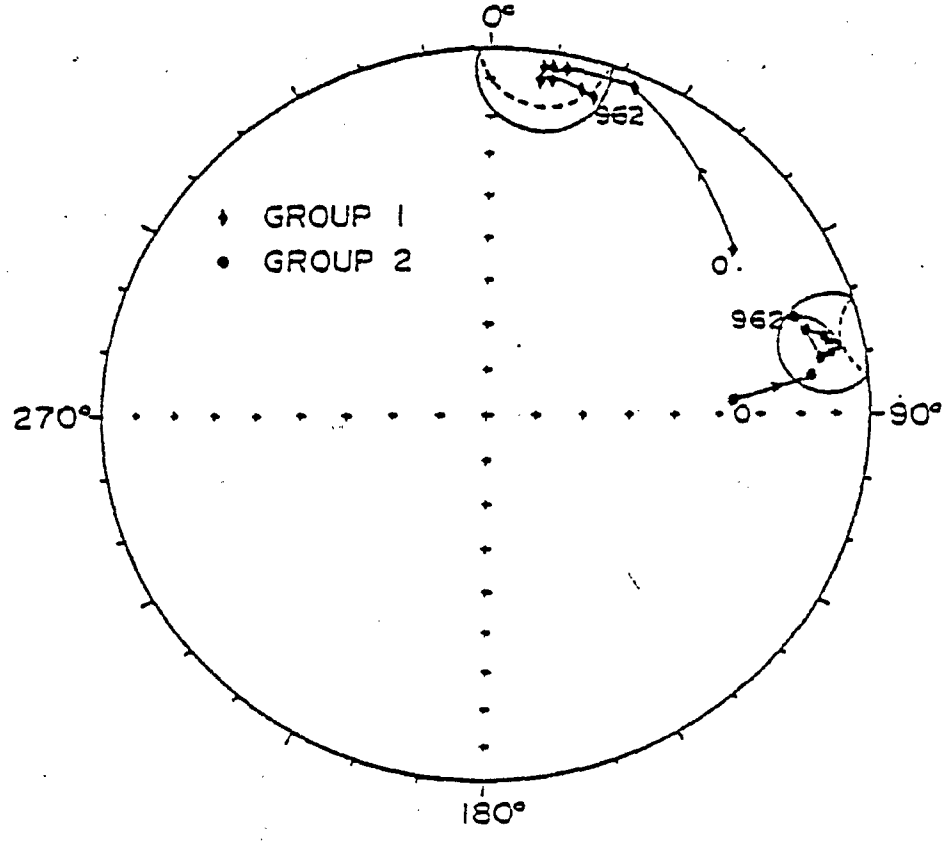

FIG. 31. Demagnetization Curves - Chemical.

a)Equal area projection showing the change in direction on progressive chemical leaching at times of 0,50,96,256,312,410,506,626 and 962 hours for IF pilot specimens. Symbols and conventions as in Figure 21.
b)Remanence Intensity is plotted as a ratio of the NRM intensity against the time of leaching.
c)Paleomagnetic Stability Index.

chemical solubility spectra.

4.8b Remaining Specimens

Of the 80 specimens used for the following experiment, a total of 39 survived the leaching for the full length of the experiment (1656 hours). Because of the lack of control in the middle period of the experiment (300 -1600 hours), due to an instrument malfunction, the further study involving 40 specimens was set up. For the purpose of this report, and because upon visual inspection the results appear identical, only the results of the latter study are discussed here.

Of the 40 specimens, 6 disintegrated within 100 hours making further measurement impossible. The data from these specimens were rejected. The banding revealed by leaching in one specimen was almost parallel and not perpendicular to the core axis indicating an orientation error. The data from this specimen was subsequently rejected. Of the remaining 33 specimens the direction isolated in 17 of them fall into group 2, and that isolated in 13 of them into group 1. The data from the remaining 3 specimens was considered insufficient to define groups 3 and 4 and were thus rejected. The survival rate is therefore 75%.

Figure 31a shows the progressive directional changes for the specimens averaged according into which group they fall. Both groups show the removal of unstable steeply inclined components within 50 - 100 hours, presumably carried either by relatively soluble, coarse grained magnetite, or by magnet-

ite within a magnetite band which is attacked faster than magnetite distributed within a cherty band. Thereafter, there is little directional change as the remaining carriers are attacked, showing that the stable direction has been isolated. Subsequent attack leaves the chemically less soluble phase, hematite, and while there is a slight change in direction, the difference is not statistically significant. The PSI curves (Fig. 31c) show this stability of directional change as initial rates of directional change exceeding 500 mdeg/hour rapidly decrease to less than 20 mdeg/hour after 300 hours. The intensity decay curves (Fig, 31b) show the efficiency of the chemical cleaning process as more than 96% of the magnetization is removed within the experimental period. The similarity of the decay curves for the two groups shows that in terms of chemical solubility spectra there is no difference between the magnetic carriers for the two components.

Vector diagrams (Fig. 32) of the progressive demagnetization indicate a component of magnetization associated with the removal of relatively soluble coarse and presumably multidomain grains of magnetite, and a component which is removed during continued leaching of the magnetite and hence attack of smaller single domain grains. There is no change in magnetization vector direction after the magnetite has been leached from the specimens. Thus, the stable direction is also carried by detrital grains of hematite or by in-

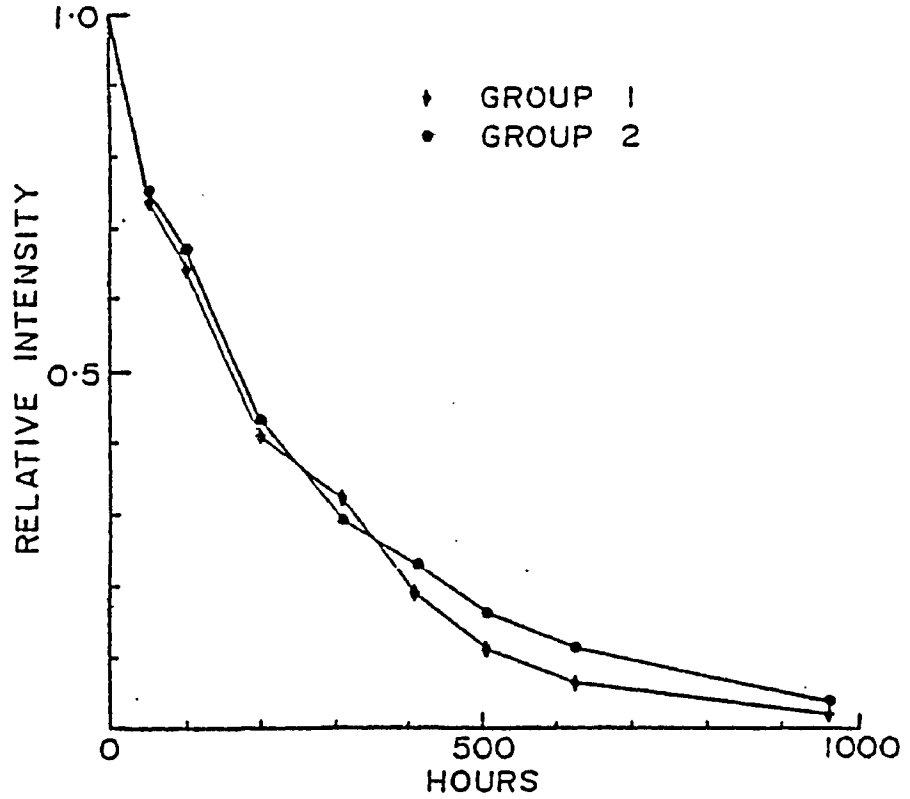

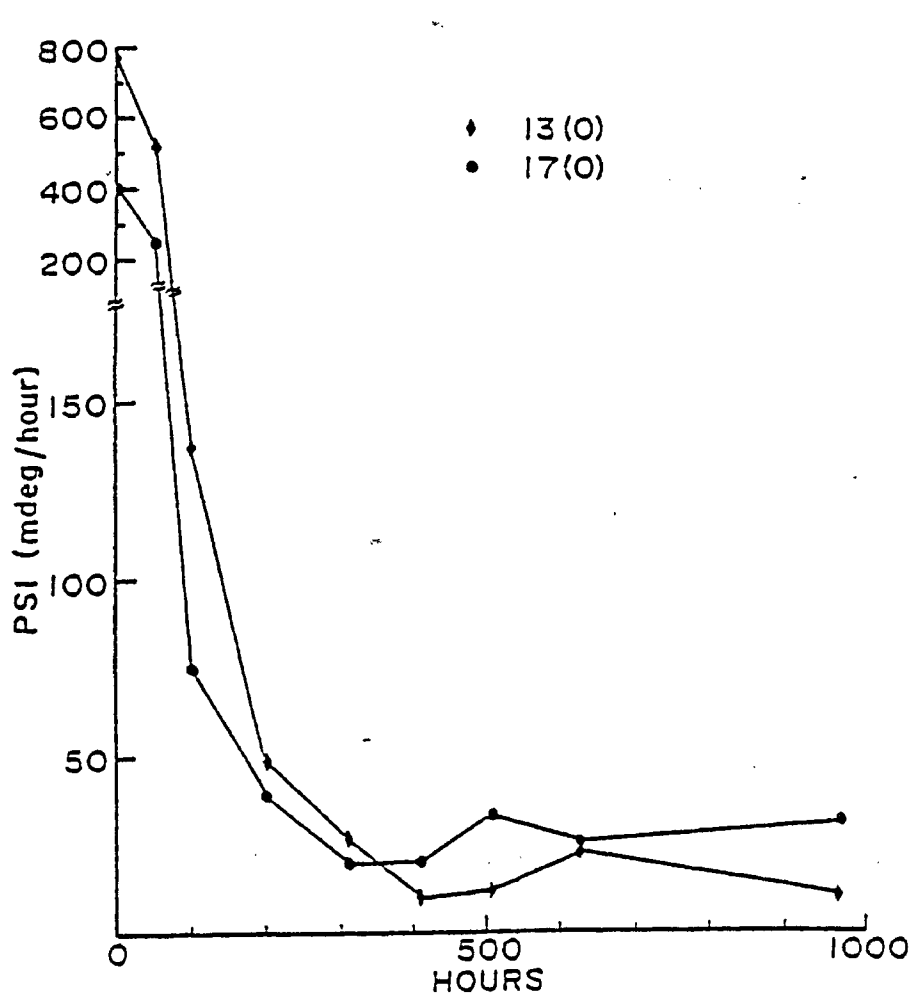

FIG. 31. contd.

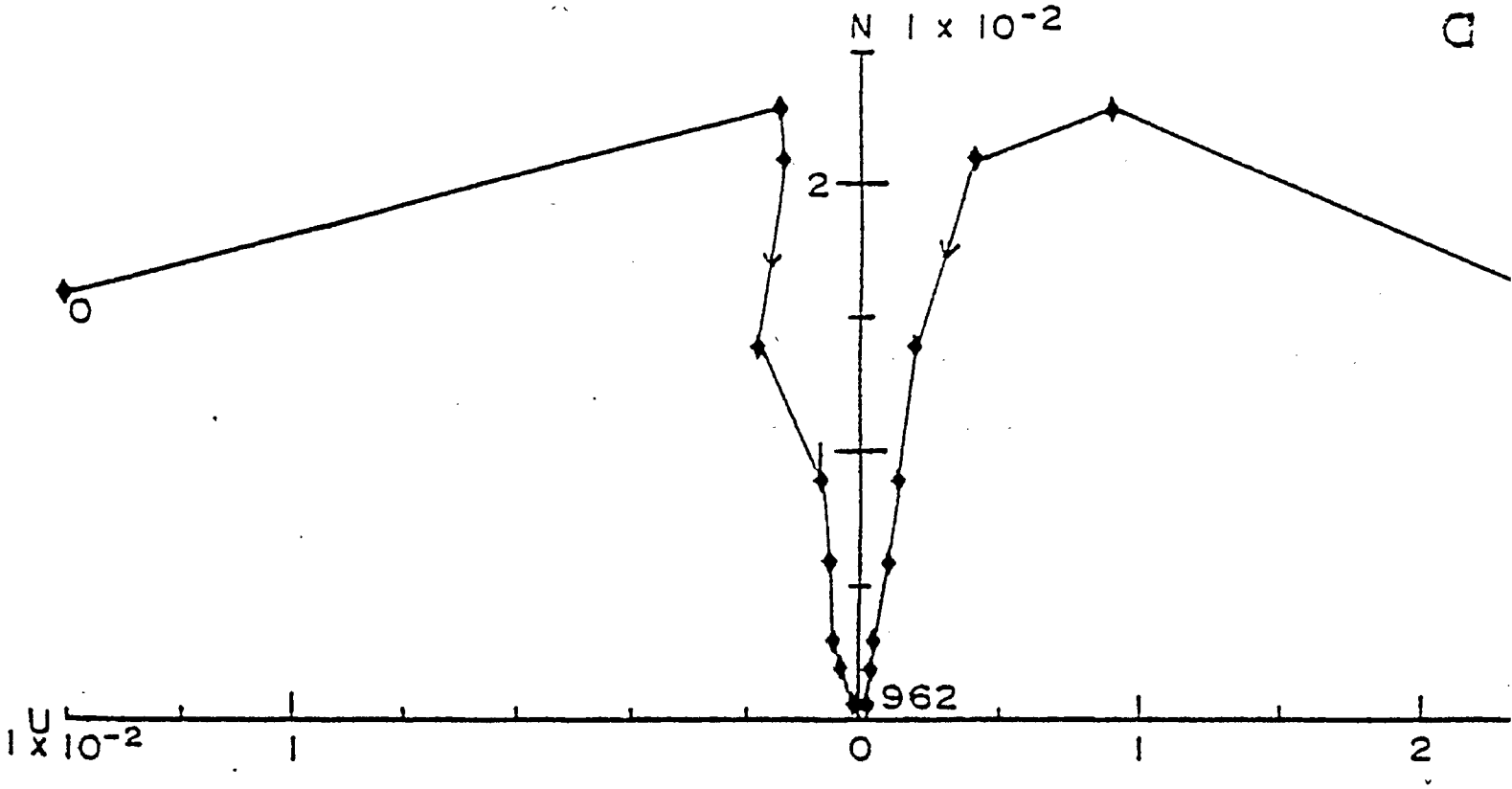

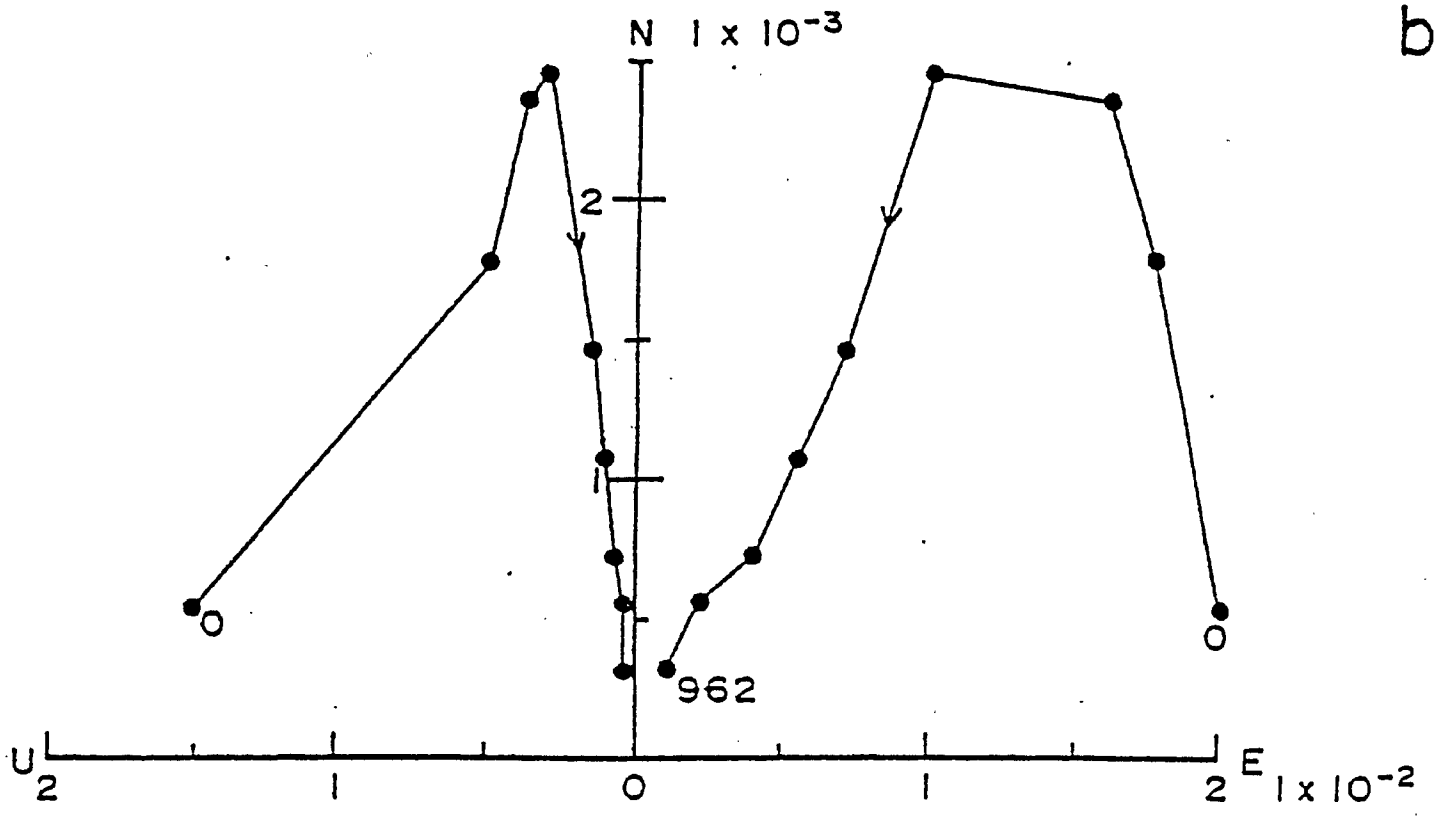

FIG. 32. Demagnetization Vector Diagrams - Chemical.

Symbols and conventions as used in Figure 22. Numbers represent hours of leaching. Intensity in $emucm^{-3}$.

completely attacked small single domain titano-magnetite grains.

Table 18 summarizes the remanence directions isolated during chemical leaching and those isolated by the various demagnetization techniques discussed previously. The excellent agreement between the techniques illustrates the presence of an A component directed at (354.3°, 2.9°), a B component at (79.1°, 1.4°) and a magnetically 'soft' C component at (278°,78°)

4.9 AF CLEANING OF HOST ROCK

4.9a Pilot Specimens

On first inspection, the pilot specimens appear to show no common behaviour on AF step demagnetization suggesting that the remanence is unstable to AF cleaning. However, after rejection of specimens showing random directional changes the surviving specimens (76%) all show a marked stability even in high demagnetizing fields. Once again, the directions of these more stable specimens cluster into four relatively poorly defined groups with antiparallel components. After grouping and averaging the directions isolating the same component, the stability of the remanence is clearly seen. Figure 33a shows the directional changes of the residual remanence. The PSI curves are shown in Figure 33c. They both illustrate the absence of any significant viscous remanence. Low initial rates of directional change in the order of 50 deg/dT remain the same throughout the demagnetization

TABLE 18. Summary of remanence directions of IF specimens during demagnetizati

Group	Number of specimens N	Mean remanence direction				
		Length R	Decl. °	Incl. +down	K	A95 °
A component						
AF pilots	17	14.854	0.0	5.7	7.5	14.0
AF remaining specimens	43	36.267	3.7	5.4	8.5	8.2
Thermal pilots	9	8.157	6.1	7.4	9.5	17.6
Thermal demag. @ 500°C	38	29.060	356.8	11.2	4.1	13.1
Thermal demag. @ 600°C	38	28.077	358.1	6.2	3.7	14.0
Chemical leaching	13	11.317	9.4	4.5	7.1	16.7
B component						
AF pilots	19	16.409	84.4	6.8	6.9	13.7
AF remaining specimens	52	45.482	80.6	6.1	10.8	6.4
Thermal pilots	7	6.152	92.3	11.6	7.2	27.2
Thermal demag. @ 500°C	42	35.671	79.2	11.3	6.5	9.4
Thermal demag. @ 600°C	42	32.452	88.1	-3.3	4.3	12.1
Chemical leaching	17	15.297	79.0	11.0	9.4	12.3
Isolated by least squares						
A component	38	33.742	354.3	2.9	8.7	8.4
B component	25	23.146	79.1	1.4	12.9	8.4
C component	27	20.074	278.4	77.7	3.8	16.7

NOTES: R is the length of vector resultant.
K is Fisher's (1953) precision parameter.
A95 is the radius of 95% confidence (Fisher 1953) in degrees.
A component refers to directions centred on (360°,0°); B component refers to directions centred on (90°,0°). In both cases, normal and reversed components have been combined.
C component refers to a population of steeply inclined directions.

a

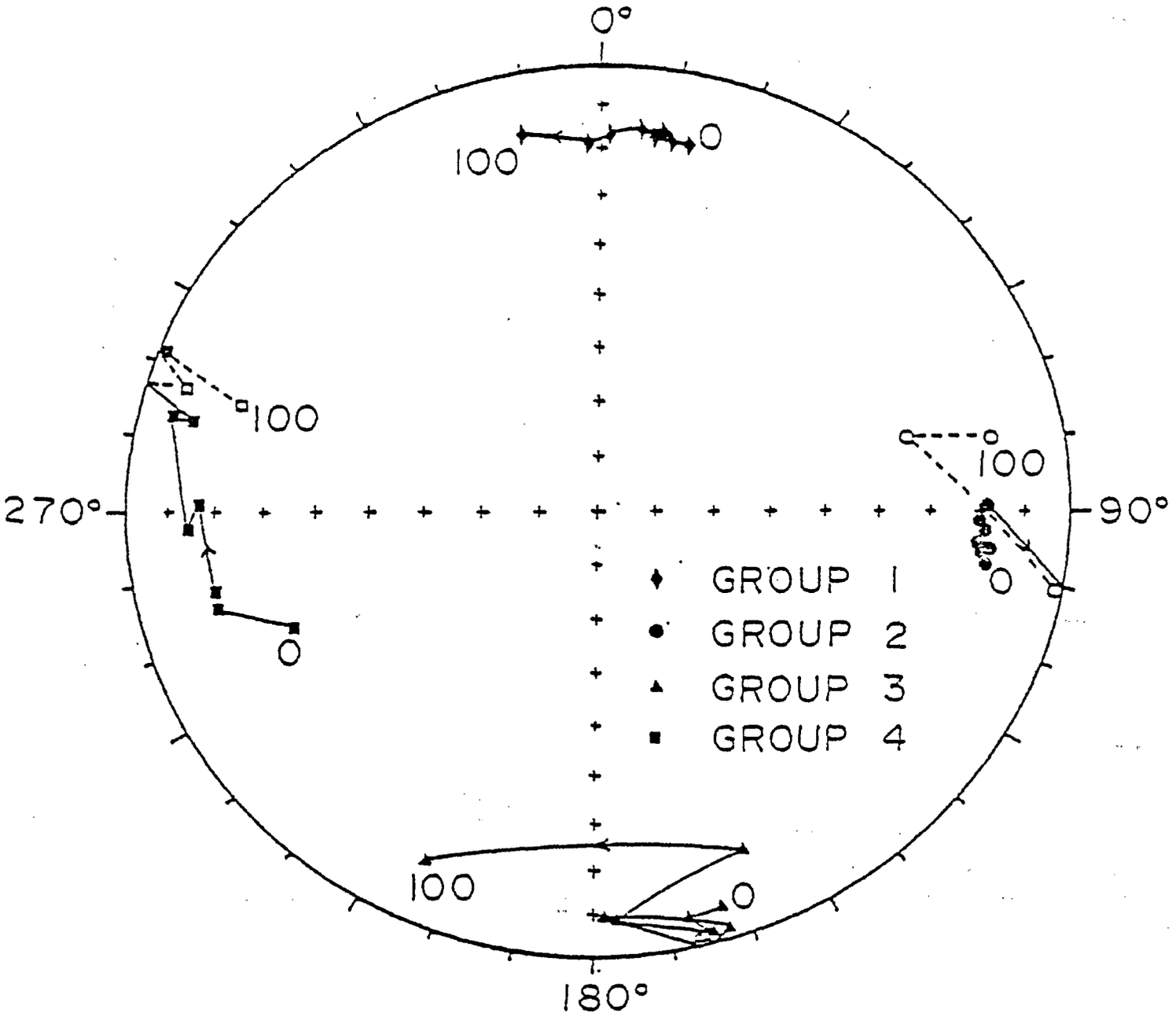

FIG. 33. AF Demagnetization Curves; Host Rock

a)Equal area projection showing the change in direction on progressive AF demagnetization in fields of 0,5,10,15,20,30,40,60,80 and 100mT, for HR pilot specimens. Symbols and conventions as used in Figure 21.

b)Remanence Intensity is plotted as a ratio of the NRM intensity against the demagnetizin field.

c)Paleomagnetic Stability Index for above directional changes.

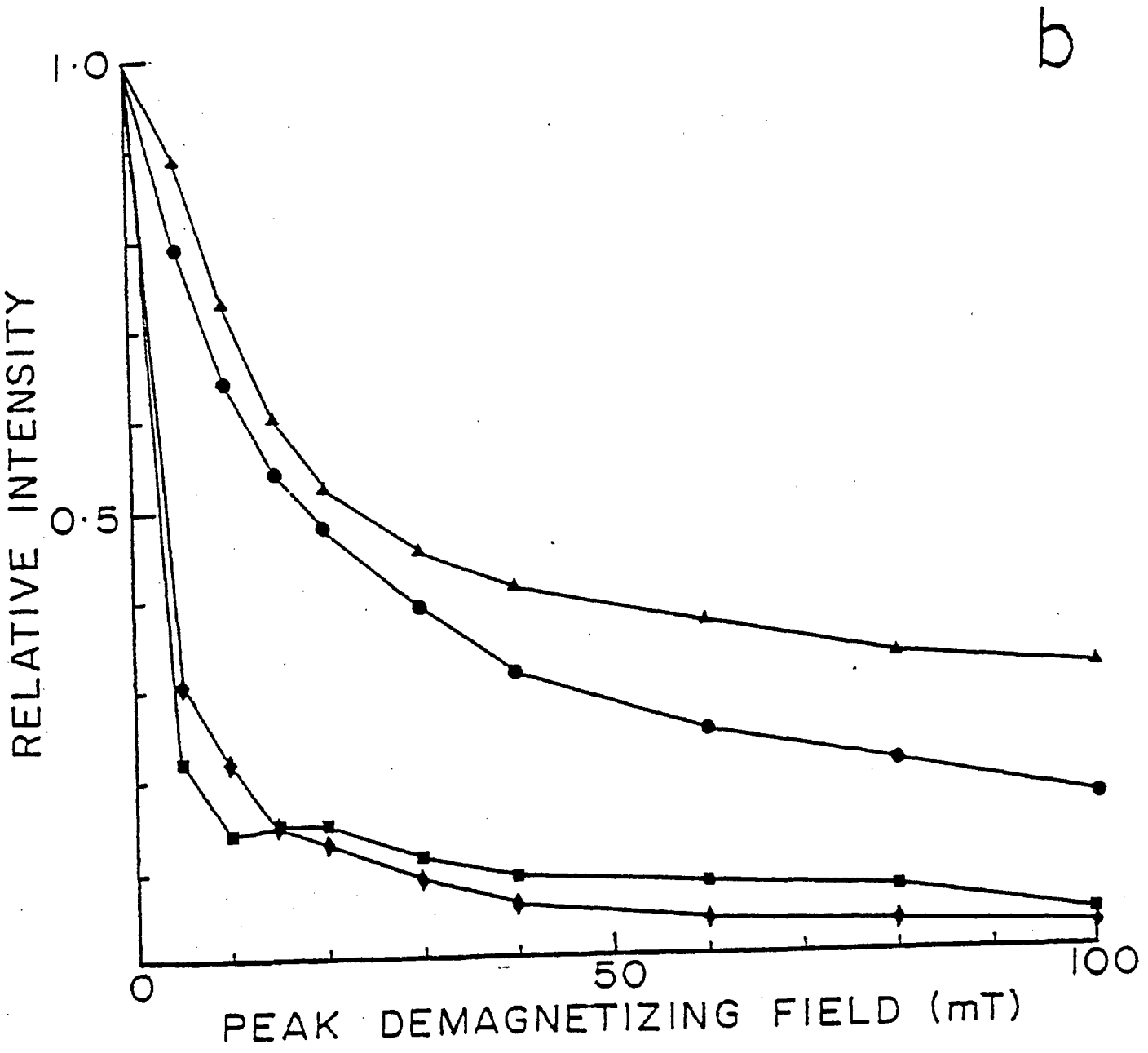

FIG. 33. contd.

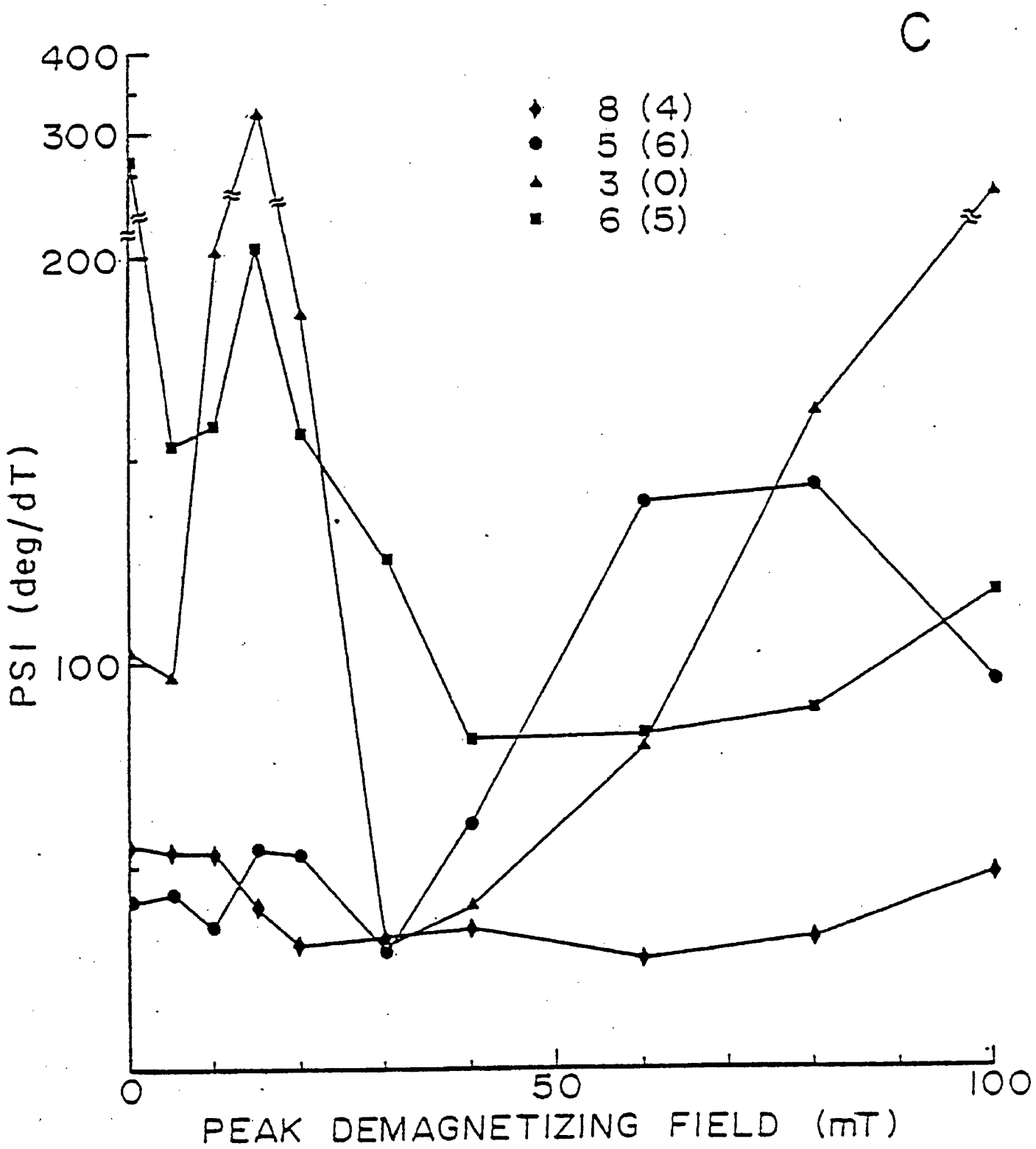

FIG. 33. contd.

process up to 60mT. Above 60mT the curves record an increasing rate of directional change from step to step as larger random ARM components are progressively added.

The intensity decay curves (Fig. 33b) show the presence of a relatively large unstable component removed in the 0 - 5mT step and thereafter a gradual intensity decay up to 100mT, where in groups 1 and 4 there is still a large component stable to AF cleaning. Thus, both the southerly directed and the easterly directed components appear to be less stable to AF demagnetization than their antiparallel components.

The optimum cleaning field has been selected on inspection of PSI mimima and agreement between the vector removed and the measured vector. In most cases, as shown by Figure 23, this field is less than 40mT and the relative intensity of the stable remanence (Fig. 24) ranges from 10% to 80% of the original intensity.

4.9b Remaining Specimens

The remaining specimens from each site were demagnetized using the optimum AF intensity as selected above. After appropriate data screening (4.5a) the site means were computed. The 13 surviving site mean directions (Table 3) form four poorly defined clusters. After grouping normal and reversed components so as to form two groups, the mean directions, although poorly defined, are in close agreement with the A and B components isolated in the IF. Six sites show the A

component with a mean of (3^{o},5^{o}) and seven sites show the B component with a mean of (82^{o},3^{o}). The one surviving diabase site falls into the A component population. These directions and those as defined by the pilot specimens are shown in Table 19.

Also shown in Table 19 are the group means of the unscreened, uncleaned NRM site means. It is evident from this that the paleopole positions obtained from the initial NRM directions are going to be just as reliable as those obtained after having gone through an elaborate series of demagnetization and screening techniques. The main problem here is one of numbers of sites, with such a high rejection percentage obviously leading to poorly defined populations. This perhaps points out that AF demagnetization is not always imperative and may in fact be misleading. Obviously, it is impossible to know in advance if the initial NRM component is useful unless the different magnetization tests are carried out, but the number of pilot tests may be reduced and the interpretation of the data improved.

4.9c Fold Test

The angular variance ratio test as described previously (4.6d) was used to compare the AF cleaned directions corrected for bedding attitude with those uncorrected for bedding. The results are summarized in Table 20. The first test compares the corrected and uncorrected directions isolating the A

TABLE 19. Summary of host-rock remanence directions

Group	Number of sites N	Number of specimens B	Mean remanence direction Length R	Decl. °	Incl. +down	K	A95 °
Initial NRM							
Group 1	14	70	11.785	6.5	15.4	5.9	17.9
Group 2	14	70	12.218	83.9	18.9	7.3	15.8
Group 3	3	15	2.503	177.9	11.9	4.0	71.9
Group 4	6	30	5.625	249.5	-1.8	13.3	19.0
AF pilots							
A component							
Normal specimens		8	5.708	5.9	14.0	3.1	38.2
Reversed specimens		3	2.719	176.0	6.3	7.1	50.0
All specimens*		11		358.6	5.0	24.6	52.8
B component							
Normal specimens		5	4.171	89.8	16.0	4.8	38.9
Reversed specimens		6	5.014	265.2	13.3	5.1	33.0
All specimens		11		103.6	4.2	116.7	23.3
Remaining specimens (AF)							
A component	6	18	4.919	3.1	4.8	4.6	34.9
B component	7	21	5.896	81.9	2.6	5.4	28.5
Thermal pilots							
A component		2	1.610	10.7	25.8	2.6	>99.9
B component		7	5.972	78.1	24.0	21.2	57.3

NOTES: R is the length of vector resultant.
K is Fisher's (1953) precision parameter. A95 is the radius of 95% confidence (Fisher 1953).
Where possible site means have been used to determine the mean remanence direction.

TABLE 20. Angular variance ratio tests of host-rock AF data

Group	Number of sites N	Mean remanence direction Length R	Decl. °	Incl. +down	K	A95 °	V	$F_{0.05}$	Result
1. A component									
Corrected	6	4.919	3.1	4.8	4.6	34.9	1.45	2.98	Positive
Uncorrected	6	4.433	332.2	45.2	3.2	44.8			
2. B component									
Corrected	7	5.897	81.9	2.6	5.4	28.5	2.12	2.69	Positive
Uncorrected	7	4.659	42.4	59.4	2.6	47.6			

NOTES: R is the length of vector resultant.
K is Fisher's (1953) precision parameter. A95 is the radius of 95% confidence (Fisher 1953).
V is the variance ratio $\delta_{corr}/\delta_{uncorr}$ of the two populations being compared.
$F_{0.05}$ is the theoretical statistic $F_{2(N_{corr}-1),2(N_{uncorr}-1),0.05}$ thereby setting the test at the 95% confidence level.

component. The variance ratio of 1.45 is less than the theoretical statistic of 2.98 at the 95% confidence level. Similarly, the seven directions isolating the B component give a variance ratio of 2.12 which is less than the theoretical statistic of 2.69 at the 95% confidence level. Thus the test is inconclusive at this confidence level. If we go to the 75% confidence level, the test results become significantly negative, indicating the direction dispersions are different. This, and the greater precision parameter, K of the corrected mean directions implies that the remanence is prefolding. Bearing in mind the poor precision of the directions, little conclusion can be drawn from this test.

4.10 THERMAL CLEANING OF HOST ROCK

As with AF cleaning, the HR appears unstable to thermal cleaning. Of the 20 pilot specimens selected, only 45% survived. Rejections were made on the basis of high PSI values and large random fluctuations in direction. Of the remaining 9 specimens, 2 isolate the A component to give a poorly defined direction at (11^{o}, -26^{o}) and the remaining 7 specimens show the B component to give a poorly defined mean direction of (78^{o}, 24^{o}). Table 19 summarizes the remanence directions for the HR during AF and thermal demagnetization.

4.11 POLE POSITIONS

The earlier discussion shows the consistent isolation of two stable, prefolding directions. Least squares analysis

of the AF cleaned specimens also isolates a third prefolding direction. These directions give apparent pole positions for the time when the remanence was acquired (Table 21). Figure 34 shows these pole positions superimposed on the apparent polar wander (APW) curve for this period (Irving 1979). Also shown are the pole positions obtained from the Sherman mine study (Symons and Stupavsky 1979). The older pole, from the B component, gives an apparent age of ∿2.7Ga, and may therefore represent the primary remanence of the IF acquired during deposition.

The A component gives a pole position with an age of ∿2.5Ga, representing a prefolding metamorphic event probably associated with the emplacement of the Algoman granite.

The 'soft' C component gives a pole position with an age of ∿2.1Ga, the explanation for which at present is uncertain bearing in mind the prefolding nature of the remanence and the ∿2.2Ga age of the surrounding flat-lying Gowganda formation. However, the large semi-axes for the 95% confidence ellipse suggest that this age may well be erroneous by a factor of 150Ma, giving a possible age of 2.35Ga for this remanence. It may thus represent a burial metamorphic event or a Nipissing component.

4.12 MAGNETIC MODEL

4.12a Infinite Depth Extent

The total intensity of the Earth's magnetic field at

TABLE 21. Pole positions for the Moose Mountain Iron-Formation

Group	Number of specimens N	Mean remanence direction Length R	Decl. °	Incl. +down	K	A95 °	Pole Position Long. (°W)	Lat. (°N)	d_p °	d_m °
A component	38	33.742	354.3	2.9	8.7	8.4	253.1	44.4	4.2	8.4
B component	25	23.146	79.1	1.4	12.9	8.4	343.5	8.0	4.2	8.4
C component	27	20.074	278.4	77.7	3.8	16.7	115.1	45.1	29.4	31.3

NOTES: Least squares isolated components reported because of greater precision.
Reversed vectors in antiparallel position.
For the pole position the longitude and latitude are in degrees west (Long. °W) and north (Lat. °N) respectively, with d_p and d_m being the semi-axes of the oval of 95% confidence along and perpendicular to the site-pole great circle.

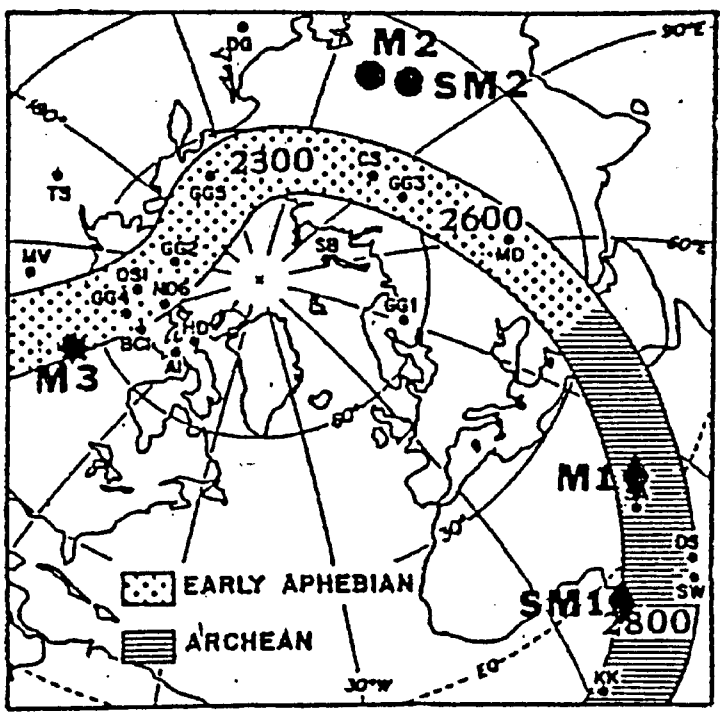

FIG. 34. Apparent polar wander (APW) curve (after Irving, 1979) showing the pole positions.
M1,M2 and M3 from the Moose Mountain mine.
SM1 and SM2 from the Sherman mine.

the Moose Mountain mine is 59,300 gammas with a direction of (8.3°W,76.0°)(C.D.M. 1961).

The magnetic anomaly produced by the Pit 2 deposit, with an average width of 50m will be used as an example. Using the determined k_1 of 0.110 cgscm^{-3} (4.2), the determined k_{11}/k_1 of 1.75 (4.3), a realistic demagnetizing factor of $F = 2\pi$ (Gay, 1963) and adding the 24% increase from the remanence effect as determined previously (4.4), the aeromagnetic anomaly at a terrain clearance of 305m (1000ft) was calculated for a variety of strike directions and dip values.

Figure 35a illustrates the results for an E - W striking deposit. The variation of peak anomaly with dip and strike is shown in Figure 35b.

The Pit 2 deposit strikes N - S and dips 70°E, giving a computed peak anomaly of 3100 gammas. The measured peak value over Pit 2 is 6200 gammas (GSC 1965), less a background value of 2050 gammas, giving a peak anomaly of 4150 gammas. Thus the calculated and measured peak values agree to within 25%. By comparison, if the pit ore zone is rotated to the horizontal, then the calculated peak anomaly is reduced to ~700 gammas or 22% of its' present value. This is an identical conclusion to that made from the Sherman mine study (Symons and Stupavsky 1979). Because of the close similarity of the magnetic characteristics for the two deposits (Table 22),

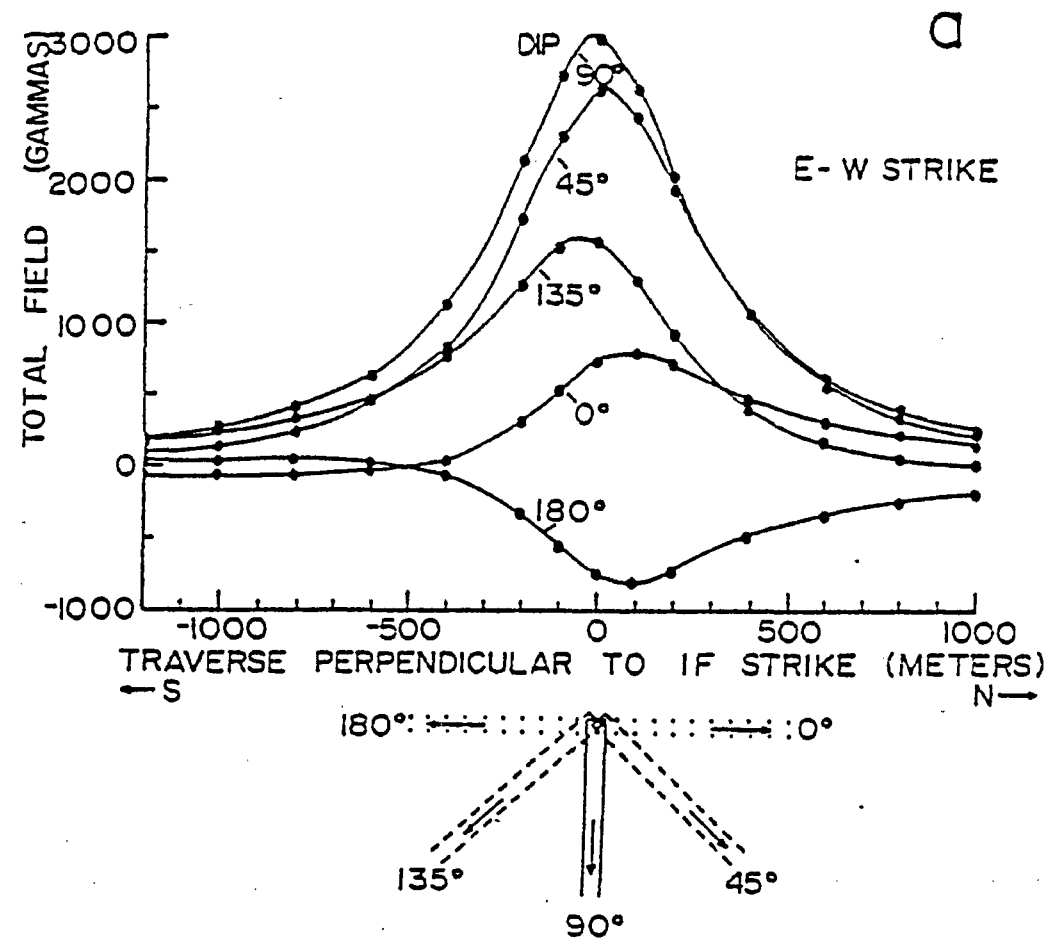

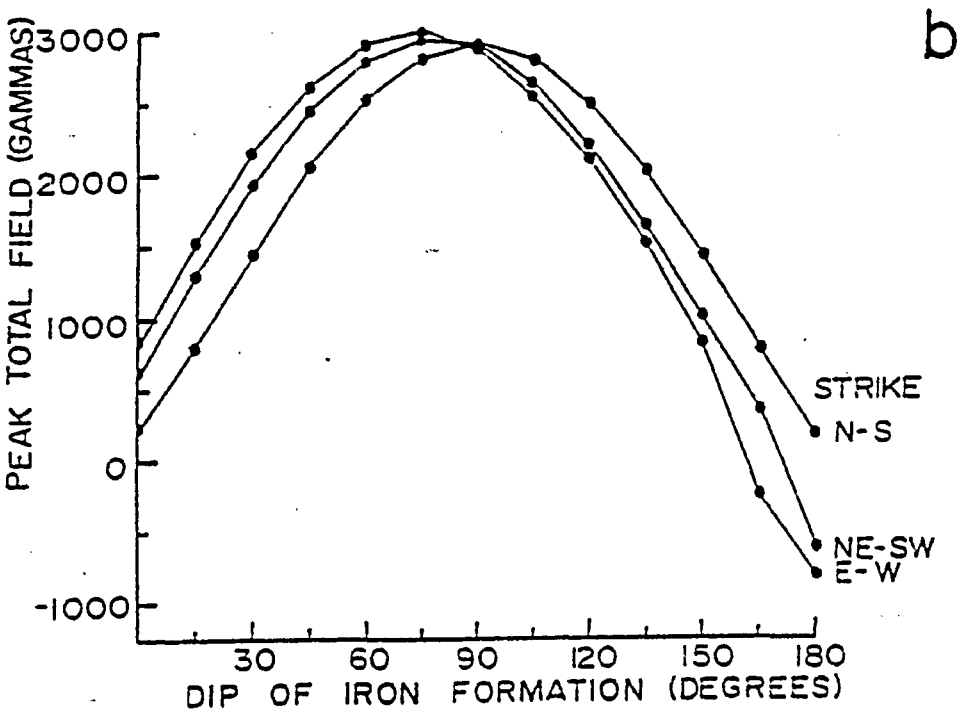

FIG. 35. Computed magnetic anomaly of IF at 305m. elevation.

TABLE 22a. Summary and comparison of magnetic properties of the Sherman mine and Moose Mountain mine iron formations

	Sherman	Moose Mountain
1.Metamorphic grade	low greenschist	upper greenschist amphibolite
2.Magnetic susceptibility 1 bedding plane, k_1 (cgs/cc)	0.096	0.110
3.Anisotropy of magnetic susceptibility, k_{11}/k_1	1.60	1.75
4.NRM remanence (emu/cc) magnetite	2.5×10^{-2}	4.8×10^{-2}
hematite	4.0×10^{-6}	3.9×10^{-6}
5.Koenigsberger ratio, Q	0.46	0.63
6.Effective Q, $Q_e = R/N\cos\theta$	0.22	0.24
	(170.0°,0.1°,5.1°)Pr	(3.7°,5.4°,8.2°)Pr
7.AF demagnetized remanence (N and R cmpnts combined)	(96.1°,-6.6°,9.3°)Pr	(80.6°,6.1°,6.4°)Pr (278.4°,77.7°,16.7°)Pr

NOTES: Remanence directions given as(Decl.,Incl.,A95).
Pr.= Pre-folding @ 95% confidence level. I.= Inconclusive fold-test.
For details of the results listed, see text.

TABLE 22b. Summary and comparison of magnetic properties of the host rock at the Sherman and Moose Mountain mines

	Sherman	Moose Mountain
1.Magnetic susceptibility 1 bedding plane, k_1 (cgs/cc)	4.9×10^{-5}	5.0×10^{-5}
2.NRM remanence (emu/cc)	2.94×10^{-6}	1.99×10^{-6}
3.Koenigsberger ratio, Q	0.104	0.063
	(168°,9°,8°)Pr	(3°,5°,35°)I
4.AF demagnetized remanence (N and R cmpnts combined)	(84°,4°,15°)I	(82°,3°,28°)I

the type curves take almost identical form.

Figures 36a and 36b are the corresponding curves to Figures 35a and 35b, but at an elevation of 50m representing a helicopter flown survey. Actual 50m data were not available for comparison.

The iron formation strike, dip and effective width for each pit are shown in Table 23. The calculated peak aeromagnetic anomaly at a terrain clearance of 305m are also shown. Using the magnetic anomaly produced by the pit 11 deposit as an example, the measured peak value is 2950 gammas, less a background value of 2050 gammas, giving a peak anomaly of 900 gammas. Thus, the calculated and measured peak values are in poor agreement at this elevation. The other pits give similar results (Table 23).

The low value of the observed anomaly and the resulting poor agreement is considered to be a consequence of an IF sheet of finite depth extent. The bipolar nature of the body would result in cancellation of the anomaly due to the N-seeking pole by that due to the S-seeking pole, particularly at high elevation. The magnetic model, assuming infinite strike and depth extent neglects the effect of this S-seeking pole. In view of the laterally discontinuous nature of the ore bodies, it is not an unrealistic interpretation that they are also vertically discontinuous.

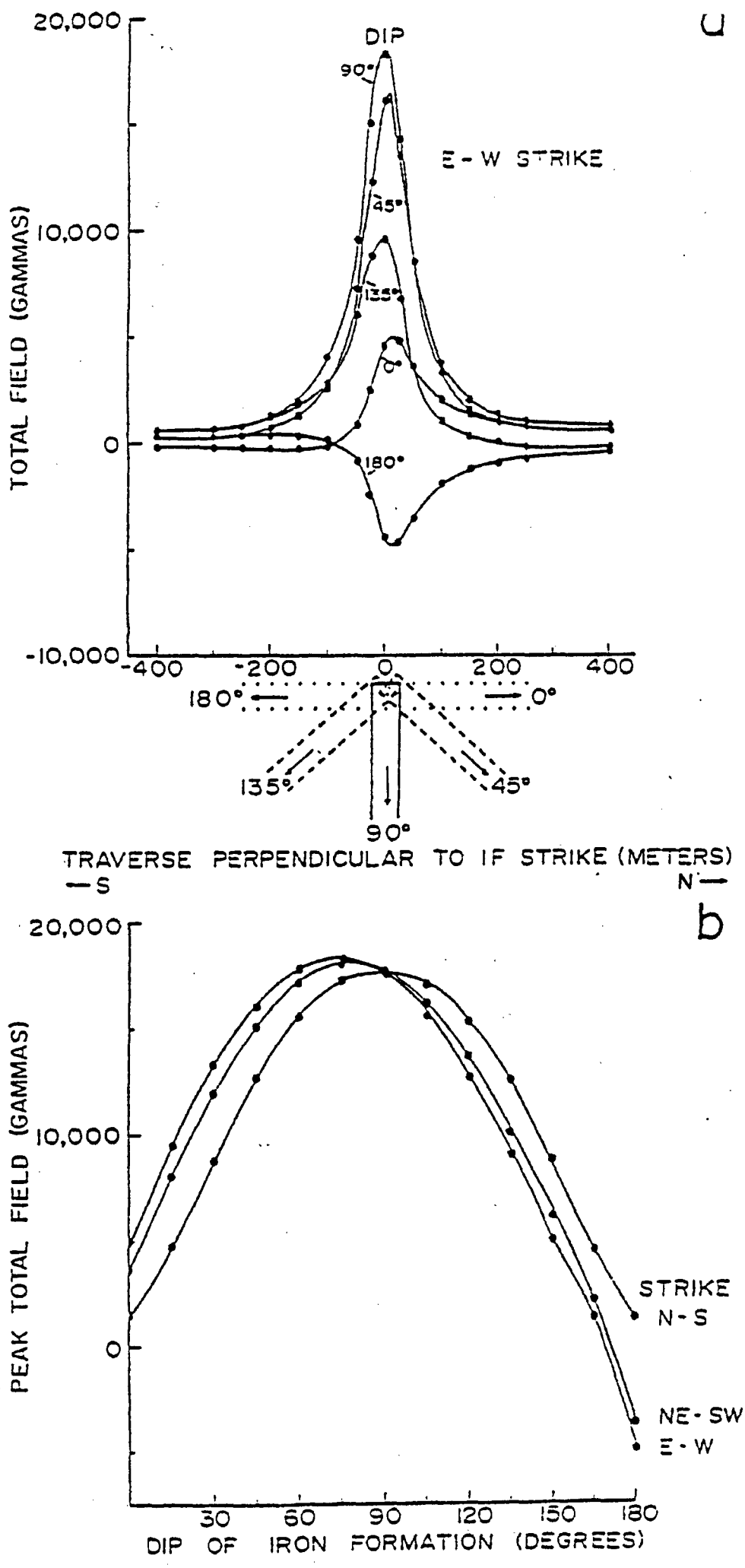

FIG. 36. Computed magnetic anomaly of IF at 50m elevation.

TABLE 23. Summary of aeromagnetic response of IF.

Pit	Strike °	Dip °	Width m.	Peak aeromagnetic response @ 305m. (gammas) Observed	Computed
1	90	80	40		2800
2S	120	70	80		6000
2N	170	70	50	4150*	3100
3	135	80	60		4200
3A	170	70	35		3000
10	90	80	65	1000	3900
11	150	65	35	900	2700

NOTES: Observed response from Map 1519G Venetian Lake, Ontario (GSC 1965).
* response of individual pits indistinguishable.
Strike reported from 0°- 180° for the purposes of the program.

TABLE 24. Summary of inferred depth extent of IF

Pit	Observed anomaly (gammas)	Inferred depth extent (metres)
2S	4150	400
10	1000	70
11	900	150

4.12b Finite Depth Extent

To confirm this interpretation, the magnetic model computations were modified to take an IF of finite depth extent into account. By computing the anomaly due to the buried S-pole and subtracting this from the anomaly due to the N-pole, the effective anomaly can be calculated.

Figure 37 shows the parameters used; the symbols used being the same as those defined by Gay (1963). Two additional parameters can be defined having the following values:

$$W = \tan^{-1}\left(\frac{y - l\cos\delta}{z + l\sin\delta}\right)$$

and;

$$z' = z + l\sin\delta$$

where l is the depth extent of the IF along the dip direction.

Thus for each component, z to be computed, a $z_{(+)}$ can be determined as due to the N-pole using values of ψ, z; and a $z_{(-)}$ can be determined as due to the S-pole using values of W, z'.

The effective value of z can thus be defined by:

$$z_{eff.} = z_{(+)} - z_{(-)}$$

The program was modified accordingly to perform this additional computation (Appendix II). The depth extent, l was then varied so as to give optimum agreement between the computed curve and the observed aeromagnetic anomaly for the Pit 11 ore body. Figure 38a shows the results with a depth extent of 150m. The agreement is excellent bearing in mind

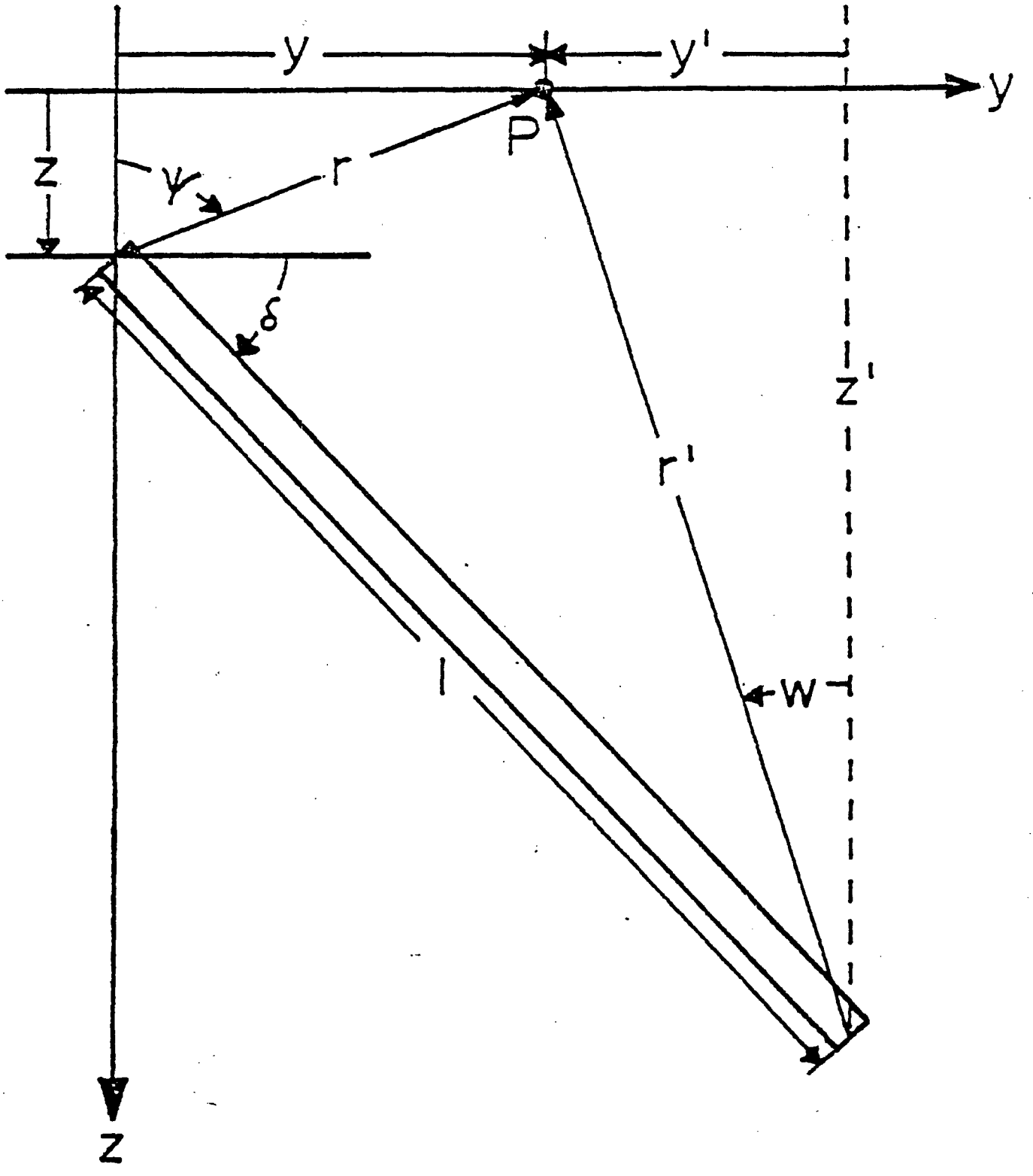

FIG. 37. Geometry of the IF of finite length in the y-z plane.

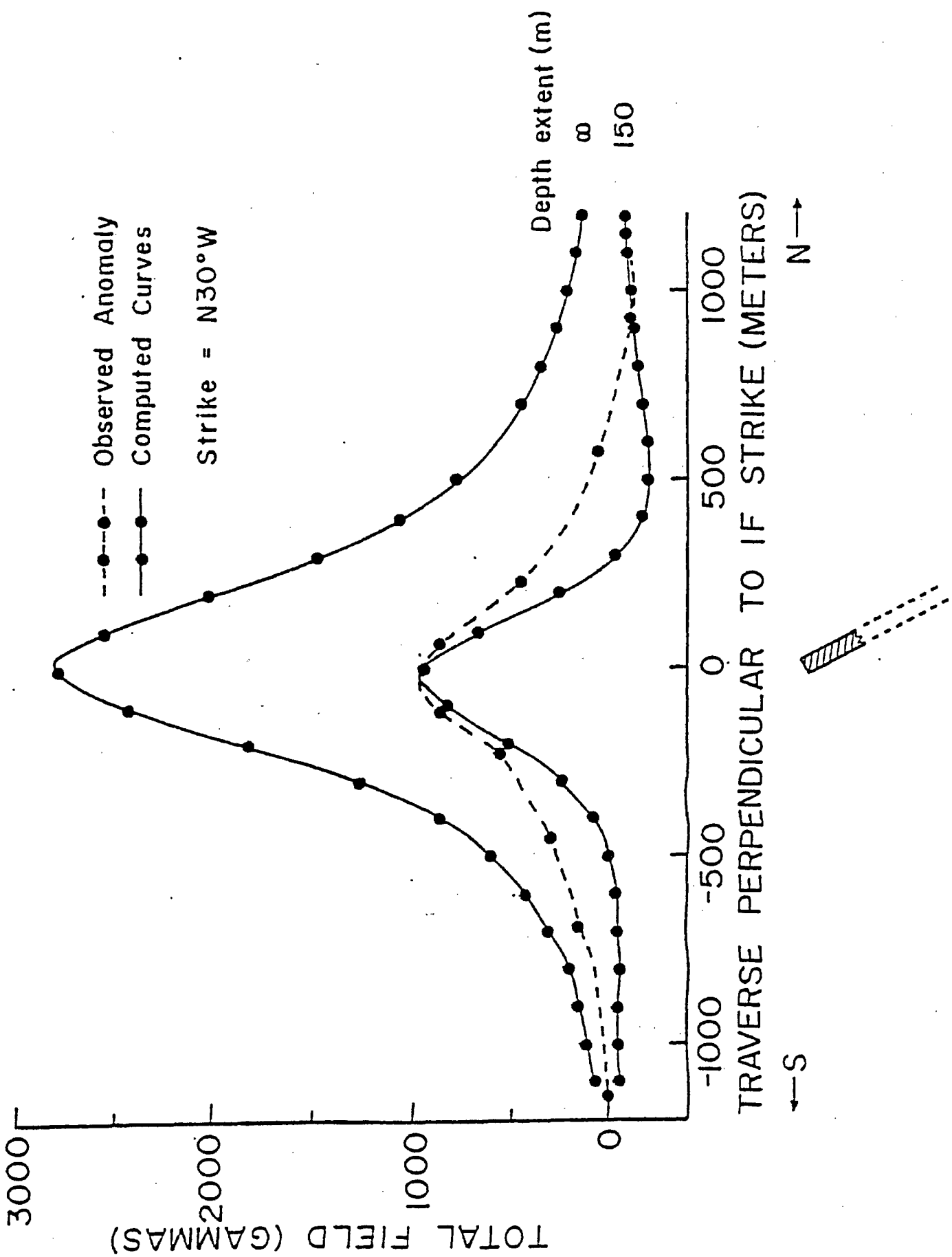

FIG. 38a. Computed and observed magnetic anomalies over Pit 11 at an elevation of 305m.

that lean IF and HR will contribute to the observed anomaly on either side of the peak anomaly. Also shown are the observed and computed anomalies for a ground survey at an assumed elevation of 5m (Lowphos Ore Ltd. 1962). The contribution at this height of the S-pole is minimal. Once again, agreement is excellent (Fig. 38b).

The other pits give similar results with depth extents of between 70m and 400m suggested. Table 24 summarizes the results. A finite depth extent is considered consistent with the observation that this IF occurs in many faulted segments.

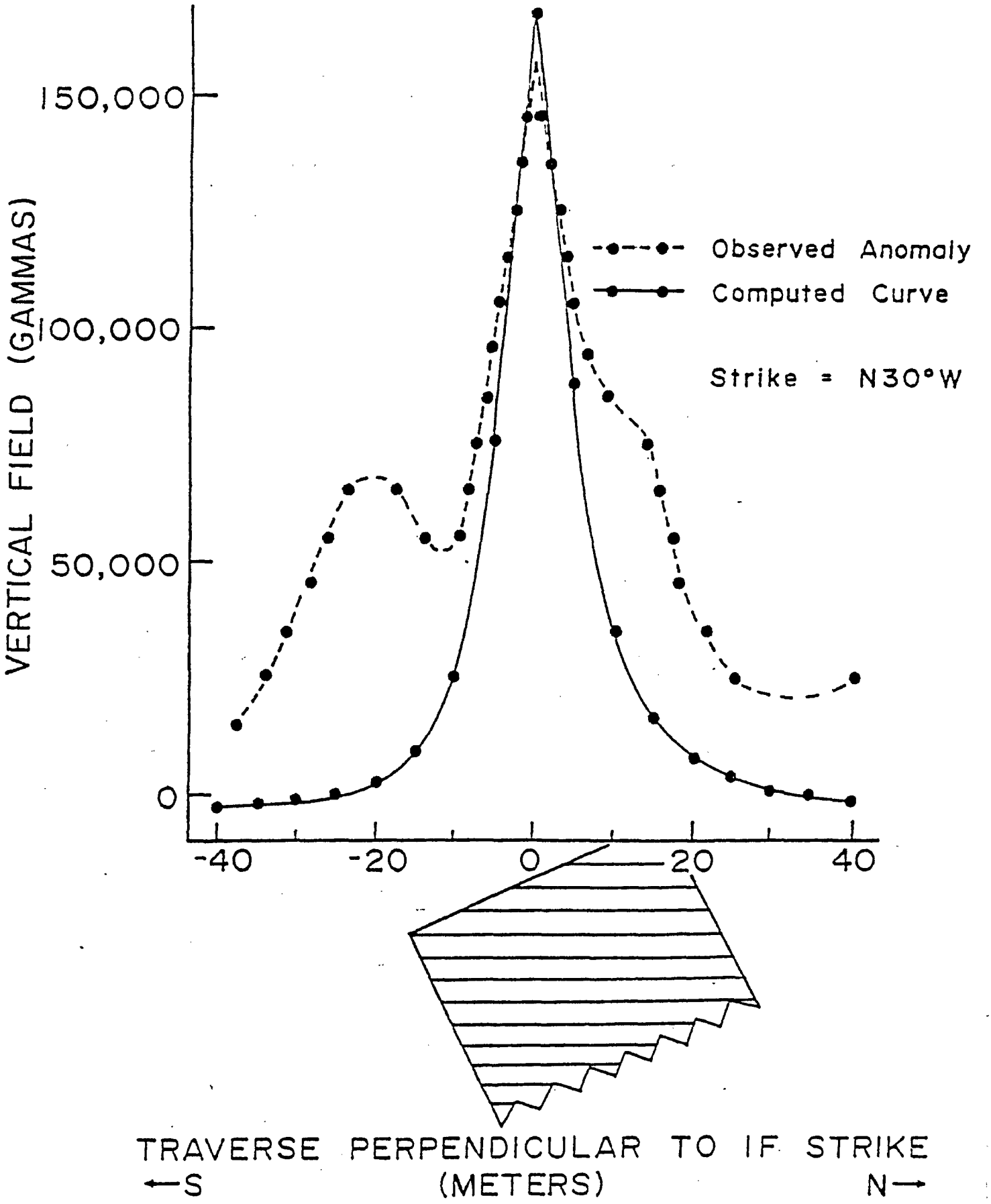

FIG. 38b. Computed and observed magnetic anomalies over Pit 11 at an elevation of 5 m.

CHAPTER V

CONCLUSIONS AND RECOMMENDATIONS

From the preceeding discussion, a number of conclusions can be drawn:

1) The striking agreement of the Moose Mountain mine magnetic parameters with those of the Sherman mine (Table 22), suggests that the genesis of the two ore bodies was very similar. The higher NRM intensities and higher anisotropy of susceptibility at Moose Mountain are thought to be the result of the higher metamorphic grade.

2) The close similarity of magnetic characteristics for these two Algoma-type banded IF suggests that the values may be representative of Algoma-type IF as a whole and may therefore be used in magnetic anomaly computation for exploration purposes.

3) For anomaly interpretation purposes the HR NRM can be omitted because the induced magnetization of the IF is approximately 18,000 times greater.

4) If the IF NRM directions were entirely aligned with the Earth's field, then the remanence would increase the induced anomaly by 63%. Thus the remanence intensity and direction is an important factor.

5) Computation of the magnetic anomaly curves, incorp-

orating the effects of anisotropy, demagnetization and remanence show that if the IF were flat-lying, the peak anomaly would be reduced to 22% of its' present value. Thus IF dip is a critical factor.

6) Variation in IF strike has little effect on the value of the peak anomaly.

7) Close agreement between observed and expected anomalies is only achieved using a model of finite depth extent. This, and the fact that the IF occurs in many faulted segments suggests a finite depth for the IF segments of between 70m and 400m.

8) The present explorational rationale of only using the most intense vertical magnetizations as targets for examination is insufficient and unjustified.

9) A more logical approach to exploration is outlined:

i) Locate potential area of interest from regional geology,

ii) Determine regional strike and dip,

iii) Using realistic values of susceptibility, anisotropy, demagnetization, remanence and depth, compute the type curves for the aeromagnetic anomaly for a number of thicknesses and depth extents,

iv) Match observed magnetic anomalies with type curves, and

v) Use detailed mapping and diamond drilling to put restraints on thickness, depth of burial and depth extent.

10) AF, thermal and chemical demagnetization of the IF

results in the isolation of two stable, well defined prefolding remanence components. An A component at (354°, 3°), and a B component at (79°, 1°).

11) These components are not significantly different from those isolated in the Sherman mine IF after tectonic correction.

12) Least squares analysis, while isolating the same components as isolated by conventional methods, also reveals a third stable component at (278°, 78°). While seemingly a prefolding remanence, the apparent age of 2.1Ga infers a postfolding origin representing a 'burial' metamorphic event, or perhaps a Nipissing related component.

13) The HR NRM directions poorly define two components not significantly different to those from the IF. These components are similar in direction to, and are statistically more precise than those obtained from AF and thermal demagnetization.

14) The inferred paleomagnetic pole position for the IF is 343°W, 8°N (d_p = 4°, d_m = 8°). This pole is based upon least squares treatment of AF demagnetization data which is statistically most precise. This pole position is in good agreement with the Precambrian apparent polar wander (APW) path for North America (Irving 1979) and gives an age of 2.7Ga.

15) The inferred pole position defined by the A component gives an age of 2.5Ga and may therefore represent a prefolding metamorphic event associated with the emplacement

of the Algoman granite.

16) The stability of the primary remanence in magnetite is attested by a blocking temperature close to the Curie point of magnetite (T_c = 580°C) and well below that for hematite (T_c = 650°C).

APPENDICES

APPENDIX I

Computer program for the calculation of the magnetic anomaly over a thin sheet of infinite strike and depth extent.

```
0001            DIMENSION V(100),Y(100),VQ(100),NAME(40)
0002            DIMENSION VH(100),T1(100),TT(100),TIT(100)
0003         10 FORMAT(8F8.0)
0004            DIMENSION X(90)
0005          1 FORMAT(40A2)
0006         61 FORMAT('0')
0007          2 FORMAT(F8.1,5F6.1,F10.7,2F6.3)
0008          3 FORMAT(1H0,123H*TOTAL FIELD IN GAMMAS*INCLINATION**ANOMALY**STRIKE
             1**DIP**A.WIDTH(M)**DEPTH(M)**CROSS DIP MS**PARALLEL DIP MS**Q-RATIO*
             2*          )
0009          4 FORMAT(1H0,5X,F8.1,13X,F6.1,14X,F6.1,F6.1,1X,F6.1,4X,F6.1,5X,F10.7
             1,5X,F10.7,3X,F7.3)
0010            PI=57.296
0011            READ1,NAME
0012          6 READ2,RINT1,RINC1,STR,DIP,T,Z,S,R,Q
0013            IF(RINT1)7,7,8
0014          8 RR=R*S
0015            S=S*(1.0+Q)
0016            R=R*S
0017            RINC1=RINC1/PI
0018            STR=STR/PI
0019            DIP=DIP/PI
0020            RINC=ATAN(TAN(RINC1)/SIN(STR))
0021            RINT=RINT1*SIN(RINC1)/SIN(RINC)
0022            B=RINC-DIP
0023            BB=ATAN(TAN(B)/(R*(1.0+12.566*S)))
0024            AMPL=S*2.0*RINT*T*COS(B)/(Z*COS(BB))
0025            AMPH=AMPL*SIN(STR)
0026            N=41
0027            DO5I=1,N
0028            A=I
0029            Y(I)=(A-1.0)*5.0-60.0
0030            PSI=ATAN(Y(I)/Z)
0031            VV=COS(PSI)*(R*COS(PSI)*COS(BB)+SIN(PSI)*SIN(BB))
0032            VVH=COS(PSI)*(COS(PSI)*SIN(BB)-R*SIN(PSI)*COS(BB))
0033            V(I)=AMPL*VV
0034            VH(I)=AMPH*VVH
0035            TT(I)=V(I)*SIN(RINC1)+VH(I)*COS(RINC1)
0036            T1(I)=V(I)*COS(RINC1)-VH(I)*SIN(RINC1)
0037            TIT(I)=SQRT(T1(I)*T1(I)+(RINT1+TT(I))*(RINT1+TT(I)))
0038            X(I)=V(I)
0039          5 CONTINUE
0040            STR=PI*STR
0041            DIP=PI*DIP
```

```
0042                RINC1=PI*RINC1
0043                Q=Q
0044                PRINT3
0045                PRINT4,RINT1,RINC1,STR,DIP,T,Z,S,RR,QQ
0046                PRINT61
0047                PRINT10,Y(1),Y(2),Y(3),Y(4),Y(5),Y(6),Y(7),Y(8)
0048                PRINT10,X(1),X(2),X(3),X(4),X(5),X(6),X(7),X(8)
0049                PRINT61
0050                PRINT10,Y(9),Y(10),Y(11),Y(12),Y(13),Y(14),Y(15),Y(16)
0051                PRINT10,X(9),X(10),X(11),X(12),X(13),X(14),X(15),X(16)
0052                PRINT61
0053                PRINT10,Y(17),Y(18),Y(19),Y(20),Y(21),Y(22),Y(23),Y(24)
0054                PRINT10,X(17),X(18),X(19),X(20),X(21),X(22),X(23),X(24)
0055                PRINT61
0056                CALL PLOT3(Y,TT,N)
0057                GO TO 6
0058              7 CALL EXIT
0059                STOP
0060                END
```

```
0001            SUBROUTINE PLOT3(X,Y,N)
0002            DIMENSION X(N),Y(N),GL(2),VL(2),DT(2),XP(11),RC(62),A(120)
                C       DATA C,BLK/1H+,1H /                                                                  002
0003            INTEGER C, BLK, A                                                                            003
0004            DATA C, BLK / '+', ' ' /                                                                     004
                C       DATA(RC(I),I=1,62)/1.E29,1.E28,1.E27,1.E26,1.E25,1.E24,1.E23,                        005
0005            DATA RC/1.E29,1.E28,1.E27,1.E26,1.E25,1.E24,1.E23,1.E22,1.E21,1.E2
                10,1.E19,1.E18,1.E17,1.E16,1.E15,1.E14,1.E13,1.E12,1.E11,1.E10,1.E9
                2.,1.E8,1.E7,1.E6,1.E5,1.E4,1.E3,1.E2,1.E1,1.,1.E-1,1.E-2,1.E-3,1.E-
                34,1.E-5,1.E-6,1.E-7,1.E-8,1.E-9,1.E-10,1.E-11,1.E-12,1.E-13,1.E-14
                4,1.E-15,1.E-16,1.E-17,1.E-18,1.E-19,1.E-20,1.E-21,1.E-22,1.E-23,1.
                5E-24,1.E-25,1.E-26,1.E-27,1.E-28,1.E-29,1.E-30,1.E-31,1.E-32/
0006            XMIN=X(1)                                                                                    014
0007            XMAX=X(1)                                                                                    015
0008            YMIN=Y(1)                                                                                    016
0009            YMAX=Y(1)                                                                                    017
0010            DO 3 I=2,N                                                                                   018
0011            XMAX=AMAX1(XMAX,X(I))                                                                        019
0012            XMIN=AMIN1(XMIN,X(I))                                                                        020
0013            YMAX=AMAX1(YMAX,Y(I))                                                                        021
0014            YMIN=AMIN1(YMIN,Y(I))                                                                        022
0015          3 CONTINUE                                                                                     023
0016            GL(1)=XMAX-XMIN                                                                              024
0017            GL(2)=YMAX-YMIN                                                                              025
0018            DO 10 J=1,2                                                                                  026
0019            DT(J)=FLOAT(J)*.01*GL(J)                                                                     027
0020            IF(DT(J).GT.1.E30) GO TO 8                                                                   028
0021            DO 5 I=1,62                                                                                  029
0022            IF(DT(J).GT.RC(I)) GO TO 6                                                                   030
0023          5 CONTINUE                                                                                     031
0024            DT(J)=1.E-32                                                                                 032
0025            GO TO 10                                                                                     033
0026          6 CR=RC(I)                                                                                     034
0027            DO 7 K=2,8                                                                                   035
0028            IF(K.EQ.7) GO TO 7                                                                           036
0029            IF(DT(J).LT.FLOAT(K)*CR) GO TO 9                                                             037
0030          7 CONTINUE                                                                                     038
0031            DT(J)=PC(I-1)                                                                                039
0032            GO TO 10                                                                                     040
0033          8 WRITE (6,100)                                                                                041
0034            RETURN                                                                                       042
0035          9 DT(J)=FLOAT(K)*CR                                                                            043
0036         10 VL(J)=.5*(FLOAT(J-J)*50.*DT(J)-GL(J))                                                        044
0037            OUTX=XMIN-VL(1)                                                                              045
0038            TOPY=YMAX+VL(2)                                                                              046
0039            U=ABS(OUTX)                                                                                  047
0040            RL=AMOD(U,DT(1))                                                                             048
```

```
0041            U=U-REM                                                          049
0042            BOTX=SIGN(U,BOTX)                                                050
0043            U=ABS(TOPY)                                                      051
0044            REM=AMOD(U,DT(2))                                                052
0045            U=U-REM                                                          053
0046            TOPY=SIGN(U,TOPY)+DT(2)                                          054
0047            DXP=10.*DT(1)                                                    055
0048            DO 17 I=1,11                                                     056
0049         17 XP(I)=BOTX+FLOAT(I-1)*DXP                                        057
0050            WRITE (6,101)                                                    058
0051            DY2=.51*DT(2)                                                    059
0052            DO 22 JJ=1,51                                                    060
0053            I=JJ-1                                                           061
0054            DO 105 J=1,101                                                   062
0055        105 A(J)=BLK                                                         063
0056            YN=TOPY-FLOAT(I)*DT(2)                                           064
0057            DO 18 J=1,N                                                      065
0058            IF(ABS(YN-Y(J)).GT.DY2) GO TO 18                                 066
0059            L=1+IFIX(.5+(X(J)-BOTX)/DT(1))                                   067
0060            A(L)=C                                                           068
0061         18 CONTINUE                                                         069
0062            IF(MOD(I,5).EQ.0) GO TO 20                                       070
0063            WRITE (6, 102) (A(J),J=1,101)                                    071
0064            GO TO 22                                                         072
0065         20 WRITE (6,103) YN , (A(J),J=1,101)                                073
0066         22 CONTINUE                                                         074
0067            WRITE (6,104) (XP(I),I=1,11)                                     075
0068            PRINT31
0069            PRINT31
0070            WRITE (6,105) XMAX,XMIN,YMAX,YMIN,DT(1),DT(2)                    076
0071            RETURN                                                           077
0072        100 FORMAT(1H1,10X,20HPLOT RANGE TOO LARGE   )
0073        101 FORMAT(1H1,12X,1H*,10(9X,1H*)/12X,103(1H*))
0074        102 FORMAT(12X,1H*,101A1,1H*)
0075        103 FORMAT(1X,F11.0,3H **,101A1,2H**)
0076        104 FORMAT(12X,103(1H*)/4X,11(9X,1H*)/6X,11(4X,F6.0))
0077        105 FORMAT(1X,6HXMAX =,F7.0,2X,6HXMIN =,F7.0,2X,6HYMAX =,F8.1,2X,6HYMI
               1N =,F7.1,2X,7HXINCR =,F6.0,2X,7HYINCR =,F7.0///)
0078         31 FORMAT('0')
0079            END                                                              085
```

APPENDIX II

Computer program for the calculation of the magnetic anomaly over a thin sheet of infinite strike and finite depth extent.

```
0001            DIMENSION V(100),VH(100),TT(100),TI(100),TTT(100),NAME(40)
0002            DIMENSION TTS(100),TIN(100),TTN(100),TTTN(100),Y(100),VC(100)
0003            DIMENSION VN(100),VHN(100),VS(100),VHS(100),TIS(100),TTS(100)
0004         10 FORMAT(8F4.0)
0005            DIMENSION X(50)
0006          1 FORMAT(40A2)
0007         61 FORMAT('0')
0008          2 FORMAT(F8.1,5F8.1,F10.7,2F8.3)
0009          3 FORMAT(1H0,123H*TOTAL FIELD IN GAMMAS*INCLINATION**ANOMALY**STRIKE
             1*DIP**MAGNETIZATION(M)**DEPTH(M)**CROSS DIP MS**PARALLEL DIP MS**Q-RATIO*
             2*      )
0010          4 FORMAT(1H0,5X,F8.1,13X,F6.1,14X,F6.1,F6.1,1X,F6.1,4X,F6.1,5X,F10.7
             1,5X,F10.7,3X,F7.3)
0011            PI=57.296
0012            READ1,NAME
0013          6 READ2,RINT1,RINC1,STR,DIP,T,Z,S,R,Q
0014            DL=200.0
0015            IF(RINT1)7,7,8
0016          8 RR=R*S
0017            S=S*(1.0+Q)
0018            RR=R*S
0019            RINC1=RINC1/PI
0020            STR=STR/PI
0021            DIP=DIP/PI
0022            RINC=ATAN(TAN(RINC1)/SIN(STR))
0023            RINT=RINT1*SIN(RINC1)/SIN(RINC)
0024            B=RINC-DIP
0025            BB=ATAN(TAN(B)/(R*(1.0+12.566*S)))
0026            AMPL=S*2.0*RINT*T*COS(B)/(Z*COS(BB))
0027            AMPH=AMPL*SIN(STR)
0028            N=41
0029            DO51I=1,N
0030            A=I
0031            Y(I)=(A-1.0)*5.0-60.0
0032            PSI=ATAN(Y(I)/Z)
0033            VVN=COS(PSI)*(R*COS(PSI)*COS(BB)+SIN(PSI)*SIN(BB))
0034            VVHN=COS(PSI)*(COS(PSI)*SIN(BB)-R*SIN(PSI)*COS(BB))
0035            VN(I)=AMPL*VVN
0036            VHN(I)=AMPH*VVHN
0037            TTN(I)=VN(I)*SIN(RINC1)+VHN(I)*COS(RINC1)
0038            TIN(I)=VN(I)*COS(RINC1)-VHN(I)*SIN(RINC1)
0039            TTTN(I)=SQRT(TIN(I)*TIN(I)+(RINT1+TTN(I))*(RINT1+TTN(I)))
0040            ZS=Z+DL*SIN(DIP)
0041            AMPLS=S*2.0*RINT*T*COS(B)/(ZS*COS(BB))
0042            AMPHS=AMPLS*SIN(STR)
```

```
0043              W=ATAN((Y(I)-DE*COS(DIP))/(Z+DE*SIN(DIP)))
0044              VVS=COS(W)*(R*COS(W)*COS(DB)+SIN(W)*SIN(DB))
0045              VVHS=COS(W)*(COS(W)*SIN(DB)-R*SIN(W)*COS(DB))
0046              VS(I)=AMPLS*VVS
0047              VHS(I)=AMPHS*VVHS
0048              TTS(I)=VS(I)*SIN(RINC1)+VHS(I)*COS(RINC1)
0049              TIS(I)=VS(I)*COS(RINC1)-VHS(I)*SIN(RINC1)
0050              TTTS(I)=SQRT(TIS(I)*TIS(I)+(RINT1+TTS(I))*(RINT1+TTS(I)))
0051              V(I)=VN(I)-VS(I)
0052              VH(I)=VHN(I)-VHS(I)
0053              TI(I)=TTN(I)-TTS(I)
0054              TI(I)=TIN(I)-TIS(I)
0055              TTT(I)=TTTN(I)-TTTS(I)
0056              X(I)=V(I)
0057            5 CONTINUE
0058              STR=PI*STR
0059              DIP=PI*DIP
0060              RINC1=PI*RINC1
0061              GO=0
0062              PRINT3
0063              PRINT4,RINT1,RINC1,STR,DIP,T,Z,S,RK,QQ
0064              PRINT61
0065              PRINT10,Y(1),Y(2),Y(3),Y(4),Y(5),Y(6),Y(7),Y(8)
0066              PRINT10,X(1),X(2),X(3),X(4),X(5),X(6),X(7),X(8)
0067              PRINT61
0068              PRINT10,Y(9),Y(10),Y(11),Y(12),Y(13),Y(14),Y(15),Y(16)
0069              PRINT10,X(9),X(10),X(11),X(12),X(13),X(14),X(15),X(16)
0070              PRINT61
0071              PRINT10,Y(17),Y(18),Y(19),Y(20),Y(21),Y(22),Y(23),Y(24)
0072              PRINT10,X(17),X(18),X(19),X(20),X(21),X(22),X(23),X(24)
0073              PRINT61
0074              CALL PLOT3(Y,TT,N)
0075              GO TO 6
0076            7 CALL EXIT
0077              STOP
0078              END
```

```
0001                SUBROUTINE PLOT3(X,Y,N)
0002                DIMENSION X(N),Y(N),GL(2),VL(2),DT(2),XP(11),RC(62),A(120)
                C   DATA C,BLK/1H+,1H /                                                    002
0003                INTEGER C, BLK, A                                                      003
0004                DATA C, BLK / '+', ' ' /                                               004
                C   DATA(RC(I),I=1,62)/1.E29,1.E28,1.E27,1.E26,1.E25,1.E24,1.E23,      005
0005                DATA RC/1.E29,1.E28,1.E27,1.E26,1.E25,1.E24,1.E23,1.E22,1.E21,1.E2
                   10,1.E19,1.E18,1.E17,1.E16,1.E15,1.E14,1.E13,1.E12,1.E11,1.E10,1.E9
                   2,1.E8,1.E7,1.E6,1.E5,1.E4,1.E3,1.E2,1.E1,1.,1.E-1,1.E-2,1.E-3,1.E-
                   34,1.E-5,1.E-6,1.E-7,1.E-8,1.E-9,1.E-10,1.E-11,1.E-12,1.E-13,1.E-14
                   4,1.E-15,1.E-16,1.E-17,1.E-18,1.E-19,1.E-20,1.E-21,1.E-22,1.E-23,1.
                   5E-24,1.E-25,1.E-26,1.E-27,1.E-28,1.E-29,1.E-30,1.E-31,1.E-32/
0006                XMIN=X(1)                                                              014
0007                XMAX=X(1)                                                              015
0008                YMIN=Y(1)                                                              016
0009                YMAX=Y(1)                                                              017
0010                DO 3 I=2,N                                                             018
0011                XMAX=AMAX1(XMAX,X(I))                                                  019
0012                XMIN=AMIN1(XMIN,X(I))                                                  020
0013                YMAX=AMAX1(YMAX,Y(I))                                                  021
0014                YMIN=AMIN1(YMIN,Y(I))                                                  022
0015              3 CONTINUE                                                               023
0016                GL(1)=XMAX-XMIN                                                        024
0017                GL(2)=YMAX-YMIN                                                        025
0018                DO 10 J=1,2                                                            026
0019                DT(J)=FLOAT(J)*.01*GL(J)                                               027
0020                IF(DT(J).GT.1.E30) GO TO 8                                             028
0021                DO 5 I=1,62                                                            029
0022                IF(DT(J).GT.RC(I)) GO TO 6                                             030
0023              5 CONTINUE                                                               031
0024                DT(J)=1.E-32                                                           032
0025                GO TO 10                                                               033
0026              6 CR=RC(I)                                                               034
0027                DO 7 K=2,8                                                             035
0028                IF(K.EQ.7) GO TO 7                                                     036
0029                IF(DT(J).LT.FLOAT(K)*CR) GO TO 9                                       037
0030              7 CONTINUE                                                               038
0031                DT(J)=RC(I-1)                                                          039
0032                GO TO 10                                                               040
0033              8 WRITE (6,100)                                                          041
0034                RETURN                                                                 042
0035              9 DT(J)=FLOAT(K)*CR                                                      043
0036             10 VL(J)=.5*(FLOAT(J-J)*50.*DT(J)-GL(J))                                  044
0037                ROTX=XMIN-VL(1)                                                        045
0038                TOPY=YMAX+VL(2)                                                        046
0039                U=ABS(ROTX)                                                            047
0040                RL=AMOD(U,DT(1))                                                       048
```

```
0041            U=U-REM
0042            BOTX=SIGN(U,BOTX)
0043            U=ABS(TOPY)
0044            REM=AMOD(U,DT(2))
0045            U=U-REM
0046            TOPY=SIGN(U,TOPY)+DT(2)
0047            DXP=10.*DT(1)
0048            DO 17 I=1,11
0049         17 XP(I)=BOTX+FLOAT(I-1)*DXP
0050            WRITE (6,101)
0051            DY2=.51*DT(2)
0052            DO 22 JJ=1,51
0053            I=JJ-1
0054            DO 105 J=1,101
0055        105 A(J)=BLK
0056            YN=TOPY-FLOAT(I)*DT(2)
0057            DO 18 J=1,N
0058            IF(ABS(YN-Y(J)).GT.DY2) GO TO 18
0059            L=1+IFIX(.5+(X(J)-BOTX)/DT(1))
0060            A(L)=C
0061         18 CONTINUE
0062            IF(MOD(I,5).EQ.0) GO TO 20
0063            WRITE (6, 102) (A(J),J=1,101)
0064            GO TO 22
0065         20 WRITE (6,103) YN , (A(J),J=1,101)
0066         22 CONTINUE
0067            WRITE (6,104) (XP(I),I=1,11)
0068            PRINT31
0069            PRINT31
0070            WRITE (6,105) XMAX,XMIN,YMAX,YMIN,DT(1),DT(2)
0071            RETURN
0072        100 FORMAT(1H1,10X,20HPLOT RANGE TOO LARGE   )
0073        101 FORMAT(1H1,12X,1H*,10(9X,1H*)/12X,103(1H*))
0074        102 FORMAT(12X,1H*,101A1,1H*)
0075        103 FORMAT(1X,F9.0,3H **,101A1,2H**)
0076        104 FORMAT(12X,103(1H*)/4X,11(9X,1H*)/6X,11(4X,F6.0))
0077        105 FORMAT(1X,6HXMAX =,F7.0,2X,6HXMIN =,F7.0,2X,6HYMAX =,F8.1,2X,6HYMI
               1N =,F7.1,2X,7HXINCR =,F6.0,2X,7HYINCR =,F7.0///)
0078         31 FORMAT('0')
0079            END
```

REFERENCES

BMDP-77., 1977. Biomedical Computer Programs P-Series, Univ. Calif. Press, Berkeley, Los Angeles, London, 215p.

C.D.M., 1961. Isoclinic, isogonic and isodynamic charts, Canada. Can. Dep. Mines Tech. Surveys.

C.M.Y., 1976. Canadian Minerals Yearbook. Can., Dep. Energy, Mines Resourc. p.254-9.

Card, K.D., 1978. Geology of the Sudbury - Manitoulin Area. Ont. Geol. Surv., Rep. 166, p.9-30.

Christie, K.W., and Symons, D.T.A., 1969. Apparatus for measuring magnetic susceptibility and its anisotropy. Geol. Surv. Can., Paper 69-41. 10p.

Dunnet, D., 1969. A technique of finite-strain analysis using elliptical particles. Tectonophysics, v. 7, p.117-136.

Elliot, D., 1970. Determination of finite strain and initial shape from deformed elliptical objects. Geol. Soc. Am., Bull., v. 81, p.2221-2236.

Fairbairn, H.W., Hurley, P.M., Card, K.D., and Knight, C.J., 1969. Correlation of radiometric ages of Nipissing diabase and Huronian metasediments with Proterozoic orogenic events in Ontario. Can. J. Earth Sci., v. 6, p.489.

Fisher, R.A., 1953. Dispersion on a sphere. Proc. Royal Soc. London, Series A, 217, p.295-305.

Fuller, M.D., and Kobayashi, K., 1967. Identification of magnetic phases in certain rocks by low temperature analysis. in Methods in Palaeomagnetism, Edited by Collinson, Creer and Runcorn. Elsevier. p.529.

Gates, T.M., and Hurley, P.M., 1973. Evaluation of Rb-Sr Dating Methods Applied to the Matachewan, Abitibi, Mackenzie and Sudbury Dike Swarms in Canada. Can. J. Earth Sci., v. 10, p.900.

Gay, S.P., 1963. Standard curves for interpretation of magnetic anomalies over long tabular bodies. Geophysics, v. 28, p.161-200.

G.S.C., 1965. Venetian Lake, Ontario. Geol. Surv. Can. Aeromagnetic Series Map 1519G, scale 1 inch to 1 mile or 1:63,360. Survey flown June 1959 to October 1960.

Henry, S.G., 1979. Chemical demagnetization methods, procedures, and applications through vector analysis. Can. J. Earth Sci., v. 16, p.1832.

Irving, E., 1979. Paleopoles and paleolatitudes of North America and speculations about displaced terrains. Can. J. Earth Sci., v. 16, p.669-694.

Kindle, L.F., 1932. Moose Mountain, Wahnapitei Area, Ontario. Ont. Dep. Mines, Annu. Rep., v. XLI, pt. 4, p.29-49.

Larochelle, A., 1969. L'application de la statistique au paléomagnétisme. Geol. Surv. Can., Paper 68-59, p.1-19.

Lowphos Ore Ltd., 1962. Moose Mountain Mine, Ground Magnetometer Survey, Ore Body 11, Sheet 1, scale 1 inch to 40 ft.

Markland, G.D., 1966. Geology of the Moose Mountain mine and its' application to Mining and Milling. Can. Min. Metall. Bull., Trans., v. 69, p.50-61.

Meyn, H.D., 1970. Geology of Hutton and Parkin Townships. Ont. Dep. Mines, Rep., 80, p.43.

O.D.M., 1967. Ont. Dep. Mines, Resident Geologists' Section Annu. Rep., Misc. Paper No. 17, Edited by J.F. Donovan, p.103.

O.D.M., 1969. Ont. Dep. Mines, Misc. Paper No. 34, Edited by D.G. Innes, p.23.

O.D.M., 1975. Ont. Dep. Mines, Annu. Rep. Regional Resident Geologists, Misc. Paper No. 64, Edited by C.R. Kustra, p.106.

Park, J.K., 1970. Acid leaching of red beds and the relative stability of the red and black components. Can. J. Earth Sci., v. 7, p.1086.

Roy, J.L., and Lapointe, P.L., 1976. The Paleomagnetism of Huronian red beds and Nipissing diabase; Post-Huronian Igneous Events and apparent polar path for the interval 2300 to 1500Ma for Laurentia. Can. J. Earth Sci., v. 13, p.749.

Seguin, M.K., 1972. Étude et application du magnétisme rémanent naturel à la découverte de gisements de taconite magnétique. Pure and Applied Geophys., v. 97, p.156-174.

Seguin, M.K., 1975. Étude des propriétés magnétiques et du paléomagnétisme de formations de fer de la portion centale de la fosse du Labrador. Résumé, 43e Congrès de l'ACFAS, v. 42, No. 1, p.78.

Seguin, M.K., 1976. Are Precambrian iron formations suitable for paleomagnetic studies? Annale de Geophysique, v. 32, p.327-334.

Shklanka, R., 1968. Iron Deposits of Ontario. Ont. Dep. Mines, Mineral Resources Circular, No. 11, p.342.

Strangway, D.W., 1965. Interpretation of the Magnetic Anomalies over some Precambrian Dikes. Geophysics, v. 30, p.783-796.

Stupavsky, M., and Symons, D.T.A., 1978. Separation of Magnetic Components from AF step Demagnetization Data by Least Squares Computer Methods. J. Geophys. Res., v. 83, p.4925-4931.

Symons, D.T.A., 1966. A paleomagnetic study on the Gunflint, Mesabi and Cayuna iron ranges in the Lake Superior region. Econ. Geol., v.61, p.1336-1361.

Symons, D.T.A., 1967. Paleomagnetic evidence on the origin of the Marquette and Steep Rock hard hematite and geothite deposits. Can. J. Earth Sci., v. 4, p.1-20.

Symons, D.T.A., and Stupavsky, M., 1974. A rational paleomagnetic stability index. J. Geophys. Res., v. 79, p.1718-1720.

Symons, D.T.A., and Stupavsky, M., 1979. Magnetic Characteristics of the Iron Formation near Temagami, Ontario. Ont. Geol. Surv., Misc. Paper 87, p.133-147.

van Schmus, R., 1965. The geochronology of the Blind River-Bruce Mines Area. J. Geol., v. 73, p.775.

Wanless, R.K., Stevens, R.D., Lachance, G.R., and Rimsaite, J.Y.H., 1965. Age determinations and geological studies. Can. Dep. Mines Tech. Surveys, Rep. 5.

Watson, G.S., 1956. Analysis of dispersion on a sphere. Monthly Notices Roy. Astron. Soc. London, Geophys. Suppl., No. 7, p.153-159.

Zijderveld, J.D.A., 1967. AF demagnetization of rocks: analysis of results. in Methods in Palaeomagnetism, Edited by Collinson, Creer and Runcorn. Elsevier. New York. p.254-286.

VITAE AUCTORIS

Born: February 9th., 1955, in Stoke-on-Trent, England.
Son of Mr. and Mrs. S.D. Walley

Education:

Secondary School:
The Grove Comprehensive School, Market Drayton, Shropshire, England.

University:
Bath University, England.

University College of Swansea, University of Wales, Swansea, S. Wales.
Bachelor of Science in Geology, 1977.
B.Sc. Thesis: The Geology of the Area around St. Geniez, near Sisteron, Alpes-de-Hautes-Provence, France.

University of Windsor, Windsor, Ontario, Canada.
M.Sc. Thesis topic: Component magnetization of the Iron Formation and deposits at the Moose Mountain Mine, Capreol, Ontario. 1980.